# VARIABLE STIFFNESS SUSPENSION SYSTEM

By

OLUGBENGA MOSES ANUBI

A DISSERTATION PRESENTED TO THE GRADUATE SCHOOL
OF THE UNIVERSITY OF FLORIDA IN PARTIAL FULFILLMENT
OF THE REQUIREMENTS FOR THE DEGREE OF
DOCTOR OF PHILOSOPHY

UNIVERSITY OF FLORIDA

2013

To my LORD and savior Jesus Christ.

To my lovely and beautiful wife Serena Leah Anubi.

To my sweet mother Victoria Anubi

ACKNOWLEDGMENTS

I express my gratitude to my supervisory committee: Dr. Carl Crane, Dr. Warren Dixon, Dr. Prabir Barooah, Dr. William Hagger, Dr. Oscar D. Crisalle, Dr. Rico Jose, and Dr. Rodney Roberts for their time, efforts, and invaluable contributions to my academic growth during my time at the University of Florida.

Many thanks to Darsan Patel for his help with experiments and data collection. I also thank every member of the Center for Intelligent Machines and Robotics (CIMAR) for their invaluable support.

Also, my appreciation goes to my parent in-law, Carl and Bernadette Sealy, for their invaluable support, prayers and mentorship.

Finally, I express my gratitude to the members of my microchurch; Serena Leah Anubi, Olawale Adeleye, Adria McKire (Adeleye to be), Oluwatosin Adeladan, Oluwabusayo Fawole (Adeladan to be), David Walker, Kerlin and Ketty Bien, Ethel Porras, Eyitayo Owoeye, Brenda Nelson, Qwamel Hanks, Orece Carty, Conrad Cole, Chelsea Brown, Otonye Braids, and Conrad Cole for their prayers, counseling, and encouragement in my walk with our Lord Jesus.

TABLE OF CONTENTS

page

ACKNOWLEDGMENTS . . . . . 4

LIST OF TABLES . . . . . 8

LIST OF FIGURES . . . . . 9

NOMENCLATURE . . . . . 13

ABSTRACT . . . . . 16

CHAPTER

1 INTRODUCTION . . . . . 18

1.1 Some Historical Notes on Vehicle Suspension . . . . . 18
1.2 Types of Suspension . . . . . 19
1.2.1 Independent Suspension . . . . . 19
1.2.2 Dependent Suspension . . . . . 20
1.2.3 Semi-independent Suspension . . . . . 21
1.3 Suspension Geometry . . . . . 22
1.4 Controlled Suspension . . . . . 24
1.4.1 Active Suspension Design . . . . . 25
1.4.2 Adaptive Suspension Design . . . . . 25
1.4.3 Semi-Active Suspension Design . . . . . 26

2 VARIATION OF STIFFNESS IN SUSPENSION DESIGN . . . . . 30

2.1 General Semi-Active Suspension . . . . . 30
2.2 Single Modulation Optimal Semi-Active Control Laws . . . . . 33
2.3 Spring and Damper Modulation . . . . . 37
2.4 Double Modulation Optimal Semi-Active Control Laws . . . . . 41
2.4.1 Sequential Modulation . . . . . 41
2.4.2 Simultaneous Modulation . . . . . 45
2.5 Simulation . . . . . 47
2.5.1 Time Domain Simulation . . . . . 48
2.5.2 Frequency Response . . . . . 50

3 VARIABLE STIFFNESS MECHANISM . . . . . 54

3.1 Forward Analysis . . . . . 54
3.1.1 Effect of $r$ on $K$ and $l_0$ . . . . . 61
3.1.2 Special Cases . . . . . 64
3.2 Reverse Analysis . . . . . 65
3.3 Dynamical Analysis . . . . . 67

4 VARIABLE STIFFNESS SUSPENSION SYSTEM: PASSIVE CASE . . . . . 70

4.1 System Description . . . . . 71
4.1.1 Variable Stiffness Concept . . . . . 71
4.1.2 Mechanism Description . . . . . 72
4.1.3 Equations of Motion . . . . . 73
4.2 System Analysis . . . . . 77
4.2.1 Performance Objective . . . . . 79
4.2.2 Constant Stiffness Case . . . . . 81
4.2.3 Passive Variable Stiffness Case . . . . . 87
4.2.4 Experiment . . . . . 90
4.2.5 Simulation . . . . . 94
4.2.5.1 Time Domain Simulation . . . . . 94
4.2.5.2 Frequency Domain Simulation . . . . . 95

5 VARIABLE STIFFNESS SUSPENSION SYSTEMS USING NONLINEAR ENERGY SINKS: ACTIVE AND SEMI-ACTIVE CASES . . . . . 100

5.1 Orthogonal Nonlinear Energy Sink . . . . . 101
5.2 Active Case . . . . . 103
5.2.1 Control Masses and Actuator Dynamics . . . . . 105
5.2.2 Control Development . . . . . 106
5.2.3 Stability Analysis . . . . . 109
5.2.4 Simulation . . . . . 111
5.3 Semi-active Case . . . . . 113
5.3.1 MR-damper Modeling . . . . . 115
5.3.2 Control Development . . . . . 120
5.3.2.1 Open Loop Tracking Error Development . . . . . 121
5.3.2.2 Closed Loop Error System Development . . . . . 123
5.3.3 Stability Analysis . . . . . 127
5.3.4 Simulation Results . . . . . 128

6 ROLL STABILIZATION ENHANCEMENT USING VARIABLE STIFFNESS SUSPENSION . . . . . 135

6.1 Mechanism Description . . . . . 136
6.2 Modeling . . . . . 137
6.2.1 Yaw Dynamics . . . . . 137
6.2.2 Roll Dynamics . . . . . 140
6.3 Kinematic Control . . . . . 142
6.3.1 Control Allocation . . . . . 144
6.3.2 Stability Analysis . . . . . 145
6.3.3 Simulation . . . . . 148
6.3.3.1 Fish hook Maneuver . . . . . 149
6.3.3.2 Double Lane Change Maneuver . . . . . 152
6.4 Dynamic Control . . . . . 153

6.4.1 Control Masses and Actuator Dynamics . . . 154
6.4.2 Control Design . . . 155
6.4.2.1 Vehicle Body Roll . . . 155
6.4.2.2 Control Masses . . . 159
6.4.2.3 Hydraulic Actuators . . . 160
6.4.3 Stability Analysis . . . 163
6.4.4 Simulation . . . 167

7 CONCLUSIONS AND FUTURE WORK . . . 171

7.1 Conclusion . . . 171
7.2 Future Work . . . 172

APPENDIX: PROOF OF THEOREMS 2.1 AND 2.2 . . . 174

A.1 Proof of Theorem 2.1 . . . 174
A.2 Proof of Theorem 2.2 . . . 176

REFERENCES . . . 180

BIOGRAPHICAL SKETCH . . . 191

LIST OF TABLES

Table page

2-1 Dynamic parameter values . . . . . 48

4-1 RMS gain values of experimental results . . . . . 91

5-1 Dynamic parameter values . . . . . 111

5-2 Hydraulic parameter values . . . . . 112

5-3 Variance gain values . . . . . 113

5-4 MR-damper parameter values . . . . . 121

5-5 Variance gain values . . . . . 130

LIST OF FIGURES


Figure page

1-1 Front wheel double wishbone suspensions . . . . . 20

1-2 McPherson suspension system . . . . . 21

1-3 Rigid axle suspension system . . . . . 22

1-4 Twist beam suspension system . . . . . 23

2-1 Quarter car - modulated spring/damper . . . . . 31

2-2 Quarter car - modulated spring and damper . . . . . 37

2-3 Time response - car body acceleration . . . . . 48

2-4 Time response - suspension deflection . . . . . 49

2-5 Time response - tire deflection . . . . . 49

2-6 Time response - performance index . . . . . 50

2-7 Frequency response - car body acceleration . . . . . 52

2-8 Frequency response - suspension deflection . . . . . 53

2-9 Frequency response - tire deflection . . . . . 53

3-1 Schematics . . . . . 55

3-2 Free body diagram . . . . . 56

3-3 Effective stiffness against $d$ . . . . . 59

3-4 Effective stiffness against $\frac{1}{d}$ . . . . . 59

3-5 Overall free length against $d$ . . . . . 60

3-6 Effective stiffness against $r$ over $d$ . . . . . 62

3-7 Variation of overall free length against $r$ over $d$ . . . . . 63

3-8 Effective stiffness against $d$ over $r$ . . . . . 63

3-9 Variation of overall free length against $d$ over $r$ . . . . . 64

3-10 Effect of aspect ratio on achievable stiffness lower bound . . . . . 67

3-11 Natural frequency . . . . . 68

4-1 Variable stiffness mechanism . . . . . 72

4-2 Variable stiffness suspension system . . . . . 73
4-3 Quarter car model - passive case . . . . . 74
4-4 Quarter car experimental setup . . . . . 91
4-5 Sinusoidal test - fixed case . . . . . 92
4-6 Sinusoidal test - passive case . . . . . 93
4-7 Drop test - car body acceleration . . . . . 93
4-8 Drop test - tire deflection acceleration . . . . . 94
4-9 Solidworks quarter car model . . . . . 95
4-10 Time domain simulation - car body acceleration . . . . . 96
4-11 Time domain simulation - suspension deflection . . . . . 96
4-12 Time domain simulation: tire deflection . . . . . 96
4-13 Time domain simulation - control mass position . . . . . 97
4-14 Frequency domain simulation - car body acceleration . . . . . 98
4-15 Frequency domain simulation - suspension deflection . . . . . 98
4-16 Frequency domain simulation - tire deflection . . . . . 99
5-1 Orthogonal nonlinear energy sink (NES) . . . . . 101
5-2 Variance Gain . . . . . 104
5-3 Quarter car model - active case . . . . . 105
5-4 Simmechanic model . . . . . 111
5-5 Car body acceleration (CBA) . . . . . 114
5-6 Suspension travel (ST) . . . . . 115
5-7 Tire deflection(TD) . . . . . 116
5-8 Control mass displacement . . . . . 116
5-9 Actuator forces . . . . . 117
5-10 Quarter car model - Semi-active case . . . . . 118
5-11 Nonparametric MR-damper model . . . . . 119
5-12 Polynomial approximation . . . . . 124

5-13 Car body acceleration (CBA) - semi-active case . . . 130
5-14 Suspension travel (ST) - semi-active case . . . 130
5-15 Tire deflection(TD) - semi-active Case . . . 131
5-16 Control mass displacement - semi-active case . . . 131
5-17 Parameter estimates - semi-active case . . . 132
5-18 Control currents . . . 133
5-19 MR-damper forces . . . 134
6-1 Half car model . . . 137
6-2 Modeling schematics . . . 138
6-3 Bicycle model . . . 138
6-4 Idealized half car model for roll dynamics modeling . . . 140
6-5 Snap shot during data collection process . . . 149
6-6 Parameter estimation validation - snake data . . . 150
6-7 Fishhook - steering command . . . 150
6-8 Fishhook - roll response . . . 151
6-9 Fishhook - control mass displacement . . . 151
6-10 Double lane change - steering command . . . 152
6-11 Double lane change - roll response . . . 152
6-12 Double lane change - control mass displacement . . . 153
6-13 Half car model . . . 153
6-14 Lateral tire force approximation . . . 157
6-15 Roll response . . . 167
6-16 Control mass displacement . . . 167
6-17 Voltage command . . . 168
6-18 Spool valve response . . . 168
6-19 Hydraulic force output . . . 168
6-20 Adaptive parameter estimation history, $\hat{\mathbf{Q}}$ . . . 169

6-21 Adaptive parameter estimation history, $\hat{\alpha}$ . . . . . 169
6-22 Adaptive parameter estimation history, $\hat{\beta}$ . . . . . 169
6-23 Adaptive parameter estimation history, $\hat{\gamma}$ . . . . . 170
6-24 Vehicle trajectory . . . . . 170

NOMENCLATURE

$l_s$ Vertical strut length.

$l_{0_s}$ Natural length of suspension spring

$l_{0_s}$ Natural length of vertical strut.

$\bigcap$ Intersection of sets

$\bigcup$ Union of sets

$\delta$ Front wheel steering angle

$\delta$ Vertical displacement of the point of application of force

$\lambda_{max}\{A\}$ The maximum eigenvalue of the matrix $A$

$\lambda_{min}\{A\}$ The minimum eigenvalue of the matrix $A$

$\mathcal{L}_s(\mathbf{q}_1, \mathbf{q}_2)$ The set of points that lie on the line segment joining the vectors $\mathbf{q}_1$ and $\mathbf{q}_2$

$\mathcal{R}$ The set of real numbers

$\mathcal{R}$ Set of real numbers

$\phi$ Vehicle body roll angle

$\psi$ Vehicle yaw angle

$\mathbf{e}_{i,n}$ The $i$th column of the identity matrix of dimension $n$

$\theta$ Angular displacement of lever about pivot

$A_{i:j,k:l}$ The sub-matrix of matrix $A$ formed by rows $i$ to $j$ and columns $k$ to $l$

$A_{i:j}$ The sub-matrix of matrix $A$ formed by rows $i$ to $j$ and all columns

$b_s$ suspension damping coefficient

$d$ Horizontal displacement of the pivot from the center of lever

$d_L$ Left control mass displacement

$d_R$ Right control mas displacement

$det\{A\}$ The determinant of the matrix $A$

$eig\{A\}$ Set of the eigenvalues of matrix $A$

$F$ External force.

$H$ Height of the control mass from the pivot point of the lower wishbone.

$H$ Height of the pivot bar

$h_u$ Half distance between points C and D.

$I$ Identity matrix

$I_c$ Moment of inertia of control arm.

$I_s$ Vehicle roll moment of inertia

$I_z$ Vehicle yaw moment of inertia

$K(d)$ Effective stiffness of the mechanism expressed as a function $d$

$k_1, k_2$ Spring constants

$k_s$ stiffness of suspension spring

$k_s, b_s$ Vertical Strut stiffness and damping coefficient

$k_t, b_t$ Tire spring constant and damping coefficient.

$k_u, b_u$ Control(Horizontal) Strut stiffness and damping

$L_1, L_2$ Horizontal distances of the vertical springs ($k_1$ and $k_2$) from center of lever

$l_D$ Length of the lower wishbone.

$l_f$ distance of front axle from the center of mass

$l_r$ distance of rear axle from the center of mass

$l_{0_1}, l_{0_2}$ Spring free lengths

$m$ Vehicle total mass

$m_s, m_u, m_d$ Sprung, unsprung and control masses.

$r$ Yaw rate

$Re\{\alpha\}$ The real part of the complex number $\alpha$

$roots(\alpha(i))$ The set of roots of the polynomial $\alpha(i)$

$tr\{A\}$ The trace of the matrix $A$

$v_x$ Longitudinal velocity

$v_y$ Lateral velocity

$x$ Distance between points O and A along the lower wishbone.

$y_s$ Vertical displacement of the sprung mass.

$y_u$ Vertical displacement of the unsprung mass.

$\{\}$ Empty set

Abstract of Dissertation Presented to the Graduate School
of the University of Florida in Partial Fulfillment of the
Requirements for the Degree of Doctor of Philosophy

VARIABLE STIFFNESS SUSPENSION SYSTEM

By

Olugbenga Moses Anubi

May 2013

Chair: Carl Crane
Major: Mechanical Engineering

Improvements over passive suspension designs is an active area of research. Past approaches utilize one of three techniques; adaptive, semi-active, or fully active suspension. An adaptive suspension utilizes a passive spring and an adjustable damper with slow response to improve the control of ride comfort and road holding. A semi-active suspension is similar, except that the adjustable damper has a faster response and the damping force is controlled in real-time. A fully active suspension replaces the damper with a hydraulic actuator, or other types of actuators like electromagnetic actuators, which can achieve optimum vehicle control, but at the cost of design complexity. The fully active suspension is also not fail-safe in the sense that performance degradation results whenever the control fails, which may be due to either mechanical, electrical, or software failures. Recently, research in semi-active suspensions has continued to advance with respect to capabilities, narrowing the gap between semi-active and fully active suspension systems. Today, semi-active suspensions (e.g using Magneto-Rheological (MR), Electro-Rheological (ER) etc) are widely used in the automobile industry due to their small weight and volume, as well as low energy consumption compared to purely active suspension systems.

However, most semi-active design concepts are focused on only varying the damping coefficient of the shock absorber while keeping the stiffness constant. Meanwhile, in suspension optimization, both the damping coefficient and the spring

rate of the suspension elements are usually used as optimization arguments. Therefore, a semi-active suspension system that varies both the stiffness and damping of the suspension element could provide more flexibility in balancing competing design objectives.

This work considers the design, analyses, and experimentation of a new variable stiffness suspension system. The design is based on the concept of a variable stiffness mechanism. The mechanism, which is a simple arrangement of two springs, a lever arm, and a pivot bar, has an effective stiffness that is a rational function of the horizontal position of the pivot. The effective stiffness is varied by changing the position of the pivot while keeping the point of application of the external force constant. The overall suspension system consists of a horizontal control strut and a vertical strut. The main idea is to vary the load transfer ratio by moving the location of the point of attachment of the vertical strut to the car body. This movement is controlled passively, semi-actively, and actively using the horizontal strut. The system is analyzed using an $\mathcal{L}_2$-gain analysis based on the concept of energy dissipation. The analyses, simulation, experimental results, show that the variable stiffness suspension achieves better performance than the constant stiffness counterpart. The performance criteria used are; ride comfort, characterized by the car body acceleration, suspension deflection, and road holding, characterized by tire deflection.

# CHAPTER 1
# INTRODUCTION

Suspension is a collective term given to the system of springs, damper and linkages that isolates a vehicle body (sprung mass) from the wheel assembly (unsprung mass). The vehicle interacts with the road via the direct contact between tire and the road. The suspension system serves to isolate the passenger from the road noise as much as possible while keeping good road contact for improved handling and mobility. The automotive suspension system consists of the tires, guiding elements which include control arms and links (A-arms), struts, leaf springs, and force elements which include springs (coil spring, air spring, or leaf spring), torsion bar,anti-roll bar, damper (passive or semi-active), bushings, etc.

## 1.1 Some Historical Notes on Vehicle Suspension

The history of vehicle suspension dates back to the era of horse drawn vehicles. By the early 19th century, most British horse carriages were equipped with wooden springs in light one-horse vehicles, and steel springs in larger vehicles. The steel springs were made of low-carbon steel and were designed in form of multiple layer leaf springs [1]. The British steel springs were not well suited for use on America's rough roads of that time. As a result, in the 1820's, the Abbot Downing Company of Concord, New Hampshire developed a system whereby the bodies of stage coaches were supported on leather straps called "thorough braces", which gave a swinging motion instead of the jolting up and down of a spring suspension.

Automotives were initially designed as self-propelled versions of horse drawn vehicles. However, the horse-drawn vehicle suspension designed for slow speeds were not suitable for higher speeds permitted by the internal combustion engine. In 1901, Mors of Paris first fitted an automobile with shock absorbers. Henri Fournier later won the prestigious Paris-to-Berlin race on June 20, 1901 with the aid of his 'Mors Machine' [2]. Leyland used torsion bars in a suspension system in 1920. In 1922,

independent front suspension was pioneered on the Lancia Lambda and became more common in mass-produced cars by 1932 [3]. Early independent suspensions were also produced by Andre Dubonnet in France in late 1920's [4]. Also in 1932, two experimental Cadillac cars were buit, one using Dubonnet's type of suspension, the other with a double-wishbone suspension of GM's design. During the great depression, there were heavy financial constraints on car manufacturing and retail prices were pressing. However, independent front suspension designs were enthusiastically accepted, and shown to the public in 1934. In 1935 Chevrolet and Pontiac had cars available with Dubonnet suspensions, while Cadillac, Buick, and Oldsmobile had double wishbone suspensions. By that time the rigid front axle was beginning to faze out in passenger cars.

## 1.2 Types of Suspension

Suspension systems are divided into three classes: independent, dependent and semi-independent suspensions.

### 1.2.1 Independent Suspension

As the name implies, the independent suspension has no mechanical linkages between the two hubs of the same axle; the force acting on one wheel does not affect the other. The linkages must be designed to constrain five out of the six degrees of freedom of the wheel hub. The unconstrained degree of freedom is the translation in a direction perpendicular to the ground. None of the many devices which are currently used fulfills this requirement exactly [5]. Independent suspensions are usually either a double wishbone type or a McPherson suspension type. Double wishbone suspensions are applied to luxury sedans and sports cars because they allow a design of the elasto-kinematic parameters that provides an optimum compromise between handling and comfort. They have two A-arms (wishbones), connected to the top and bottom of the wheel hub via a ball and socket joint. Figure 1-1 shows double wishbone suspensions of the high and low types. If the upper A-arm is replace by a prismatic

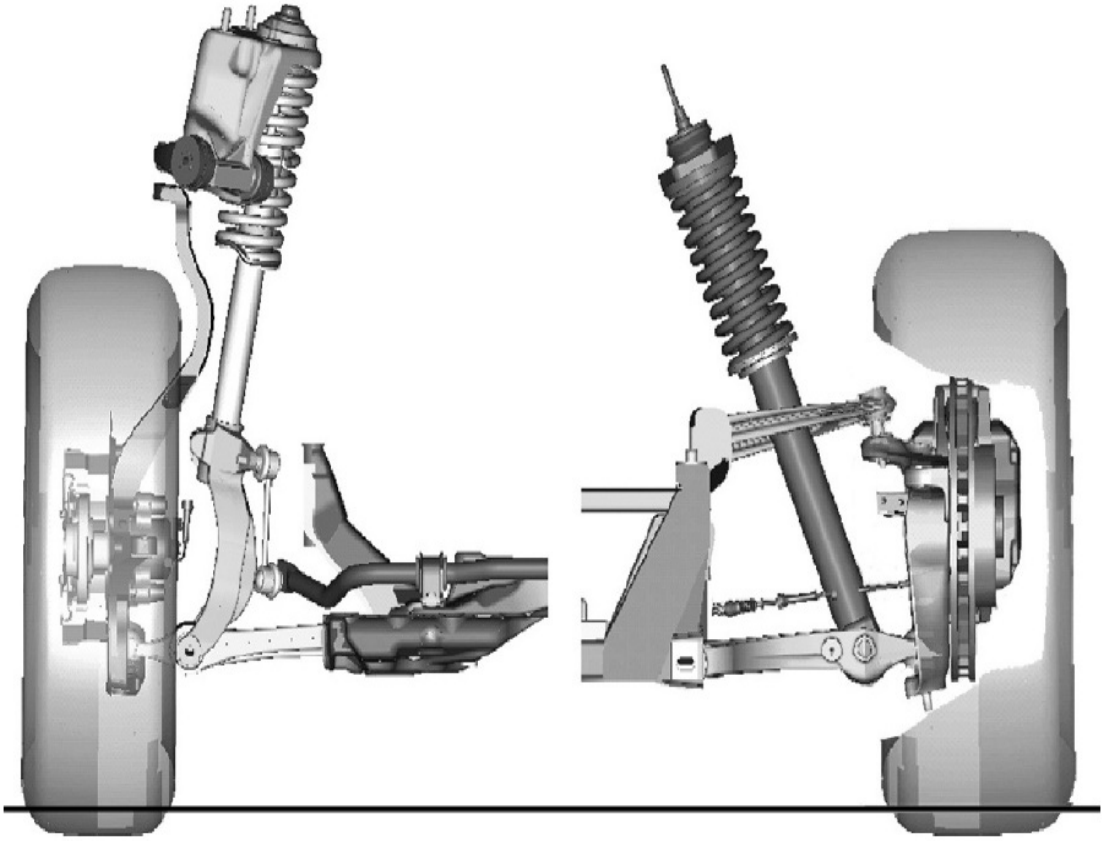

Figure 1-1. Front wheel double wishbone suspensions [5].
Left: high type, Right: low type.

joint, a McPherson suspension results as shown in Figure 1-2. It is simple and allows more room for the engine. As a result, it has become a common solution for automotive front axles, particularly in small cars. Other forms of independent suspension generally used for rear suspension due to their minimal invasiveness into the chassis include the trailing arm suspension, semi-trailing arm suspension, guided-trailing arm suspension, and multilink suspension.

### 1.2.2 Dependent Suspension

Dependent suspensions have rigid axles which provide a rigid linkage between the two wheels of the same axle (see Figure 1-3). The dynamic response of the wheels

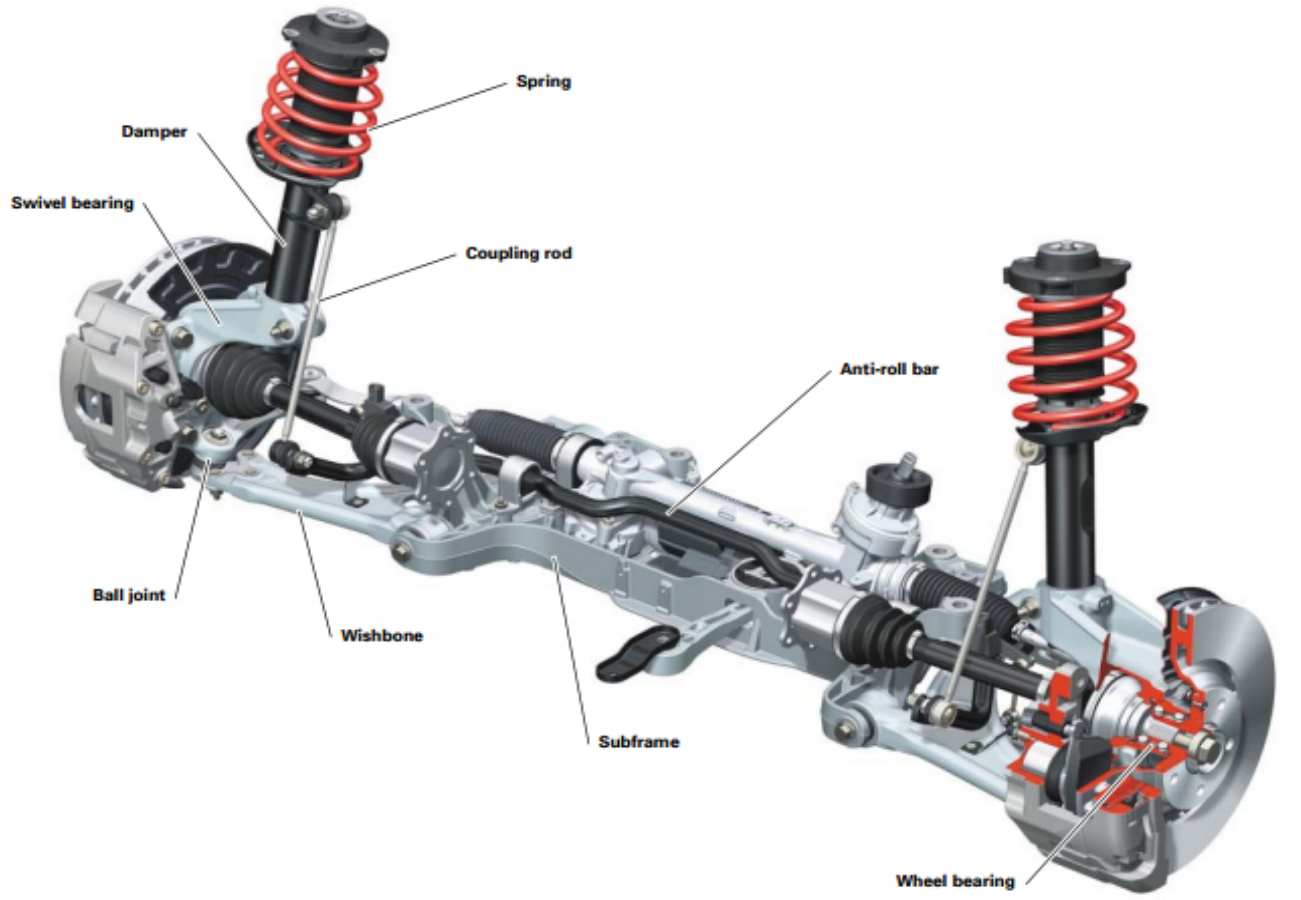


Figure 1-2. McPherson suspension system [6].

caused by road excitations are coupled with each other. This suspension is widely used in industrial vehicles and off road vehicles.

### 1.2.3 Semi-independent Suspension

This type of suspension has intermediate characteristics between the first two categories. An example is the twist beam suspension which is essentially comprised of two trailing arms fixed to the chassis with an elastic bushing and connected by a cross beam. The springs and shock absorbers are fixed between the arms and the car body. This suspension system is depicted in Figure 1-4.

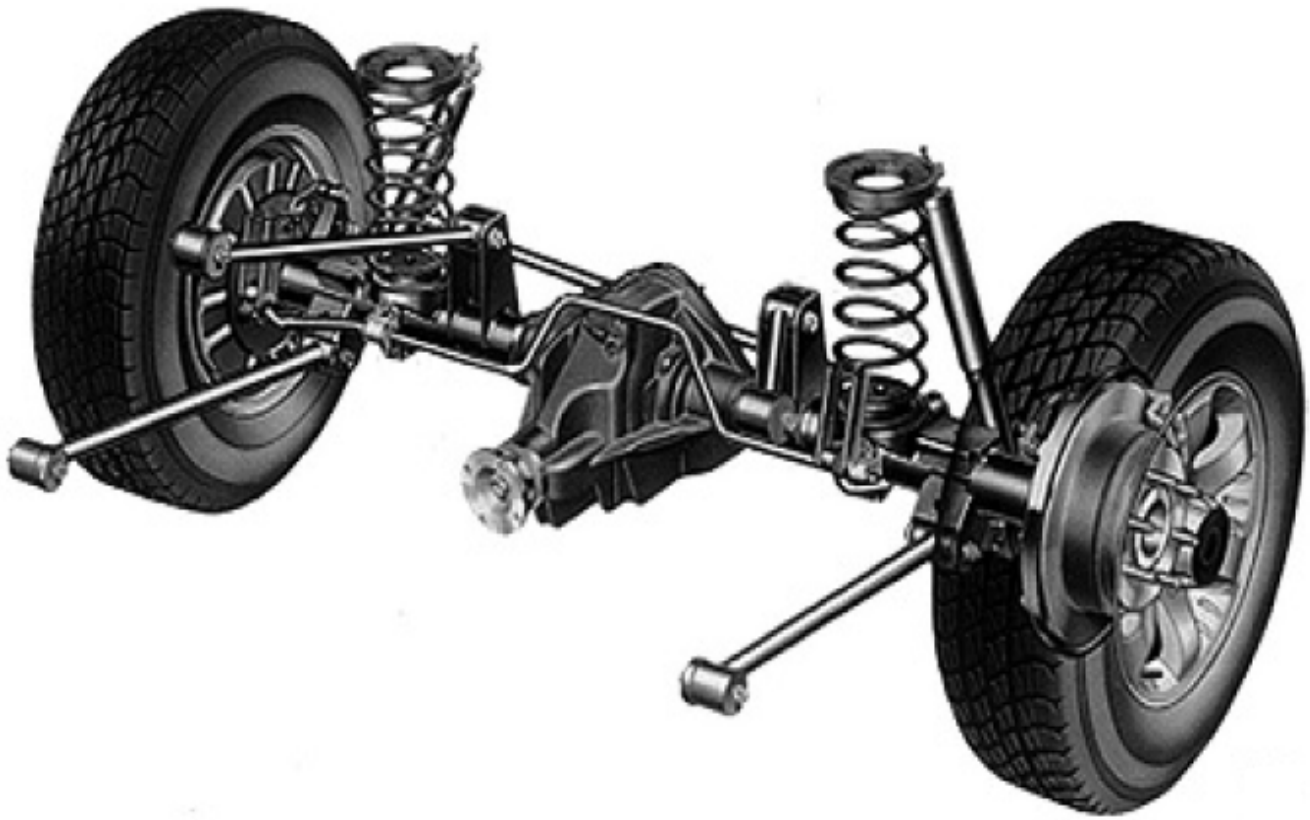

Figure 1-3. Rigid axle suspension system [5].

### 1.3 Suspension Geometry

This describes the kinematic relationships between the various suspension elements, the sprung, and unsprung masses. Some of the terminologies used to describe these relationships are described as follows:

**Bump:** The vertical displacement of the entire sprung mass.

**Body Roll:** The rotation of the sprung mass about the body longitudinal axis, arising from cornering activity and road roughness. The longitudinal axis is forward in both ISO and SAE systems. Thus, clockwise rotation as seen from the rear defines positive roll angle.

**Suspension Roll:** As formally defined by SAE, suspension roll is the rotation of the sprung mass about a fore-aft axis with respect to a transverse line joining a pair of

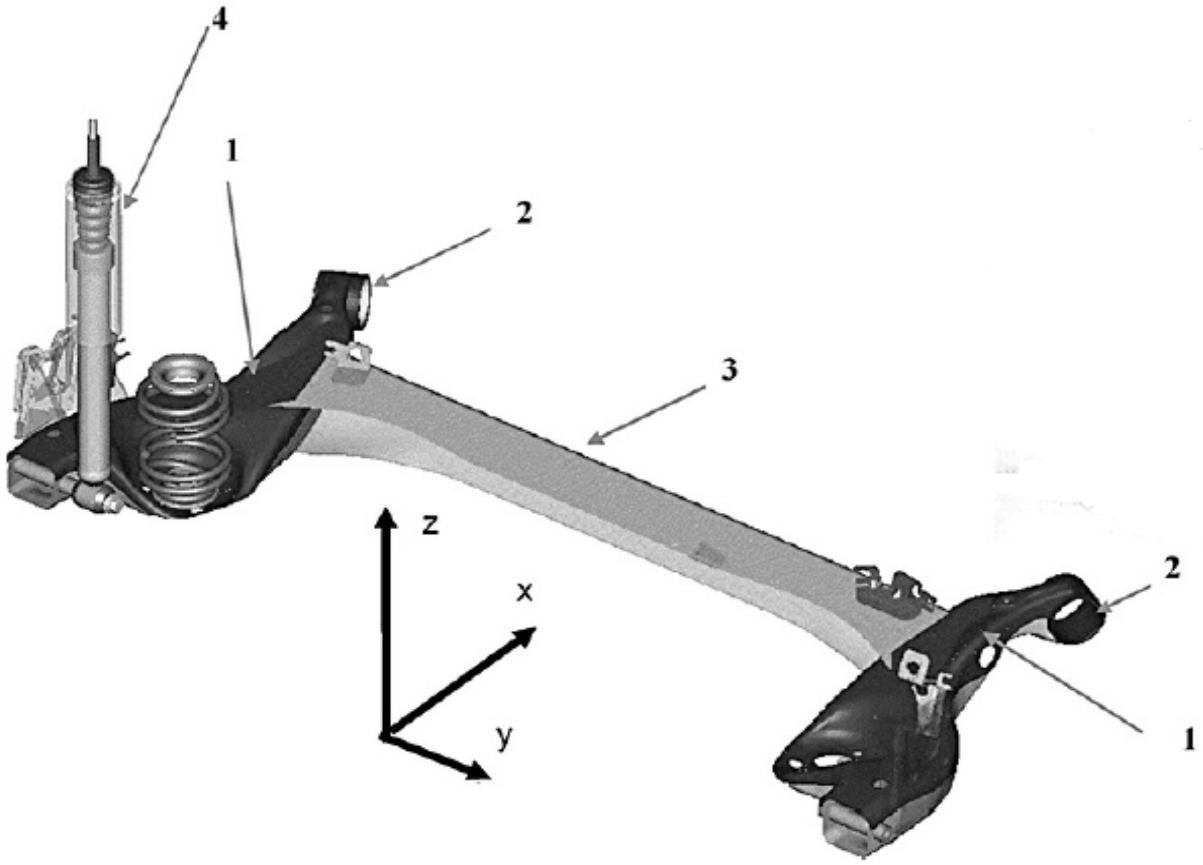


Figure 1-4. Twist beam suspension system [5].

wheel centers. If the ground is flat and front and rear wheels centers have parallel transverse lines, the definition is straight forward. Otherwise, some mean ground plane must be adopted.

**Pitch:** The rotation of the sprung mass about a transverse axis, resulting in either a ”nose-up” or a ”nose-down” configuration. This motion is usually associated with acceleration and braking. In the SAE axis system, the ”nose-up” configuration defines positive pitch while in the ISO axis system, the ”nose-down” configuration defines positive roll.

**Roll Center:** This is the point about which the sprung mass pivots during a roll situation. It is a dynamic point - it moves around throughout the suspension travel.

**Pitch Center:** This is the point about which the sprung mass pivots during a pitch situation. It is a dynamic point - it moves around throughout the suspension travel.

**Camber:** The tilting of the tire as seen from either the front or rear view. Leaning of the tire inboard towards the chassis defines a negative camber.

**Toe:** The tilting of the tire in a static situation as seen from either the top or bottom view. Turning in of the front of the tire is referred to as ”toe-in”.

**Steering Axis:** The axis about which the wheel/tire rotates during steering. It is also known as the ”King Pin Axis”.

**Caster:** The tilting of the steering axis as seen from side view. It creates camber change with steering input. It also creates a restoring torque (aligning moment) for centering the steering wheel.

**Caster Trail:** The distance between the center of the tire contact patch and the point of intersection of the steering axis and the ground plane as seen from the side view. This also generates self a aligning moment for the steering wheel.

**Scrub Radius:** The distance between the center of the tire contact patch and the point of intersection of the steering axis and the ground plane as seen from either the front view or rear view.

**Steering Arm:** The line between the steering axis and the steering linkage (tie rod).

**Bump Travel:** The maximum possible vertical upward displacement of the wheel from the equilibrium position relative to the sprung mass.

**Droop Travel:** The maximum possible vertical downward displacement of the wheel from the equilibrium position relative to the sprung mass.

## 1.4 Controlled Suspension

To improve on the performance of suspension system, researchers have attempted to systematically modulate the suspension force. Improvements over passive suspension designs is an active area of research [7–17]. Past approaches utilize one of three techniques [18], adaptive [19], semi-active [9, 20] or fully active suspension [19, 21].

### 1.4.1 Active Suspension Design

A fully active suspension replaces the damper with a force generator which could be hydraulic, electric, or pneumatic. This can achieve optimum vehicle control, but at the cost of design complexity, expensive actuators, etc. In the work of Fialho and Balas [19], a novel approach to the design of road adaptive active suspensions via a combination of linear parameter-varying control and nonlinear backstepping techniques was presented. Two levels of adaptation were considered: the lower level control design shapes the nonlinear characteristics of the vehicle suspension as a function of road conditions, while the higher level design involves adaptive switching between these different nonlinear characteristics, based on the road conditions. In [22], an active suspension control approach combining a filtered feedback control scheme and an ”input decoupling transformation” was used for a full-vehicle suspension system. Recently, Bose Corp. has developed an automobile active suspension system using an electromagnetic actuator [23]. The Bose system equips each wheel with a separate electromagnetic motor similar to those used in roller coasters. Rather than revolving, the electromagnetic motors telescope up or down to imitate the behavior of a typical shock absorber. This active system have been shown to have enormous improvement with regard to ride comfort and handling.

### 1.4.2 Adaptive Suspension Design

An adaptive suspension utilizes a passive spring and an adjustable damper with slow response to improve the control of ride comfort and road holding. In [24], the concept of adaptive suspension, in which the passive suspension parameters were controlled actively in response to various measured signals, was applied to road vehicles. In [25], a vehicle suspension system in which a computer controls damping and spring forces to optimize ride and handling characteristics under a wide range of driving conditions was presented.

### 1.4.3 Semi-Active Suspension Design

The original concept of semi-active suspension dates back to Karnopp [13–15], where it was introduced as an alternative to the costly, highly complicated, and power-demanding active systems. While fully active suspension systems are theoretically unrestricted energy wise, semi-active elements must be either dissipative or conservative in their energy demand. So far, semi-active designs fall into a general class of variable damper, variable lever arm, and variable stiffness [12].

Variable damper type semi-active devices are capable of varying the damping coefficients across their terminals. Initial practical implementations were achieved using a variable orifice viscous damper. By closing or opening the orifice, the damping characteristics change from soft to hard and vice versa. With time, the use of electro-rheological (ER) and magneto-rheological (MR) fluids replaced the use of variable orifices [18, 26, 27]. ER and MR fluids are composed of a suspension of polarized solid particles dispersed in a nonconducting liquid. When an electric ( or magnetic for MR) field is imposed, the particles become aligned along the direction of the imposed field. When this happens, the yield stress of the fluid changes, hence the damping effect. The controllable rheological properties make ER and MR fluids suitable for use as smart materials for active devices, transforming electrical energy to mechanical energy.

Variable lever arm type semi-active suspensions conserve energy between the suspension and spring storage. They are characterized by controlled force variation which consumes minimal power. The main idea behind their operation is the variation of the force transfer ratio which is achieved by moving the point of force application [16, 17, 28–30]. If this point moves orthogonally to the acting force, theoretically no mechanical work is involved in the control.

Variable stiffness semi-active suspensions exhibit a variable stiffness feature. This is achieved either by changing the free length of a spring or by a mechanism which changes its effective stiffness characteristics as a result of one or more moving parts. In

[12], an example of a hydro-pneumatic spring with a variable stiffness characteristic was given.

On the other hand, Semi-active suspension control methods are varied. Skyhook(SH) control is one of the first approaches to be applied in commercial vehicles [31], in which a fictitious damper (called skyhook damper) is placed between the sprung mass and the inertia frame, the suspension damping coefficient is then modulated to mimic the behavior of the skyhook damper. In this linear model- based control design, the damping coefficient is switched continuously between the minimum and maximum values. A similar concept called ground-hook has also been developed for road friendly suspensions [11]. This control concepts has also been applied to semi-active suspensions. Also, the Acceleration Driven Damping (ADD) technique was developed from an optimal control approach [32]. SH and ADD have complementary characteristics: SH provides large benefits around the rattle space frequency while the ADD provides large benefits around the tire hop frequency. They both perform similarly to the passive suspension otherwise. In their specific domains, SH and ADD provide quasi-optimal performances [33]. That is, it is impossible to achieve (with the same semi-active shock-absorber) better performances. The result provided a lower-bound to the filtering capabilities of a controllable semi-active suspension. In [33], a mixed SH and ADD (SH-ADD) control method was introduced. SH-ADD provides an optimal mix of SH and ADD techniques. The optimality analysis in [33] indicates that the SH-ADD is a close approximation to the best possible algorithm for semi-active suspensions for a given comfort-based objective function.

In both SH and ADD, and subsequently SH-ADD, the damper is modeled as a linear damper whose damping coefficient is adjusted using the corresponding algorithm. These approaches do not allow the use of more realistic MR-damper models. In [20], a quarter vehicle model equipped with a semi-active damper was reformulated in the Linear Parameter Varying (LPV) framework using a nonlinear static semi-active damper

model. The method incorporate the MR damper dissipativity constraint. However, the model of suspension used is an idealized linear model which undermines the kinematic details of the suspension mechanism as well as the rotational characteristics of the unsprung mass. A new model of the MacPherson suspension system was introduced in [34] and later used in [35]. The model incorporates the kinematic details of the suspension system as well as the rotational motion of the unsprung mass. The conventional idealized linear quarter car model was shown to be a special case of the MacPherson model since the transfer function of the linearized MacPherson model coincides with the conventional model if the lower support point of the damper is located at the mass center of the unsprung mass. The resonance frequencies of the MacPherson model were also shown to agree better with experimental results than the conventional linear model.

Anubi et. al [36, 37] considers the control design and analysis of a suspension system using the new nonlinear modeling of the MacPherson Suspension system equipped with an MR damper. The damper force was modeled using the nonlinear static semi-active damper model given in [38]. The controller was designed using an $\mathcal{L}_2$-gain analysis based on the concept of energy dissipation. The controller is effectively a smooth saturated PID which allows the dissipativity constraint of the MR damper to be satisfied. The performance of the closed-loop system is compared with a purely passive MacPherson suspension system and a semi-active damper, whose damping coefficient is tuned by the SH-ADD method. It was shown via simulation that the developed controller outperforms the passive case at both the rattle space and tire hop frequencies and the SH-ADD at tire hop frequency while showing close performance to the SH-ADD at the rattle space frequency. Time domain simulation results confirmed that the developed controller satisfies the dissipative constraint.

Other control concepts that have been applied to semi-active and active suspensions include; optimal control [9, 10, 39, 40], robust control [41], and robust optimal control [19, 20, 42],etc.

# CHAPTER 2
# VARIATION OF STIFFNESS IN SUSPENSION DESIGN

Variation of the damping coefficient has been the main focus of researches in semi-active suspension designs in the past. In this chapter, a combined variation of stiffness and damping coefficient is considered. First, two fundamental theorems in the optimal control of semi-active suspension are extended to cover stiffness variation as well. It was then shown that a better performance, in terms of ride comfort and handling, is achievable by varying the stiffness alongside the damping coefficient over varying either damping or stiffness alone. Two additional control laws are presented for varying the damping and stiffness of a semi-active suspension based on a quarter car model. The first varies the damping and stiffness sequentially while the second vary them simultaneously.

## 2.1 General Semi-Active Suspension

The term ”general semi-active” refers to any semi-active device which modulates either the damping coefficient or the stiffness of the suspension element. Figure 2-1 shows a quarter car model of a general semi-active suspension. It is a two degree of freedom model which captures the basic element of the vertical dynamics of the car. The sprung mass $m_s$ is the mass of the car body (chassis). The unsprung mass $m_u$ is the mass of the wheel assembly. $k_s$ and $b_s$ are the stiffness and the damping coefficient of the passive suspension element respectively. $z_r$ denotes the road disturbance and $v$ denotes the value of the modulated variable of the semi-active suspension. It is used here generically to represent either the stiffness or damping coefficient, depending on whether the semi-active device is a variable damper rate type or variable spring rate type.

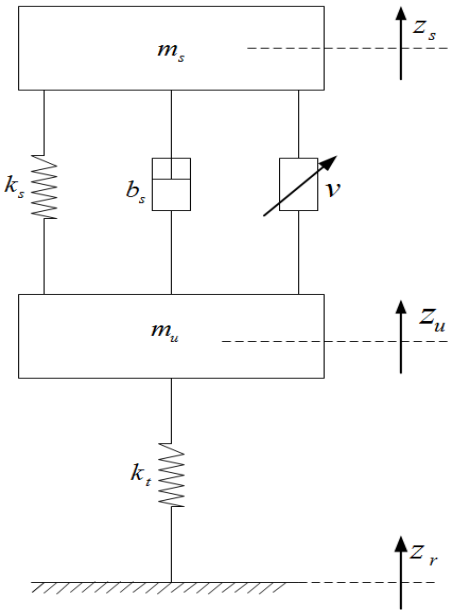


Figure 2-1. Quarter car - modulated spring/damper

Let

$$\mathbf{x} = \begin{bmatrix} x_1 \\ x_2 \\ x_3 \\ x_4 \end{bmatrix} = \begin{bmatrix} z_s - z_u \\ \dot{z}_s \\ z_u - z_r \\ \dot{z}_u \end{bmatrix} \tag{2–1}$$

be the state vector of the system, the vertical dynamics of the car is given by the following state equation

$$\begin{aligned} \dot{\mathbf{x}} &= A\mathbf{x} + \phi(\mathbf{x})v + \mathbf{L}\dot{z}_r \\ &= A\mathbf{x} - \mathbf{b}\left(\mathbf{T}^T\mathbf{x}\right)v + \mathbf{L}\dot{z}_r, \end{aligned} \tag{2–2}$$

where

$$A = \begin{bmatrix} 0 & 1 & 0 & -1 \\ -\frac{k_s}{m_s} & -\frac{b_s}{m_s} & 0 & \frac{b_s}{m_s} \\ 0 & 0 & 0 & 1 \\ \frac{k_s}{m_u} & \frac{b_s}{m_u} & -\frac{k_t}{m_u} & -\frac{b_s}{m_u} \end{bmatrix}$$

$$\mathbf{b} = \begin{bmatrix} 0 & \frac{1}{m_s} & 0 & -\frac{1}{m_u} \end{bmatrix}^T$$

$$\mathbf{L} = \begin{bmatrix} 0 & 0 & -1 & 0 \end{bmatrix}^T,$$

and $\mathbf{T} = \begin{bmatrix} 0 & 1 & 0 & -1 \end{bmatrix}^T$ if the modulated element is a damper, in which case the control variable $v$ is the variable damping coefficient of the shock absorber, or $\mathbf{T} = \begin{bmatrix} 1 & 0 & 0 & 0 \end{bmatrix}^T$ if the modulated element is a spring in which case $v$ becomes the variable stiffness of the spring.

The following assumptions are made:

1. The horizontal movement of the sprung mass, $m_s$, is neglected, i.e only the vertical displacement $z_s$ is considered.

2. The values of $z_s$ and $z_u$ are measured from their static equilibrium points. Hence, the effect of gravity is neglected in this model

3. The spring and damping forces are in the linear regions of their operating ranges.

It is also assumed that the road input $z_r$ is a stationary Wiener process and its derivative $\dot{z}_r$ is a white noise with intensity $\Xi$ . For the theoretical analysis part of this paper, it will assumed that $\dot{z}_r = 0$. In other words, the analysis is carries out for the deterministic case.

***Performance Characterization***: The performance of the suspension system is characterized by the ride comfort, suspension travel and road holding capability. These performance criteria are measured in terms of the chassis acceleration, $\ddot{z}_s$, suspension deflection $z_s - z_u$, and tire deflection $z_u - z_r$ respectively. Thus, the performance index

$J(\mathbf{x}, v)$, expressed as the weighted sum of the parameters above is defined as follows:

$$J(\mathbf{x}, v) = \int_{t_0}^{t_f} \left( \ddot{z}_s{}^2 + \rho_1^2 (z_s - z_u)^2 + \rho_2^2 (z_u - z_r)^2 \right) dt \tag{2–3}$$

$$= \int_{t_0}^{t_f} g(\mathbf{x}, v) dt. \tag{2–4}$$

$$= \int_{t_0}^{t_f} \left( \mathbf{x}^T Q \mathbf{x} - 2 \frac{w(\mathbf{x}) \mathbf{a}^T \mathbf{x} v}{m_s} + \frac{w(\mathbf{x})^2}{m_s^2} v^2 \right) dt \tag{2–5}$$

where

$$w(\mathbf{x}) = \mathbf{T}^T \mathbf{x} \tag{2–6}$$

$$\mathbf{a} = \begin{bmatrix} -\frac{k_s}{m_s} & -\frac{b_s}{m_s} & 0 & \frac{b_s}{m_s} \end{bmatrix}^T \tag{2–7}$$

$$Q = \begin{bmatrix} \rho_1^2 + \frac{k_s^2}{m_s^2} & \frac{k_s b_s}{m_s^2} & 0 & -\frac{k_s b_s}{m_s^2} \\ \frac{k_s b_s}{m_s^2} & \frac{b_s^2}{m_s^2} & 0 & -\frac{b_s^2}{m_s^2} \\ 0 & 0 & \rho_2^2 & 0 \\ -\frac{k_S b_s}{m_s^2} & -\frac{b_s^2}{m_s^2} & 0 & \frac{b_s^2}{m_s^2} \end{bmatrix}. \tag{2–8}$$

$\rho_1, \rho_2 \in \Re$ are the performance weights on the suspension deflection and road holding respectively. The units of $\rho_1$ and $\rho_2$ are time$^{-2}$.

### 2.2 Single Modulation Optimal Semi-Active Control Laws

This section presents the optimal modulation of the suspension element in the suspension system described above. The results in this section exist in literature (see [9, 10]). However, the focus restricts semi-active suspension systems to modulated dampers. This section extends the focus to include modulated springs, thus general in a sense. The design objective is to find the optimal control $v^*$ that minimizes $J(\mathbf{x}, v)$ subject to the dynamic constraint in (2–9), saturation constraint in (2–10), and the initial

condition in (2–11).

$$\dot{\mathbf{x}} = A\mathbf{x} + \phi(\mathbf{x})v \tag{2–9}$$

$$0 \leq v \leq \bar{v} \tag{2–10}$$

$$\mathbf{x}(0) = \mathbf{x}_0. \tag{2–11}$$

First, the saturation constraint (2–10) is ignored and it is shown that for the case where $v$ is allowed to vary boundlessly, the optimal control makes the semi-active suspension achieve the same performance as the optimal fully active suspension system. The following theorem expresses the fact that any semi-active device, if modulated boundlessly, can achieve the same performance as an optimal active one.

**Theorem 2.1.** *If the constraint* (2–10) *is ignored, the optimal control that minimizes the performance index* (2–3) *is*

$$v^* = \begin{cases} \frac{m_s}{2w(\boldsymbol{x})}\left(2\boldsymbol{a}^T + m_s\boldsymbol{b}^T P\right)\boldsymbol{x} & \text{if} \quad \boldsymbol{T}^T\boldsymbol{x} \neq 0 \\ 0 & \text{if} \quad \boldsymbol{T}^T\boldsymbol{x} = 0 \end{cases} \tag{2–12}$$

*where* $P \in \Re^{4\times 4}$ *is a positive definite solution to the ricatti equation*

$$\dot{P} + P\bar{A}^T + \bar{A}P - P\bar{B}P + \bar{Q} = 0 \tag{2–13}$$

*where*

$$\bar{A} = A^T - m_s\boldsymbol{a}\boldsymbol{b}^T$$

$$\bar{Q} = Q - \boldsymbol{a}\boldsymbol{a}^T$$

$$\bar{B} = \frac{1}{2}m_s^2\boldsymbol{b}\boldsymbol{b}^T.$$

*The value function* $J(\boldsymbol{x}^*, v^*)$ *is given by*

$$J(\boldsymbol{x}^*, v^*) = \frac{1}{2}\boldsymbol{x}^T(t_0)P(t_0)\boldsymbol{x}(t_0) \tag{2–14}$$

*which is the same for an optimal fully active suspension system [9]. Hence, the unconstrained optimal modulation of any single element semi-active suspension system is equivalent to the optimal active counterpart.*

The proof of this theorem is given in the Appendix A.1. The following theorem puts the saturation constraint into consideration.

**Theorem 2.2.** *The solution $v^*$ to the optimal control problem statement with constraint (2–10) is given by*

$$v^* = \begin{cases} 0 & \text{if } v' \leq 0 \\ \frac{m_s^2}{2w(\boldsymbol{x})^2} v' & \text{if } 0 < v' < \frac{2\bar{v}}{m_s^2} \boldsymbol{x}^T \boldsymbol{T}\boldsymbol{T}^T \boldsymbol{x} \\ \bar{v} & \text{if } v' \geq \frac{2\bar{v}}{m_s^2} \boldsymbol{x}^T \boldsymbol{T}\boldsymbol{T}^T \boldsymbol{x} \end{cases} \tag{2–15}$$

*where*

$$v' = \frac{w(\boldsymbol{x})}{m_s} \left(2\boldsymbol{a}^T + m_s \boldsymbol{b}^T P\right) \boldsymbol{x}. \tag{2–16}$$

*and $P \in \Re^{4\times 4}$ is the solution to the Riccati equation*

$$\dot{P} + PA_r(\boldsymbol{x}, P) + A_r^T(\boldsymbol{x}, P)P - PB_r(\boldsymbol{x}, P)P + Q_r(\boldsymbol{x}, P) = 0 \tag{2–17}$$

*where*

$$A_r(\boldsymbol{x}, P) = \begin{cases} A & \text{if } v' \leq 0 \\ \bar{A}^T & \text{if } 0 < v' < \frac{2\bar{v}}{m_s^2} \boldsymbol{x}^T \boldsymbol{T}\boldsymbol{T}^T \boldsymbol{x} \\ A - \bar{v}\boldsymbol{b}\boldsymbol{T}^T & \text{if } v' \geq \frac{2\bar{v}}{m_s^2} \boldsymbol{x}^T \boldsymbol{T}\boldsymbol{T}^T \boldsymbol{x} \end{cases}, \tag{2–18}$$

$$B_r(\boldsymbol{x}, P) = \begin{cases} 0 & \text{if } v' \leq 0 \\ \bar{B} & \text{if } 0 < v' < \frac{2\bar{v}}{m_s^2} \boldsymbol{x}^T \boldsymbol{T}\boldsymbol{T}^T \boldsymbol{x} \\ 0 & \text{if } v' \geq \frac{2\bar{v}}{m_s^2} \boldsymbol{x}^T \boldsymbol{T}\boldsymbol{T}^T \boldsymbol{x} \end{cases} \tag{2–19}$$

*and*

$$Q_r(\boldsymbol{x}, P) = \begin{cases} 2Q & \text{if } v' \leq 0 \\ \bar{Q}^T & \text{if } 0 < v' < \frac{2\bar{v}}{m_s^2}\boldsymbol{x}^T\boldsymbol{T}\boldsymbol{T}^T\boldsymbol{x} \\ Q^* & \text{if } v' \geq \frac{2\bar{v}}{m_s^2}\boldsymbol{x}^T\boldsymbol{T}\boldsymbol{T}^T\boldsymbol{x} \end{cases} \tag{2–20}$$

*with*

$$Q^* = \bar{Q} + \frac{2}{m_s^2}\left(\bar{v}\boldsymbol{T} - m_s\boldsymbol{a}\right)\left(\bar{v}\boldsymbol{T} - m_s\boldsymbol{a}\right)^T.$$

*The value function in this case is*

$$J(\boldsymbol{x}^*, v^*) = \boldsymbol{x}^T(t_0)P_a\boldsymbol{x}(t_0) + \int_{t_0}^{t_f}\left(\frac{w(\boldsymbol{x}^*)v^*}{m_s} - \left(m_s\boldsymbol{b}^T P_a + \boldsymbol{a}^T\right)\boldsymbol{x}^*\right)^2 dt \tag{2–21}$$

*where* $P_a = P_a^T > 0$ *is the solution to the algebraic riccati equation*

$$P_a\bar{A}^T + \bar{A}P_a - P_a\bar{B}P_a + \bar{Q} = 0 \tag{2–22}$$

*which corresponds to the unconstrained optimal active suspension control law[9].*

The proof of this theorem is given in Appendix A.2.

**Remark 2.1.** *It can be shown, by taking limits from left and right, that the control law* (2–15) *is continuous and that it's derivative*

$$\frac{\partial v^*}{\partial \boldsymbol{x}} = M_1(\boldsymbol{x})\boldsymbol{x} \tag{2–23}$$

*where*

$$M_1(\boldsymbol{x}) = \begin{cases} \frac{m_s}{2}\frac{(2\boldsymbol{a}+m_sP\boldsymbol{b})\boldsymbol{T}^T - \boldsymbol{T}\left(2\boldsymbol{a}^T+m_s\boldsymbol{b}^TP\right)}{\boldsymbol{x}^T\boldsymbol{T}\boldsymbol{T}^T\boldsymbol{x}} & \text{if } 0 < v' < \frac{2\bar{v}}{m_s^2}\boldsymbol{x}^T\boldsymbol{T}\boldsymbol{T}^T\boldsymbol{x} \\ 0 & \text{Otherwise} \end{cases} \tag{2–24}$$

*is not.*

**Remark 2.2.** *The optimal solution partitions the state space into three regions namely* $\mathcal{R}_1 = \{\boldsymbol{x} \mid v' \leq 0\}, \mathcal{R}_2 = \left\{\boldsymbol{x} \mid 0 < v' < \frac{2\bar{v}}{m_s^2}\boldsymbol{x}^T\boldsymbol{T}\boldsymbol{T}^T\boldsymbol{x}\right\}, \mathcal{R}_3 = \left\{\boldsymbol{x} \mid v' \geq \frac{2\bar{v}}{m_s^2}\boldsymbol{x}^T\boldsymbol{T}\boldsymbol{T}^T\boldsymbol{x}\right\} \subset \Re^4$.

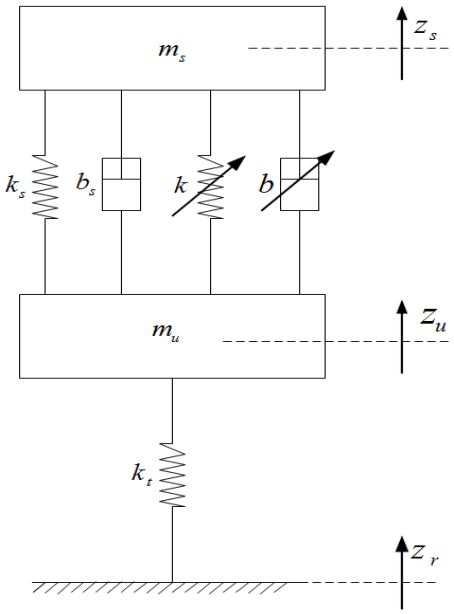


Figure 2-2. Quarter car - modulated spring and damper

*Different control actions are taken as the state trajectory changes from one region to the other. If* $\boldsymbol{x} \in \mathcal{R}_1$*, no control action is taken. This is because semi-active devices only dissipate energy and are not capable of supplying energy. This behavior is imposed on the model by the inequality constraint* $v \geq 0$ *and is ignored in Theorem 2.1. If* $\boldsymbol{x} \in \mathcal{R}_2$*, optimal energy dissipation is achieved because the physical limit of the device is not exceeded. Moreover, if the state trajectory is in region* $\mathcal{R}_3$*, the unconstrained optimal energy dissipation requirement exceeds the physical limit of the semi-active device, thus the control action is clipped as* $v = \bar{v}$*.*

The next section describes the variation of both stiffness and damping and possible improvements in overall energy dissipation.

## 2.3 Spring and Damper Modulation

Figure 2-2 shows the quarter car model of a semi-active suspension system with variable stiffness and damping suspension elements, shown in parallel with traditional

spring and damper elements. Since both the spring and damper can be modulated, let

$$\mathbf{v} = \begin{bmatrix} v_1 \\ v_2 \end{bmatrix} \tag{2–25}$$

and

$$\mathbf{T}_i = \begin{cases} \begin{bmatrix} 0 & 1 & 0 & -1 \end{bmatrix}^T & \text{if the } i\text{th element is a damper} \\ \\ \begin{bmatrix} 1 & 0 & 0 & 0 \end{bmatrix}^T & \text{if the } i\text{th element is a spring} \end{cases} \tag{2–26}$$

$$i = 1, 2.$$

Then, the equation of motion is expressed as the state equation

$$\dot{\mathbf{x}} = A\mathbf{x} + \phi(\mathbf{x})\mathbf{v} + \mathbf{L}\dot{z}_r \tag{2–27}$$

where $\phi : \Re^4 \mapsto \Re^{2\times 1}$ is given by

$$\begin{aligned} \phi(\mathbf{x}) &= -\mathbf{b}\mathbf{x}^T T \\ &= -\mathbf{b}\mathbf{w}^T(\mathbf{x}) \end{aligned} \tag{2–28}$$

with $T = \begin{bmatrix} \mathbf{T}_1 & \mathbf{T}_2 \end{bmatrix}$, and the saturation constraint is given by

$$\mathbf{0} \leq \mathbf{v} \leq \bar{\mathbf{v}}. \tag{2–29}$$

Following Remark 2.2, the question arises, of how to improve the energy dissipation in the region $\mathcal{R}_3$ without necessarily changing the limit of the semi-active device. Theorem 2.3, which is one of the main results of this chapter, shows that by modulating

a second suspension element[1] , it is possible to improve performance if saturation occurs in the first.

**Theorem 2.3.** *Suppose that the stiffness and damping coefficient of a semi-active suspension are bounded in accordance to the inequality* (2–29)*. The performance, defined in terms of the performance index* (2–3)*, achieved by optimally varying both the stiffness and damping is better (lower performance index) than that achieved by varying either the stiffness or damping alone.*

*Proof.* It is sufficient to show that the value function associated with the optimal modulation of stiffness and damping is less than that associated with the optimal modulation of either stiffness or damping alone. Let

$$v_2 = \alpha v_1. \tag{2–30}$$

Then, the performance index (2–4) is written as

$$J(\mathbf{x}, \mathbf{v}) = J(\mathbf{x}, v_1, \alpha) = \int_{t_0}^{t_f} g(\mathbf{x}, v_1, \alpha) dt. \tag{2–31}$$

Claim: Suppose $v_1^* = v^*$ is given by Theorem 2.2. There exists $\alpha^*$ satisfying

$$0 \leq \alpha^* v_1^* \leq \bar{v}_2 \tag{2–32}$$

and $\mathbf{x}^* : \Re \mapsto \Re^4$ such that given

$$J(\mathbf{x}^*, v_1^*, \alpha) \triangleq \min_{0 \leq v_1 \leq \bar{v}_1} J(\mathbf{x}, v_1, \alpha) \tag{2–33}$$

then

$$J(\mathbf{x}^*, v_1^*, \alpha^*) \leq J(\mathbf{x}^*, v_1^*, \alpha) \quad \forall \alpha \text{ such that } 0 \leq \alpha v_1^* \leq \bar{v}_2. \tag{2–34}$$

[1] This is either a damper or a spring depending on whether the original is a spring or a damper respectively

Proof of Claim: The dynamics (2–27) is expanded as

$$\begin{aligned}\dot{\mathbf{x}} &= A\mathbf{x} - \mathbf{b}\mathbf{x}^T T\mathbf{v} + \mathbf{L}\dot{z}_r \\ &= A\mathbf{x} - \mathbf{b}\mathbf{x}^T \left(\mathbf{T}_1 + \alpha\mathbf{T}_2\right) v_1 + \mathbf{L}\dot{z}_r \\ &= A\mathbf{x} - \mathbf{b}w(\mathbf{x},\alpha)v_1 + \mathbf{L}\dot{z}_r \end{aligned} \tag{2–35}$$

where

$$w(\mathbf{x},\alpha) = \left(\mathbf{T}_1 + \alpha\mathbf{T}_2\right)^T \mathbf{x}. \tag{2–36}$$

Let $J_a \triangleq \mathbf{x}^T(t_0)P_a\mathbf{x}(t_0)$ be the value function for the active suspension, then (2–21) becomes

$$\begin{aligned} J(\mathbf{x}^*, v_1^*, \alpha) &= J_a + \int_{t_0}^{t_f} \left( \frac{w(\mathbf{x}^*,\alpha)v_1^*}{m_s} - \left(m_s\mathbf{b}^T P_a + \mathbf{a}^T\right)\mathbf{x}^* \right)^2 dt. \\ &= J_a + \frac{1}{m_s^2}\int_{t_0}^{t_f} \left(v_1^*\mathbf{T}_2^T\mathbf{x}^*\left(\alpha - \alpha_s\right)\right)^2 dt \end{aligned} \tag{2–37}$$

where

$$\alpha_s = \frac{m_s\left(m_s\mathbf{b}^T P_a + \mathbf{a}^T\right)\mathbf{x}^*}{v_1^*\mathbf{T}_2^T\mathbf{x}^*} - \frac{\mathbf{T}_1^T\mathbf{x}^*}{\mathbf{T}_2^T\mathbf{x}^*}. \tag{2–38}$$

Thus $J(\mathbf{x}^*, v_1^*, \alpha)$ is convex in $\alpha$, and the minimizer

$$\alpha^* = arg \min_{0\le\alpha v_1^*\le\bar{v}_2} \int_{t_0}^{t_f} \left( \frac{w(\mathbf{x}^*,\alpha)v_1^*}{m_s} - \left(m_s\mathbf{b}^T P_a + \mathbf{a}^T\right)\mathbf{x}^* \right)^2 dt \tag{2–39}$$

exists for all $t_0, t_f \in \Re^+, t_f > t_0$. Following an engineering approach, the integrand is minimized at every instant of time and $\alpha^*$ is given by

$$\alpha^* = \begin{cases} 0 & \text{if } \alpha_s \le 0 \\ \alpha_s & \text{if } 0 \le \alpha_s \le \frac{\bar{v}_2}{v_1^*} \\ \frac{\bar{v}_2}{v_1^*} & \text{if } \alpha_s \ge \frac{\bar{v}_2}{v_1^*} \end{cases}. \tag{2–40}$$

Thus

$$
\begin{aligned}
&J(\mathbf{x}^*, k^*, \alpha) - J(\mathbf{x}^*, k^*, \alpha^*) \\
&= \begin{cases}
\frac{1}{m_s^2} \int_{t_0}^{t_f} \left(v_1^* \mathbf{T}_2^T \mathbf{x}^*\right)^2 \alpha(\alpha - 2\alpha_s) dt & \text{if } \alpha_s \leq 0 \\
\frac{1}{m_s^2} \int_{t_0}^{t_f} \left(v_1^* \mathbf{T}_2^T \mathbf{x}^*\right)^2 (\alpha - \alpha_s)^2 dt & \text{if } 0 \leq \alpha_s, \leq \frac{\bar{v}_2}{v_1^*} \\
\frac{1}{m_s^2} \int_{t_0}^{t_f} \left(v_1^* \mathbf{T}_2^T \mathbf{x}^*\right)^2 \left(\alpha - \frac{\bar{v}_2}{v_1^*}\right) \left(\alpha + \frac{\bar{v}_2}{v_1^*} - 2\alpha_s\right) dt & \text{if } \alpha_s \geq \frac{\bar{v}_2}{v_1^*}
\end{cases}
\end{aligned}
$$

$\Longrightarrow$

$$
J(\mathbf{x}^*, v_1^*, \alpha) - J(\mathbf{x}^*, v_1^*, \alpha^*) \geq 0 \quad \forall \alpha \text{ such that } 0 \leq \alpha v_1^* \leq \bar{v}_2.
$$

□

### 2.4 Double Modulation Optimal Semi-Active Control Laws

While the engineering approach is sufficient to show the result in the above theorem, the resulting steepest gradient control is not truly optimal unless no saturation occurs along the whole trajectory [10]. As a result, two additional control laws are presented. The first minimizes the residual performance index subject to the resulting closed loop dynamics from the optimal modulation of the first suspension element while the second simultaneously modulates the two suspension elements to minimize the overall performance index subject to the combined dynamics.

#### 2.4.1 Sequential Modulation

The main idea here is to optimally modulate the first suspension element, keeping the second constant, and then optimally modulate the second element with respect to the residual performance index of the first subject to the resulting closed loop dynamics from the first modulation. The deterministic open loop dynamics is given by

$$
\dot{\mathbf{x}} = A\mathbf{x} - v_1 w_1(\mathbf{x})\mathbf{b} - v_2 w_2(\mathbf{x})\mathbf{b} \tag{2–41}
$$

(2–42)

where

$$w_i(\mathbf{x}) = \mathbf{T}_i^T \mathbf{x}, \quad i = 1, 2. \tag{2–43}$$

Let $v_1$ be given by Theorem 2.2, i.e

$$v_1 = v_1^* = \begin{cases} 0 & \text{if } v_1' \leq 0 \\ \frac{m_s^2}{2w_1(\mathbf{x})^2} v_1' & \text{if } 0 < v_1' < \frac{2\bar{v}_1}{m_s^2} \mathbf{x}^T \mathbf{T}_1 \mathbf{T}_1^T \mathbf{x} \\ \bar{v}_1 & \text{if } v_1' \geq \frac{2\bar{v}_1}{m_s^2} \mathbf{x}^T \mathbf{T}_1 \mathbf{T}_1^T \mathbf{x} \end{cases} \tag{2–44}$$

where

$$v_1' = \frac{w_1(\mathbf{x})}{m_s} \left(2\mathbf{a}^T + m_s \mathbf{b}^T P_1\right) \mathbf{x} \tag{2–45}$$

and $P_1 \in \Re^{4\times 4}$ is the solution to the riccati equation (2–17). Then, the resulting closed loop dynamics is given by

$$\begin{aligned} \dot{\mathbf{x}} &= \left(A - v_1^* \mathbf{b} \mathbf{T}_1^T\right) \mathbf{x} - v_2 w_2(\mathbf{x}) \mathbf{b} \\ &= A_1(\mathbf{x}, P_1) \mathbf{x} - v_2 w_2(\mathbf{x}) \mathbf{b}, \end{aligned} \tag{2–46}$$

where

$$A_1(\mathbf{x}, P_1) = A - v_1^* \mathbf{b} \mathbf{T}_1^T. \tag{2–47}$$

The residual value function is

$$J(\mathbf{x}, v_1^*, v_2) = \int_{t_0}^{t_f} g_2(\mathbf{x}, v_1^*, v_2)\, dt \tag{2–48}$$

where

$$g_2\left(\mathbf{x}, v_1^*, v_2\right) = \mathbf{x}^T \mathbf{a}_1 \mathbf{a}_1^T \mathbf{x} + \mathbf{x}^T \begin{bmatrix} \rho_1^2 & 0 & 0 & 0 \\ 0 & 0 & 0 & 0 \\ 0 & 0 & \rho_2^2 & 0 \\ 0 & 0 & 0 & 0 \end{bmatrix} \mathbf{x}, \tag{2–49}$$

$$\mathbf{a}_1\left(\mathbf{x}, P_1\right) = \mathbf{a} - \frac{1}{m_s} v_1^* \mathbf{T}_1. \tag{2–50}$$

The new objective is now to minimize the performance index (2–48) subject to the dynamic constraint (2–46) and the inequality constraint (2–51).

$$0 \leq v_2 \leq \bar{v}_2, \tag{2–51}$$

The resulting control law is given by Theorem 2.4.

**Theorem 2.4.** *Given the dynamic constraint* (2–46) *and the inequality constraint* (2–51)*, the optimal value of* $v_2$ *that minimizes the performance index* (2–48) *is given by*

$$v_2^* = \begin{cases} 0 & \text{if } v_2' \leq 0 \\ \frac{m_s^2}{2w_2(\boldsymbol{x})^2} v_2' & \text{if } 0 < v_2' < \frac{2\bar{v}_2}{m_s^2} \boldsymbol{x}^T \boldsymbol{T}_2 \boldsymbol{T}_2^T \boldsymbol{x}, \\ \bar{v}_2 & \text{if } v_2' \geq \frac{2\bar{v}_2}{m_s^2} \boldsymbol{x}^T \boldsymbol{T}_2 \boldsymbol{T}_2^T \boldsymbol{x}, \end{cases} \tag{2–52}$$

*where*

$$v_2' = \frac{w_2(\boldsymbol{x})}{m_s} \left(2\boldsymbol{a}_1 + m_s \boldsymbol{b}^T P_2\right)^T \boldsymbol{x}, \tag{2–53}$$

*and* $P_2$ *is the solution to the riccati equation*

$$\begin{aligned} &\dot{P}_2 + P_2 \bar{A}_1\left(\boldsymbol{x}, P_1, P_2\right) + \bar{A}_1^T\left(\boldsymbol{x}, P_1, P_2\right) P_2 \\ &\quad - w_1\left(\boldsymbol{x}\right) \boldsymbol{b}\boldsymbol{x}^T M_1^T\left(\boldsymbol{x}, P_1\right) P_2 + 2\bar{Q}_1\left(\boldsymbol{x}, P_1\right) = 0, \quad P_2(t_f) = 0, \end{aligned} \tag{2–54}$$

*where*

$$\bar{A}_1(\boldsymbol{x}, P_1, P2) = A - \boldsymbol{b}\left(v_1^* \boldsymbol{T}_1^T + v_2^* \boldsymbol{T}_2^T\right) \tag{2–55}$$

$$\bar{Q}_1(\boldsymbol{x}, P_1) = \left(\boldsymbol{a}_1 - \frac{1}{m_s} M_1(\boldsymbol{x}, P_1)\, \boldsymbol{x}\boldsymbol{x}^T \boldsymbol{T}_1\right) \boldsymbol{a}_1^T + \begin{bmatrix} \rho_1^2 & 0 & 0 & 0 \\ 0 & 0 & 0 & 0 \\ 0 & 0 & \rho_2^2 & 0 \\ 0 & 0 & 0 & 0 \end{bmatrix},$$

*$P_1$ is the solution to the riccati equation (2–17) and $M_1(\boldsymbol{x}, P_1)$ is given by (2–24) .*

*Proof.* Using the calculus of variation, the Hamiltonian

$$H = g_2(\mathbf{x}, v_1^*, v_2) + \mathbf{p}_2^T \left(A_1(\mathbf{x}, P_1)\mathbf{x} - v_2 w_2(\mathbf{x})\mathbf{b}\right) - \lambda_1 v_2 + \lambda_2 (v_2 - \bar{v}_2) \tag{2–56}$$

is defined, where $\lambda_1, \lambda_2$ are the Lagrange multipliers for the inequality constraint (2–51) and $\mathbf{p}_2$ is the Lagrange multiplier for the residual closed loop dynamic constraint (2–46), and the necessary optimality conditions are given by

$$\begin{aligned} -\dot{\mathbf{p}}_2 &= \frac{\partial g_2(\mathbf{x}, v_1^*, v_2)}{\partial \mathbf{x}} + \frac{\partial}{\partial \mathbf{x}} \mathbf{p}_2^T \left(A_1(\mathbf{x}, P_1)\mathbf{x} - v_2 w_2(\mathbf{x})\mathbf{b}\right) \\ &= 2\bar{Q}_1(\mathbf{x}, P_1)\mathbf{x} + \left(A^T - (v_1^* \mathbf{T}_1 + v_2 \mathbf{T}_2)\mathbf{b}^T - \bar{M}_1 \mathbf{x}\mathbf{x}^T \mathbf{T}_1 \mathbf{b}^T\right)\mathbf{p}_2 \qquad (2–57) \\ 0 &= \frac{\partial g_2(\mathbf{x}, v_1^*, v_2)}{\partial v_2} - \mathbf{p}_2^T \mathbf{b} \mathbf{T}_2^T \mathbf{x} - (\lambda_1 - \lambda_2) \\ &= -\frac{2}{m_s} w_2(\mathbf{x})\, \mathbf{a}_1^T \mathbf{x} + \frac{2}{m_s^2} w_2(\mathbf{x})^2 v_2 - w_2(\mathbf{x})\, \mathbf{b}^T \mathbf{p}_2 - (\lambda_1 - \lambda_2) \qquad (2–58) \end{aligned}$$

If $w_2(\mathbf{x}) \neq 0$, $v_2$ is obtained from (2–58) as

$$v_2 = \frac{m_s^2}{2w_2(\mathbf{x})^2} (v_2' + \lambda_1 - \lambda_2). \tag{2–59}$$

Now, $\frac{\partial H}{\partial \lambda_1} = \frac{\partial H}{\partial \lambda_2} = 0$, together with the three cases; $(\lambda_1 > 0, \lambda_2 = 0), (\lambda_1 = \lambda_2 = 0)$ and $(\lambda_1 = 0, \lambda_2 > 0)$, yields

$$v_2^* = \begin{cases} 0 & \text{if } v_2' \leq 0 \\ \frac{m_s^2}{2w_2(\mathbf{x})^2} v_2' & \text{if } 0 < v_2' < \frac{2\bar{v}_2}{m_s^2} w_2(\mathbf{x})^2 \\ \bar{v}_2 & \text{if } v_2' \geq \frac{2\bar{v}_2}{m_s^2} w_2(\mathbf{x})^2 \end{cases}. \tag{2–60}$$

Let $\mathbf{p}_2 = P_2\mathbf{x}$, where $P_2 = P_2^T > 0$, $P_2 \in \Re^{4\times 4}$, then (2–57) becomes

$$\begin{aligned} \dot{\mathbf{p}}_2 &= \dot{P}_2\mathbf{x} + P_2\dot{\mathbf{x}} \\ &= -2\bar{Q}_1(\mathbf{x}, P_1)\mathbf{x} - \left(\bar{A}_1^T(\mathbf{x}, P_1, P_2) - w_1(\mathbf{x})\mathbf{b}\mathbf{x}^T M_1^T(\mathbf{x}, P_1)\right) P_2\mathbf{x} \end{aligned} \tag{2–61}$$

or

$$\left(\dot{P}_2 + P_2\bar{A}_1(\mathbf{x}, P_1, P_2) + \bar{A}_1^T(\mathbf{x}, P_1, P_2) P_2 - w_1(\mathbf{x})\mathbf{b}\mathbf{x}^T M_1^T(\mathbf{x}, P_1) P_2 + 2\bar{Q}_1(\mathbf{x}, P_1)\right)\mathbf{x} = 0,$$

which, provided that $\mathbf{x} \neq 0$ and $P_2(t_f) = 0$, yields the riccati equation (2–54). □

### 2.4.2 Simultaneous Modulation

Here, the overall performance index is minimized subject to the overall dynamics. First, the car body acceleration is given by

$$\ddot{z}_s = \mathbf{a}^T\mathbf{x} - \frac{1}{m_s}\mathbf{x}^T T\mathbf{v}. \tag{2–62}$$

Then the objective function (2–4) is expanded as follows

$$\begin{aligned} g(\mathbf{x}, \mathbf{v}) &= \ddot{z}_s{}^2 + \rho_1^2(z_s - z_u)^2 + \rho_2^2(z_u - z_r)^2 \\ &= \mathbf{x}^T Q\mathbf{x} - \frac{2}{m_s}\mathbf{a}^T\mathbf{x}\mathbf{x}^T T\mathbf{v} + \frac{1}{m_s^2}\mathbf{v}^T T^T\mathbf{x}\mathbf{x}^T T\mathbf{v} \end{aligned} \tag{2–63}$$

$$\begin{aligned} &= \mathbf{x}^T Q\mathbf{x} + \frac{v_1^2 w_1(\mathbf{x})^2}{m_s^2} + \frac{v_2^2 w_2(\mathbf{x})^2}{m_s^2} - 2\frac{v_1 w_1(\mathbf{x})\mathbf{a}^T\mathbf{x}}{m_s} \\ &\quad -2\frac{v_2 w_2(\mathbf{x})\mathbf{a}^T\mathbf{x}}{m_s} - 2\frac{v_1 v_2 w_1(\mathbf{x}) w_2(\mathbf{x})}{m_s^2}. \end{aligned} \tag{2–64}$$

However,

$$-2\frac{v_1 v_2 w_1(\mathbf{x})\, w_2(\mathbf{x})}{m_s^2} \leq \frac{v_1^2 w_1(\mathbf{x})^2}{m_s^2} + \frac{v_2^2 w_2(\mathbf{x})^2}{m_s^2}. \tag{2–65}$$

Therefore, $g(\mathbf{x}, \mathbf{v})$ is upper bounded as

$$g(\mathbf{x}, \mathbf{v}) \leq \bar{g}(\mathbf{x}, \mathbf{v}) \tag{2–66}$$

where

$$\begin{aligned}\bar{g}(\mathbf{x}, \mathbf{v}) = \mathbf{x}^T Q \mathbf{x} + 2\frac{v_1^2 w_1(\mathbf{x})^2}{m_s^2} + 2\frac{v_2^2 w_2(\mathbf{x})^2}{m_s^2} \\ -2\frac{v_1 w_1(\mathbf{x})\, \mathbf{a}^T \mathbf{x}}{m_s} - 2\frac{v_2 w_2(\mathbf{x})\, \mathbf{a}^T \mathbf{x}}{m_s}.\end{aligned} \tag{2–67}$$

In order to avoid the singularity associated with the rank 1 matrix $T^T \mathbf{x}\, \mathbf{x}^T T$, the performance index $J(\mathbf{x}, \mathbf{v})$ is redefined as

$$J(\mathbf{x}, \mathbf{v}) = \int_{t_0}^{t_f} \bar{g}(\mathbf{x}, \mathbf{v}) dt \tag{2–68}$$

and the simultaneous double modulation optimal control law is given in Theorem 2.5.

**Theorem 2.5.** *The optimal control law* $\boldsymbol{v}^* = \begin{bmatrix} v_1^* & v_2^* \end{bmatrix}^T$ *that minimizes the performance index* (2–68) *subject to the deterministic dynamic constraint* (2–41) *and the saturation constraint* (2–29) *is given by*

$$v_i^* = \begin{cases} 0 & \text{if } v_i' \leq 0 \\ \frac{m_s^2}{4 w_i(\boldsymbol{x})^2} v_i' & \text{if } 0 < v_i' < \frac{4\bar{v}_i}{m_s^2} \boldsymbol{x}^T \boldsymbol{T}_i \boldsymbol{T}_i^T \boldsymbol{x}, \quad i = 1, 2. \\ \bar{v}_i & \text{if } v_i' \geq \frac{4\bar{v}_i}{m_s^2} \boldsymbol{x}^T \boldsymbol{T}_i \boldsymbol{T}_i^T \boldsymbol{x}, \end{cases} \tag{2–69}$$

*where*

$$v_i' = \frac{w_i(\boldsymbol{x})}{m_s} \left(2\boldsymbol{a} + m_s \boldsymbol{b}^T P\right)^T \boldsymbol{x}, \tag{2–70}$$

*and* $P > 0$ *is the solution to the riccati equation*

$$\dot{P} + P\bar{A}_1(\boldsymbol{x}, P) + \bar{A}_1^T(\boldsymbol{x}, P)P + \bar{Q}_2(\boldsymbol{x}, P) - \frac{4}{m_s}\left(\boldsymbol{a}\boldsymbol{v}^{*T}T^T + T\boldsymbol{v}^*\boldsymbol{a}^T\right) = 0$$
$$P(t_f) = 0 \tag{2–71}$$

*where*

$$\bar{Q}_2(\boldsymbol{x}, P) = 2Q + \frac{4}{m_s^2}\left(v_1^*\boldsymbol{T}\boldsymbol{T}_1^T + v_2^*\boldsymbol{T}\boldsymbol{T}_2^T\right). \tag{2–72}$$

*Furthermore, the value function is given by*

$$J(\boldsymbol{x}^*, \boldsymbol{v}^*) = \frac{1}{2}\boldsymbol{x}(t_0)^T P(t_0)\boldsymbol{x}(t_0). \tag{2–73}$$

*Proof.* The proof of this theorem follows by defining the Hamiltonian

$$H = \bar{g}(\mathbf{x}, \mathbf{v}) + \mathbf{p}^T\left(A\mathbf{x} - \mathbf{b}\mathbf{x}^T T\mathbf{v}\right) - \boldsymbol{\lambda}_1^T\mathbf{v} + \boldsymbol{\lambda}_2^T(\mathbf{v} - \bar{\mathbf{v}}), \tag{2–74}$$

where **p** is the Lagrange multiplier for the dynamic constraint (2–41) and $\boldsymbol{\lambda}_1$,$\boldsymbol{\lambda}_2$ are the Lagrange multiplier vectors for the saturation constraint (2–29) and following similar procedure used in Appendix A.2. □

**Remark 2.3.** *The sequential modulation law is the true optimal. This assertion follows from the following fact*

$$\min_{\boldsymbol{0}\le\boldsymbol{v}\le\bar{\boldsymbol{v}}} J(\boldsymbol{x}, \boldsymbol{v}) = \min_{0\le v_1\le\bar{v}_1}\min_{0\le v_2\le\bar{v}_2} J(\boldsymbol{x}, \boldsymbol{v}) = \min_{0\le v_2\le\bar{v}_2}\min_{0\le v_1\le\bar{v}_1} J(\boldsymbol{x}, \boldsymbol{v}). \tag{2–75}$$

*However, while the simultaneous modulation is not the true optimal, it is optimal in the sense of minimizing the more conservative performance index* (2–68)*. The conservation is introduced in* (2–65) *and it is shown later, using simulation results, that the performance degradation resulting from this conservatism is negligible.*

## 2.5 Simulation

The performances of the controllers developed in this paper are evaluated via simulation. The simulation parameter values are given in table 2-1. The mass, stiffness

Table 2-1. Dynamic parameter values

| Parameter | Value |
|---|---|
| $m_s$ | 315 $kg$ |
| $m_u$ | 37.5 $kg$ |
| $b_s$ | 1500 $N/m/s$ |
| $k_s$ | 29500$N/m$ |
| $k_t$ | 210000 $N/m$ |

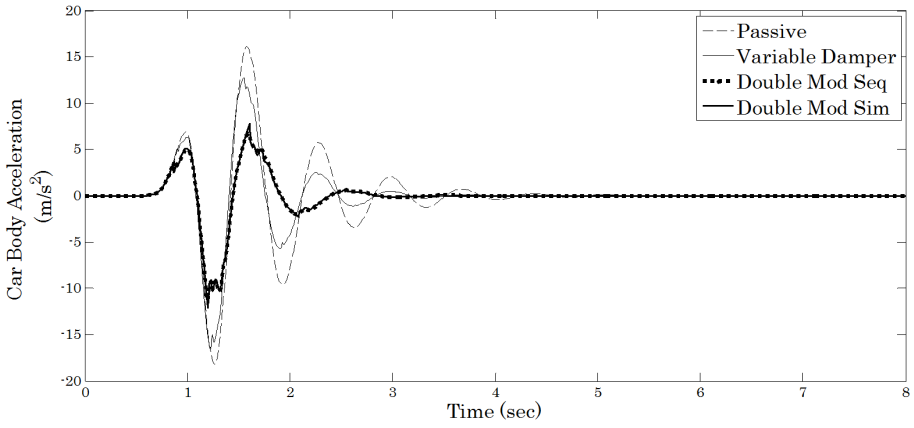


Figure 2-3. Time response - car body acceleration

and damping values are the ones given in the “Renault Mégane Coupé” model [43]. For the modulated elements, the damping coefficient and the spring constant are allowed to vary in the interval $[900 \quad 1670]N/m/s$ and $[17000 \quad 30600]N/m$ respectively. The values of $\rho_1$ and $\rho_2$ are both taken to be $1s^{-2}$ for this simulation.

### 2.5.1 Time Domain Simulation

For the time domain simulation, the vehicle traveling at a steady horizontal speed of 40$mph$ is subjected to a speed hump of height 25$cm$ and length of about $4m$. The road profile is generated using a gaussian function of height 25$cm$ and spread 3.5$m$. The responses [2] are compared for the passive suspension, single modulation damper, double modulation suspension controlled by the sequential law, and double modulation

[2] This includes the car body acceleration, suspension deflection, and tire deflection.

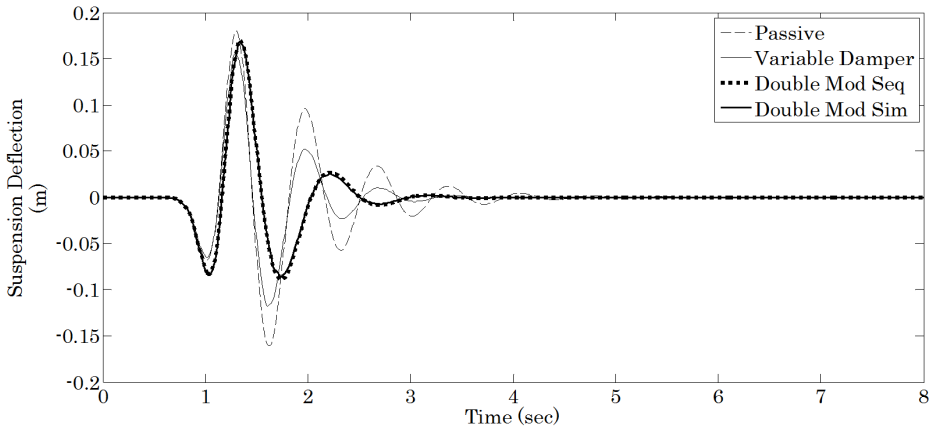


Figure 2-4. Time response - suspension deflection

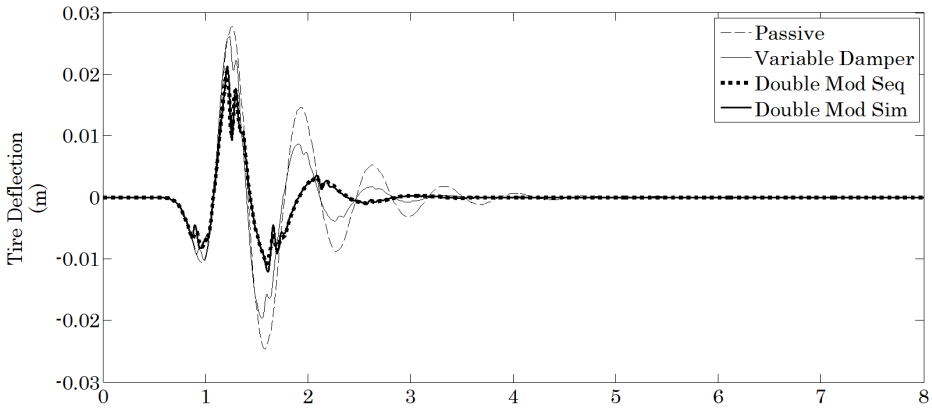


Figure 2-5. Time response - tire deflection

suspension controlled by the simultaneous law. Figures 2-3, 2-4 and 2-5 show the car body acceleration, suspension deflection, and tire deflection respectively, from which it seen that a combined modulation of damper and spring allows getting globally much better performance than a single modulation of either the damper or spring alone. It is also seen that the performances of the proposed double modulation laws are very close. Figure 2-6 shows the performance index plots, from which it is also seen that the performance degradation resulting from the conservatism in the simultaneous law is negligible.

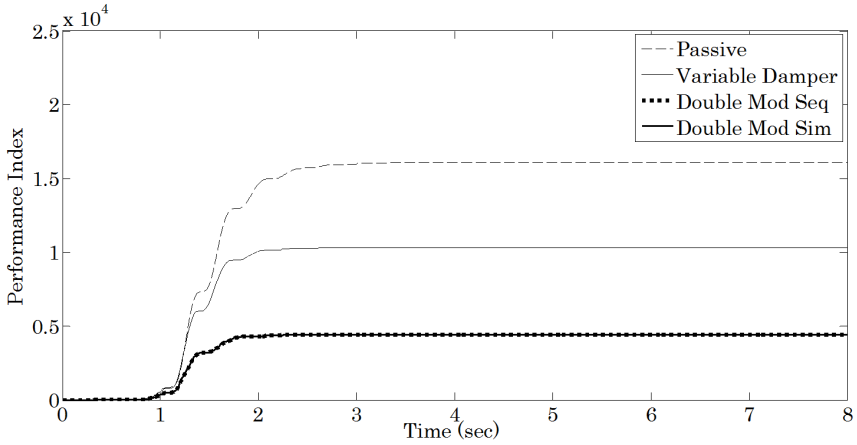


Figure 2-6. Time response - performance index

### 2.5.2 Frequency Response

An approximate frequency response is obtained using the concept of a sinusoidal input describing function[44]. The closed loop system is given by

$$\dot{\mathbf{x}} = A\mathbf{x} - f(\mathbf{x})\mathbf{b} + \mathbf{L}\dot{z}_r \tag{2–76}$$

where

$$f(\mathbf{x}) = v_1^* w_1(\mathbf{x}) + v_2^* w_2(\mathbf{x}). \tag{2–77}$$

Let

$$\mathbf{x}(j\omega) \approx \mathbf{a}_x \cos(\omega t) + \mathbf{b}_x \sin(\omega t) \tag{2–78}$$

be the nearly sinusoidal response of (2–76) to the input signal

$$\dot{z}_r = a_r \cos(\omega t), \quad a_r \in \Re^+. \tag{2–79}$$

Then, the nonlinear function $f(\mathbf{x})$ is then approximated as

$$f(\mathbf{x}) \approx a_0(\mathbf{a}_x, \mathbf{b}_x) + a_1(\mathbf{a}_x, \mathbf{b}_x)\cos(\omega t) + b_1(\mathbf{a}_x, \mathbf{b}_x)\sin(\omega t) \tag{2–80}$$

$$= a_0 + \mathbf{M}^T(\mathbf{a}_x, \mathbf{b}_x)\mathbf{x} + N(\mathbf{a}_x, \mathbf{b}_x)\dot{z}_r \tag{2–81}$$

where

$$\mathbf{M}(\mathbf{a}_x, \mathbf{b}_x) = \frac{b_1(\mathbf{a}_x, \mathbf{b}_x)\mathbf{b}_x}{\mathbf{b}_x^T\mathbf{b}_x} \tag{2–82}$$

$$N(\mathbf{a}_x, \mathbf{b}_x) = \frac{a_1(\mathbf{a}_x, \mathbf{b}_x)\mathbf{b}_x^T\mathbf{b}_x - b_1(\mathbf{a}_x, \mathbf{b}_x)\mathbf{b}_x^T\mathbf{a}_x}{a_r\mathbf{b}_x^T\mathbf{b}_x}. \tag{2–83}$$

The basis for this approximation is that the unique equilibrium point, $\mathbf{x} = \mathbf{0}$, is asymptotically stable which implies that the first harmonic of the response is dominant over higher harmonics. As a result, the the nonlinear function is approximated by it's sinusoidal input describing function. Substituting (2–78),(2–79), and (2–80) into (2–76) and doing harmonic balancing[44] yields

$$\begin{aligned} \mathbf{b}a_0(\mathbf{a}_x, \mathbf{b}_x) &= \mathbf{0} \\ A\mathbf{b}_x - \omega\mathbf{a}_x - \mathbf{b}b_1(\mathbf{a}_x, \mathbf{b}_x) &= \mathbf{0} \\ A\mathbf{a}_x - \omega\mathbf{b}_x - \mathbf{b}a_1(\mathbf{a}_x, \mathbf{b}_x) + \mathbf{L}a_r &= \mathbf{0} \end{aligned} \tag{2–84}$$

Now, evaluating the Fourier coefficients $a_0$, $a_1$ and $b_1$ for the function (6–117) is difficult, or at least tedious. Since the Fourier coefficients minimizes the mean squared approximation error, numeric estimates at each frequency are obtained by numerically minimizing the objective function

$$J(\mathbf{x}) = \frac{1}{2}\sum_{k=1}^{n}\left(f(\mathbf{a}_x\cos(\omega t_k) + \mathbf{b}_x\sin(\omega t_k)) - a_0 - a_1\cos(\omega t_k) - b_1\sin(\omega t_k)\right)^2 \tag{2–85}$$

subject to the constraints (2–84). The gain of the frequency response is then given by

$$G(\omega, a_r) = \left|\hat{C}\left(j\omega\mathbf{I} - \hat{A}\right)^{-1}\hat{L} - \hat{D}\right| \tag{2–86}$$

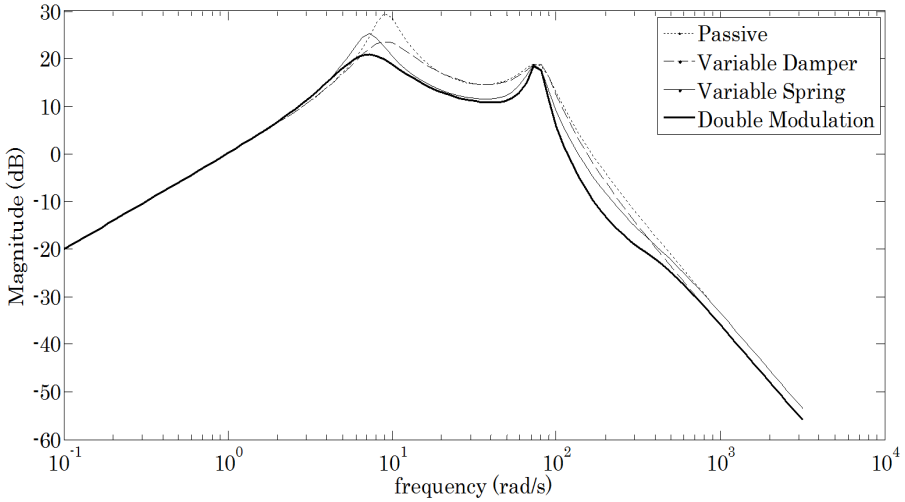


Figure 2-7. Frequency response - car body acceleration

where

$$\hat{A} = A - \mathbf{b}\mathbf{M}^T(\mathbf{a}_x, \mathbf{b}_x)$$

$$\hat{B} = \mathbf{L} - \mathbf{b}N(\mathbf{a}_x, \mathbf{b}_x)$$

$$\hat{C} = \begin{bmatrix} \mathbf{a}^T - \frac{1}{m_s}\mathbf{M}^T(\mathbf{a}_x, \mathbf{b}_x) \\ \rho_1 \quad 0 \quad 0 \quad 0 \\ 0 \quad 0 \quad \rho_2 \quad 0 \end{bmatrix}$$

$$\hat{D} = \frac{1}{m_s}\begin{bmatrix} N(\mathbf{a}_x, \mathbf{b}_x) \\ 0 \\ 0 \end{bmatrix}.$$

Figures 2-7, 2-8, and 2-9 show the frequency responses for the car body acceleration, suspension deflection, and tire deflection respectively. The frequency response is obtained for the passive, single modulation damper, single modulation spring, and double modulation controlled by the simultaneous law. Around the rattle space frequency, the variable damper performs better than the variable spring. This performance relation is reversed around the tire hop frequency. The reason for this is because of the difference in stiffness/damping requirements at both frequencies. It is seen also that

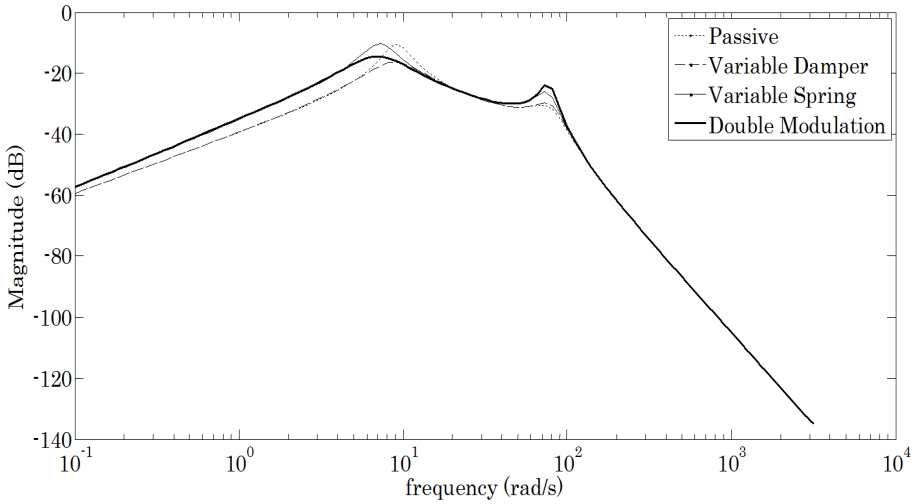


Figure 2-8. Frequency response - suspension deflection

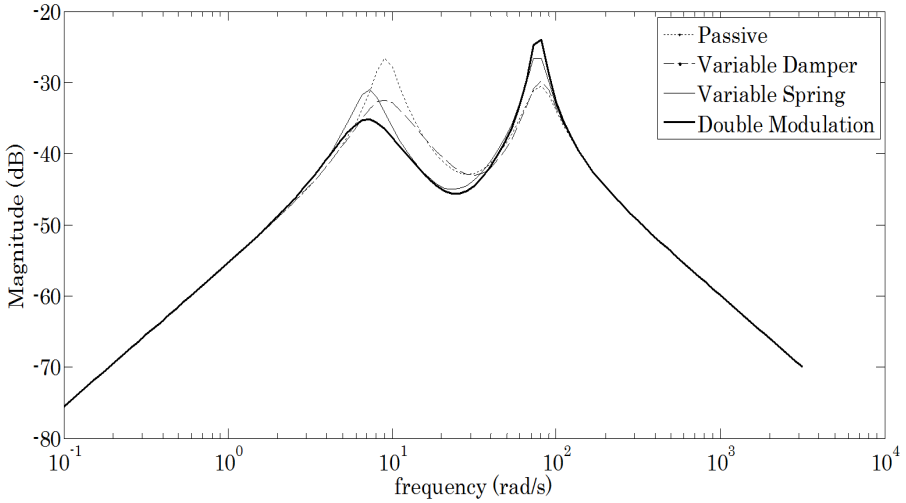


Figure 2-9. Frequency response - tire deflection

the double modulation responses track the single modulation damper responses at low frequencies and track the single modulation spring responses at high frequencies.

# CHAPTER 3
# VARIABLE STIFFNESS MECHANISM

The design and analysis of a mechanism with variable stiffness is examined. The mechanism, which is a simple arrangement of two springs, a lever arm and a pivot bar, has an effective stiffness that is a rational function of the horizontal position $d$ of the pivot. The external pure force acting on the system is constrained to always remain vertical. The effective stiffness is varied by changing $d$ while keeping the point of application of the external load constant. The expression for the effective stiffness is derived. A reverse analysis is also carried out on the mechanism. Special design cases are considered. The dynamic equation of the system is derived and used to deduce the natural frequency of the mechanism from which some insights were gained on the dynamic behavior of the mechanism.

The schematics for the system is shown in Figure 3-1. The force $F$ is constrained to move vertically and the pivot bar is constrained to move horizontally. The left and right springs, of spring constants $k_1$ and $k_2$ respectively, can only be deflected vertically (there is a sliding motion allowed between the spring and the pivot bar). $l_{0_1}$ and $l_{0_2}$ are the free lengths of the left and right springs respectively. The effective stiffness is varied by changing $d$, the horizontal position of the lever pivot point, while keeping the point of application of external load constant.

## 3.1 Forward Analysis

Given all the system parameters , $k_1, k_2, L_1, L_2, l_{0_1}, l_{0_2}$ , the external force $F$, and the horizontal distance $d$ of the pivot bar from the point of application of $F$, it is required to find the expression for the effective stiffness $K$ and the effective free length $l_0$ of the mechanism. Let $F_1$ and $F_2$ be the spring forces acting on the lever at points A and B with heights $x_1$ and $x_2$ from the ground respectively (Figure 3-2). Let the functions $\Delta(x, l_b, l_c)$

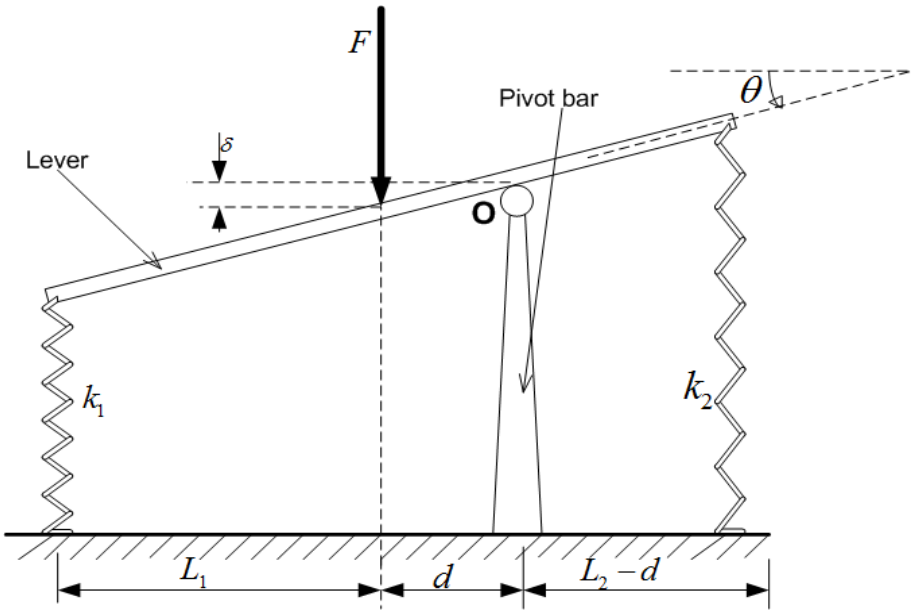


Figure 3-1. Schematics

and $\bar{\Delta}(x, l_b, l_c)$ be defined as

$$\bar{\Delta}(x, l_b, l_c) = \begin{cases} 1, & x \in \begin{pmatrix} l_b & l_c \end{pmatrix} \\ 0, & x \notin \begin{pmatrix} l_b & l_c \end{pmatrix} \end{cases} \tag{3–1}$$

and

$$\Delta(x, l_b, l_c) = \begin{cases} 0, & x \in \begin{pmatrix} l_b & l_c \end{pmatrix} \\ 1, & x \notin \begin{pmatrix} l_b & l_c \end{pmatrix} \end{cases} . \tag{3–2}$$

Thus, $F_1$ and $F_2$ can be written as

$$F_1 = \bar{\Delta}(x_1, l_{b_1}, l_{c_1})(x_1 - l_{0_1})k_1 + \Delta(x_1, l_{b_1}, l_{c_1})P_1 \tag{3–3}$$

$$F_2 = \bar{\Delta}(x_2, l_{b_2}, l_{c_2})(x_2 - l_{0_2})k_2 + \Delta(x_2, l_{b_2}, l_{c_2})P_2 \tag{3–4}$$

where

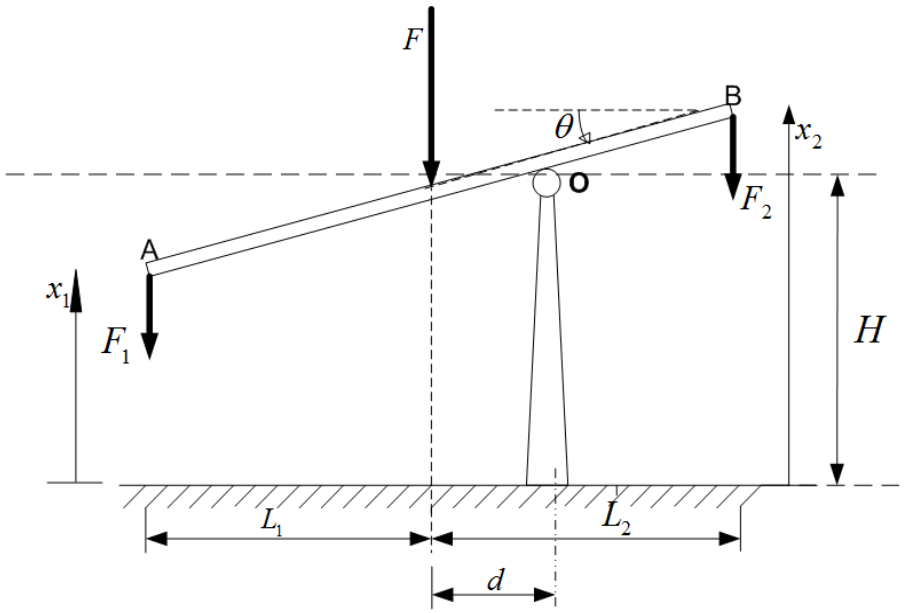


Figure 3-2. Free body diagram

$l_{b_1}$ and $l_{b_2}$ are the block lengths[1] of the left and right springs respectively

$l_{c_1}$ and $l_{c_2}$ are the open lengths[2] of the left and right springs respectively

$P_1$ and $P_2$ are the pure reaction forces of the blocked springs.

Equations (3–3) and (3–4) capture the cases when the springs behave as rigid bars (blocked or open) or as compliant members ($x_1 \in (l_{b_1} \; l_{c_1}), x_2 \in (l_{b_2} \; l_{c_2})$ ). Taking moments about point **O** and dividing by $d$ gives

$$F = -F_1 \frac{L_1 + d}{d} + F_2 \frac{L_2 - d}{d} \tag{3–5}$$

[1] the block length of a compression spring is defined as the maximal length of the spring after total blocking i.e when it is fully compressed

[2] the open length of a tension spring is defined as the length of the spring when it is fully stretched

with

$$x_1 = H - \frac{L_1 + d}{d}\delta$$
$$x_2 = H + \frac{L_2 - d}{d}\delta \tag{3–6}$$

Substituting (3–3),(3–4) and (3–6) in (3–5) yields

$$F = K\delta - C \tag{3–7}$$

where

$$K = k_1\bar{\Delta}_1\frac{(L_1 + d)^2}{d^2} + k_2\bar{\Delta}_2\frac{(L_2 - d)^2}{d^2} \tag{3–8}$$

$$C = k_1\bar{\Delta}_1\frac{(H - l_{0_1})(L_1 + d)}{d} + k_2\bar{\Delta}_2\frac{(H - l_{0_2})(L_2 - d)}{d} + \Delta_1 P_1\frac{L_1 + d}{d} + \Delta_2 P_2\frac{L_2 - d}{d} \tag{3–9}$$

where

$$\bar{\Delta}_1 = \bar{\Delta}(x_1, l_{b_1}, l_{c_1})$$
$$\bar{\Delta}_2 = \bar{\Delta}(x_2, l_{b_2}, l_{c_2})$$
$$\Delta_1 = \Delta(x_1, l_{b_1}, l_{c_1})$$
$$\Delta_2 = \Delta(x_2, l_{b_2}, l_{c_2})$$

Consider when the left spring is blocked i.e $x_1 = l_{b_1}$, $\bar{\Delta}_1 = 0 \;\; \Rightarrow \Delta_1 = 1$ , the system of Figure 3-2 becomes statically indeterminate and rigid provided that $x_2 \leq l_{c_2}$. However, any decrease in $F$ will cause the system to revert to the state where both springs are neither blocked nor open. A similar argument exists for the case where the left spring is open instead, and also for when the right spring is open or blocked. Thus (3–8)

becomes

$$K = \begin{cases} k_1 \frac{(L_1+d)^2}{d^2} + k_2 \frac{(L_2-d)^2}{d^2} & x_1 \in (l_{b_1} \;\; l_{c_1}), x_2 \in (l_{b_2} \;\; l_{c_2}) \\ \\ \infty & \textit{Otherwise} \end{cases} \tag{3–10}$$

Equation (3–10) is the expression for the overall stiffness of the system from which it is easily seen that the system is rigid when either or both the left and right springs become blocked or open or $d = 0$. It is, however, possible in design to restrict $x_1$ and $x_2$ in the range where $K$ never goes unbounded except in the neighborhood of $d = 0$. This is possible by using springs of zero free length and also satisfying the condition

$$H\left(1 + \frac{L_2}{L_1}\right) \leq l_{c_2} \tag{3–11}$$

The ratio $\frac{L_2}{L_1}$ is termed ***the aspect ratio*** and the space $\{(l_{b_1} \;\; l_{c_1}) \times (l_{b_1} \;\; l_{c_1})\} \setminus \{d = 0\}$***the useful space*** of the mechanism.

Now, consider the mechanism of Figure 3-1 restricted to the useful space and whose aspect ratio is such that the condition in (3–11) is satisfied. The plot of the effective stiffness $K$ is shown in Figures 3-3 and 3-4 from which it is easily seen that the minimum stiffness occurs at the boundary of the parameter $d$ and are given by:

$$K_{min} = \begin{cases} k_2(r+1)^2, & r < 1 \\ \\ 4min(k_1, k_2), & r = 1 \\ \\ k_1\left(\frac{1}{r}+1\right)^2, & r > 1 \end{cases} \tag{3–12}$$

where $r = \frac{L_2}{L_1}$ is the aspect ratio of the mechanism. Figure 3-4 shows the variation of $K$ with respect to $\frac{1}{d}$ which is a good way to visualize the behavior of the system as $d \to \infty$. Let $l_0$ be the overall free length of the system, then

$$l_0 = H - \delta_0 \tag{3–13}$$

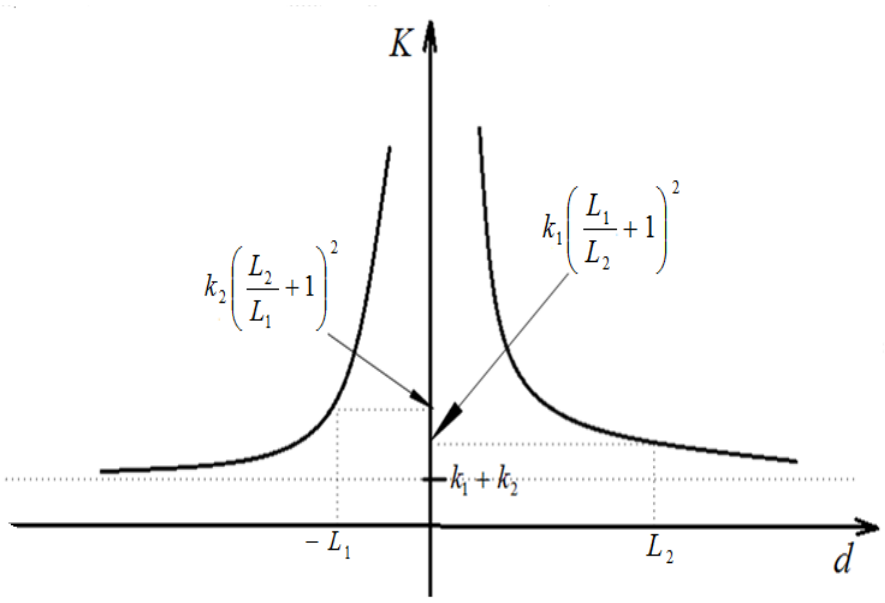


Figure 3-3. Effective stiffness against $d$

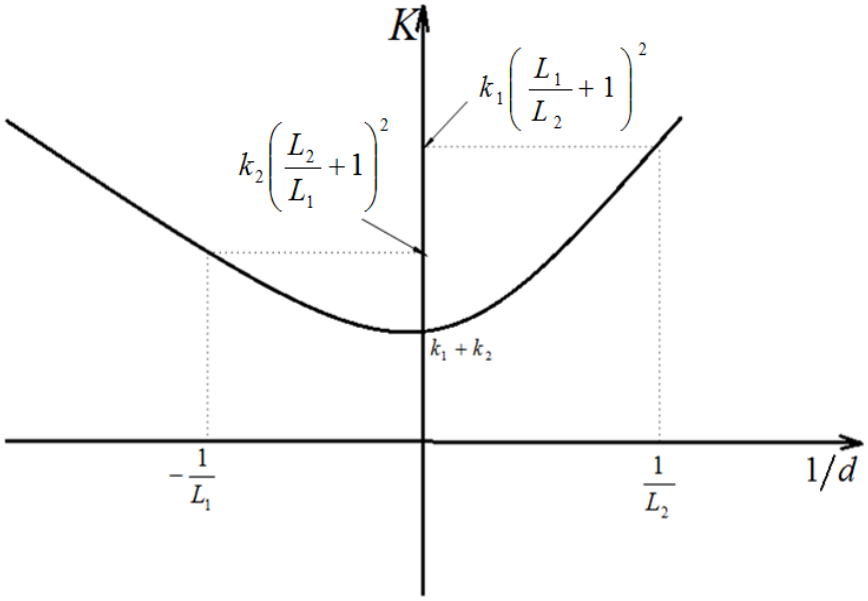


Figure 3-4. Effective stiffness against $\frac{1}{d}$

where $\delta_0$ is the deflection when $F = 0$ which is given by

$$\delta_0 = \frac{C}{K}$$

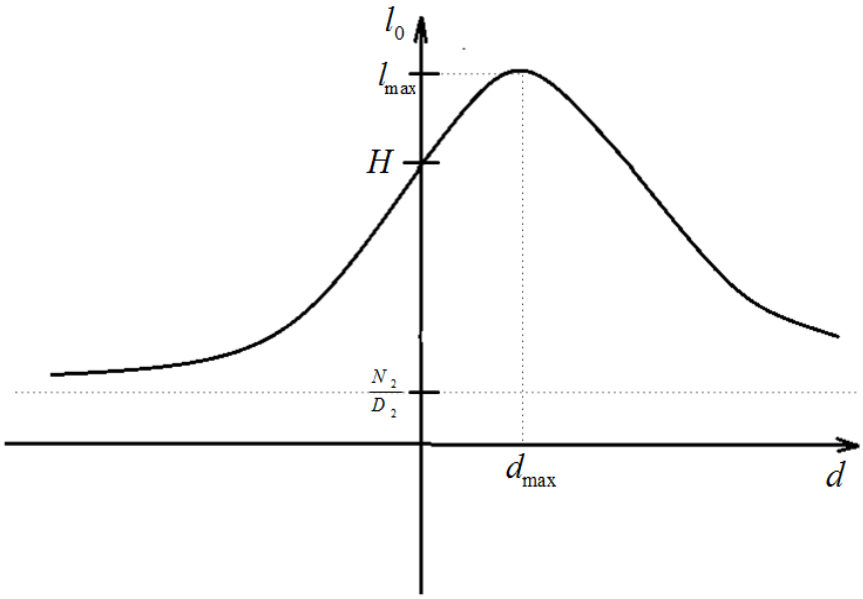


Figure 3-5. Overall free length against $d$

Thus the overall free length becomes

$$l_0 = H - \frac{C}{K} \tag{3–14}$$

$$= \frac{N_2 d^2 + N_1 d + N_0}{D_2 d^2 + D_1 d + D_0} \tag{3–15}$$

where

$$N_0 = H(k_1 L_1^2 + k_2 L_2^2)$$

$$N_1 = k_1 L_1 (H + l_{0_1}) - k_2 L_2 (H + l_{0_2})$$

$$N_2 = k_1 l_{0_1} + k_2 l_{0_2}$$

$$D_0 = k_1 L_1^2 + k_2 L_2^2$$

$$D_1 = 2(k_1 L_1 - k_2 L_2)$$

$$D_2 = k_1 + k_2$$

Figure 3-5 shows the variation of the overall free length with respect to $d$. The

maximum free length occurs when $d = d_{max}$, where $d_{max}$ is the solution to

$$\begin{vmatrix} D_1 & D_2 \\ N_1 & N_2 \end{vmatrix} d_{max}^2 + \begin{vmatrix} D_0 & D_2 \\ N_0 & N_2 \end{vmatrix} d_{max} + \begin{vmatrix} D_0 & D_1 \\ N_0 & N_1 \end{vmatrix} = 0. \tag{3–16}$$

However, from a practical point of view, it might be desired to keep the mechanism overall free length constant for all values of $d$. In that case, an additional constraint on (3–14) can be written as

$$N_2 d^2 + N_1 d + N_0 = \lambda \left( D_2 d^2 + D_1 d + D_0 \right), \quad \lambda \in \Re$$

or

$$(N_2 - \lambda D_2) d^2 + (N_1 - \lambda D_1) d + (N_0 - \lambda D_0) = 0$$

which implies that

$$\begin{bmatrix} k_1 + k_2 \\ 2(k_1 L_1 - k_2 L_2) \\ K_1 L_1^2 + k_2 L_2^2 \end{bmatrix} = \lambda \begin{bmatrix} k_1 l_{0_1} + k_2 l_{0_2} \\ k_1 L_1 (H + l_{0_1}) - k_2 L_2 (H + l_{0_2}) \\ H(k_1 L_1^2 + k_2 L_2^2) \end{bmatrix} \tag{3–17}$$

Any combination of the system parameters $k_1$,$k_2$,$l_{0_1}$,$l_{0_2}$,$L_1$,$L_2$,$H$ that satisfies (3–17) would result in a constant overall free length for all values of $d$. One example of such a case is given as

$$l_{0_1} = l_{0_2} = H \;\Rightarrow\; l_0 = H \quad \forall d.$$

### 3.1.1 Effect of $r$ on $K$ and $l_0$

In order to study the effect of the aspect ratio, $r$, on the effective stiffness and overall free length, a numerical example is given. The values of the system parameters were

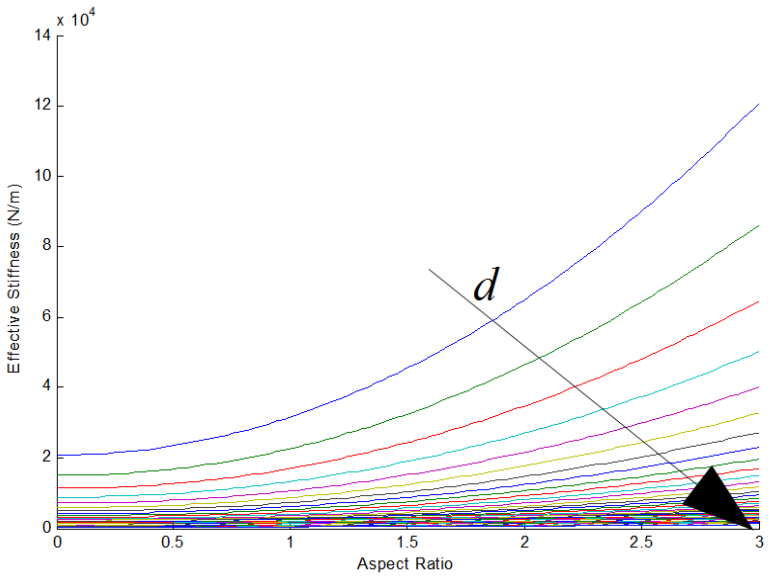


Figure 3-6. Effective stiffness against $r$ over $d$

set as follows:

$$k_1 = 3N/cm$$

$$k_2 = 4.5N/cm$$

$$l_{0_1} = 0.2cm$$

$$l_{0_2} = 0.5cm$$

$$H = 0.35cm$$

$r$ and $d$ were varied uniformly in the intervals $[0\ \ 3]$ and $[0.1\ \ 1]$ respectively. For each value of $d$, the effective stiffness and overall free length were plotted against $r$. Figure 3-6 shows a parabolic relationship between the overall stiffness and the aspect ratio. It also shows that this variation vanishes as $d \to \infty$ as $K$ becomes fairly constant with respect to $r$.This observation agrees with (3–12) and Figure 3-3 from which it is also easily seen that

$$\lim_{d\to\infty} K = k_1 + k_2.$$

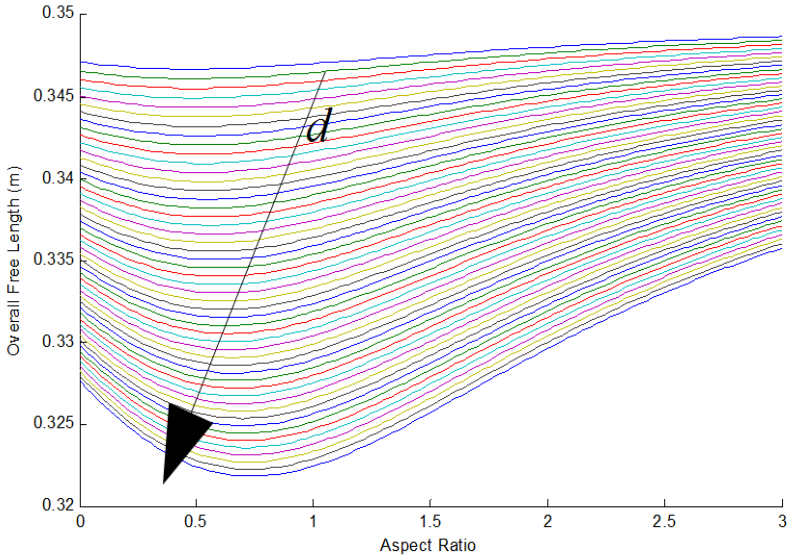


Figure 3-7. Variation of overall free length against $r$ over $d$

Figure 3-7 shows the variation of the overall free length with respect to the aspect ratio $r$ over the offset distance $d$. Figure 3-8 shows that the aspect ratio controls the curvature

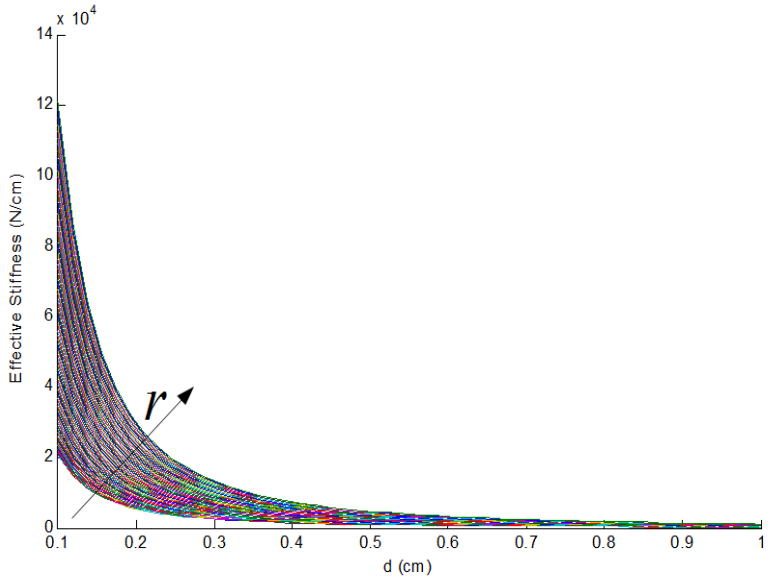


Figure 3-8. Effective stiffness against $d$ over $r$

of $K$. This is very useful in design because it helps to shape the sensitivity of $K$ to the $d$ value over a given interval. In the same vein, Figure 3-9 shows the variation of the

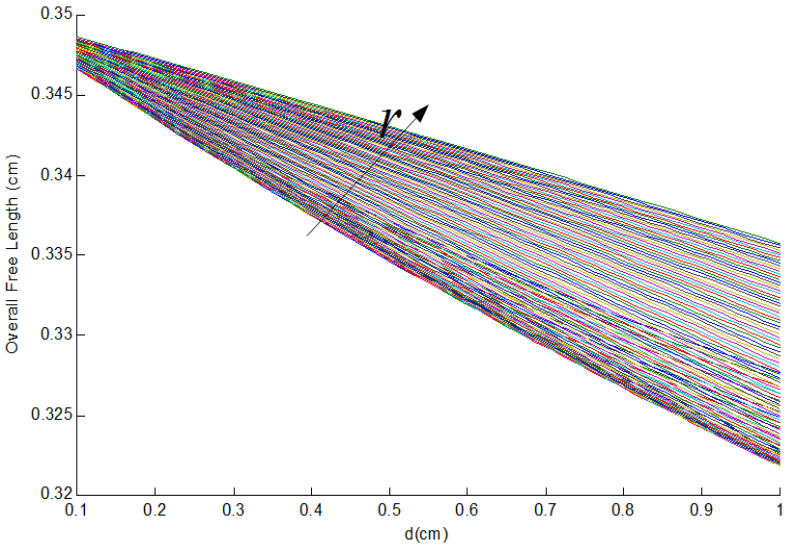


Figure 3-9. Variation of overall free length against $d$ over $r$

overall free length with respect to $d$ over $r$. In the next section, the additional constraint imposed by some special design cases are examined.

### 3.1.2 Special Cases

The special cases considered here are those that arise by pre-stressing the left and right springs in some ways. First, the cases are highlighted as follows

1. Pre-stressed: Here, both springs are always either in tension or compression. There are four sub-cases under this.
   a. both springs in tension. $l_{0_1}, l_{0_2} \ll H$.
   b. both springs in compression. $l_{0_1}, l_{0_2} \gg H$.
   c. left spring in compression and right spring in tension. $l_{0_1} \gg H, l_{0_2} \ll H$. This configuration results in an unstable system except for some values of $d$ which depends on the external force $F$
   d. right spring in compression and left spring in tension. $l_{0_1} \ll H, l_{0_2} \gg H$. This configuration also results in an unstable system as in Case 1-c above.

2. Partially Stressed: Here, only one of the springs is pre-stressed while the other remains unstressed. There are also four sub-cases under this case. As noted in Case 1-c, all the sub-cases here are only stable for some values of $d$ which depends on $F$
   a. left spring in tension. $l_{0_1} \ll H, l_{0_2} = H$.
   b. left spring in compression. $l_{0_1} \gg H, l_{0_2} = H$.
   c. right spring in tension. $l_{0_1} = H, l_{0_2} \ll H$.

d. right spring in compression. $l_{0_1} = H, l_{0_2} \gg H$

3. Unstressed: Here, neither of the springs is stressed. i.e $l_{0_1} = l_{0_2} = H$. This case is exactly the example given earlier as one of the members of the class that satisfy Eqn.(3–17)

One interesting thing about all these cases is that none of them changes the effective stiffness of the mechanism. They only change the overall free length. This shows that no matter how the system is pre-stressed, the effective stiffness remains the same.

### 3.2 Reverse Analysis

Given the desired overall spring constant, the goal of this section is to find the corresponding control parameter $d$ required to achieve the given stiffness. Judging from the form of the stiffness equation (3–10), all that needs to be done is set $K$ to the desired values and solve the resulting quadratic equation for $d$. However, the solution is not guaranteed to be always real. Thus, in addition to solving the quadratic equation, this section also details the derivation of a special constraint that must be imposed on the set value for $K$. This is achieved by constraining the discriminant of the quadratic equation to be always positive. Let $K_d$ be the desired overall stiffness of the mechanism. Setting $K = K_d$ in (3–10) yields

$$K_d d^2 = k_1(L_1 + d)^2 + k_2(L_2 - d)^2$$

or

$$(K_d - k_1 - k_2)d^2 - 2(k_1 L_1 - k_2 L_2)d - (k_1 L_1^2 + k_2 L_2^2) = 0 \tag{3–18}$$

whose solution is given by

$$d = \frac{B \pm \sqrt{B^2 + AC}}{A} \tag{3–19}$$

where

$$A = K_d - k_1 - k_2$$

$$B = k_1 L_1 - k_2 L_2$$

$$C = k_1 L_1^2 + k_2 L_2^2.$$

But $d \in \Re$ requires that

$$B^2 + AC \geq 0$$

which also implies that

$$K_d(k_1 L_1^2 + k_2 L_2^2) \geq k_1 k_2 (L_1 + L_2)^2. \tag{3–20}$$

Substituting $L_2 = rL_1$ into (3–20) yields

$$K_d(k_1 + r^2 k_2) L_1^2 \geq k_1 k_2 (1 + r)^2 L_1^2$$

or

$$K_d \geq \frac{k_1 k_2 (1 + r)^2}{k_1 + r^2 k_2} \tag{3–21}$$

Equation (3–21) gives a set of mechanism stiffness achievable by given design parameters. Again, the usefulness of the aspect ratio $r$ is evident - as this boundary can be stretched by adjusting the system aspect ratio. Figure3-10 shows the variation of the lower bound of achievable effective stiffness with respect to the aspect ratio. As can be seen from the figure, the whole system equivalently tends to the left spring as the aspect ratio tends to infinity. Similarly, the system equivalently tends to the right spring as the aspect ratio tends to zero. The maximum lower bound occurs when the aspect ratio becomes the ratio of the left and right spring constants. When this happens, the limiting behavior of the mechanism becomes that of a serial connection of the left and right springs. Also, from (3–21)

$$\frac{1}{K_d} \leq \frac{1}{k_2(1 + r)^2} + \frac{1}{k_1 \left(\frac{1}{r} + 1\right)^2} \tag{3–22}$$

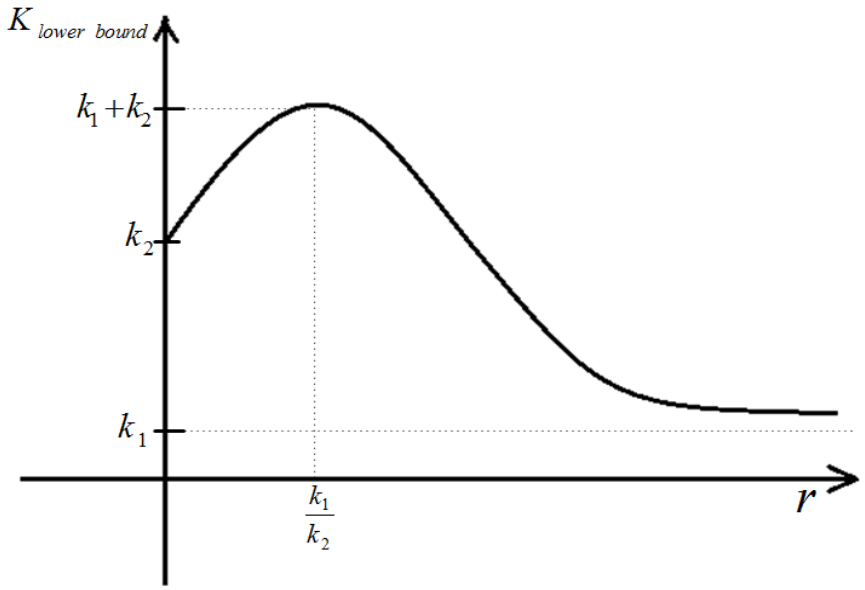


Figure 3-10. Effect of aspect ratio on achievable stiffness lower bound

from which it is concluded that the maximum compliance achievable in the assembly is the equivalent compliance of the parallel connection of two simple springs of spring constants $(1+r)^2k_2$ and $(1+\frac{1}{r})^2k_1$.

### 3.3 Dynamical Analysis

In this section, the natural frequency of the mechanism is deduced from the analysis of the system dynamics. First, the equation of motion is derived using Newton's laws of motion. Taking a moment about point **O** of Figure 3-2 yields

$$-Kd^2tan\theta + mgd + Fd - (md^2sec^2\theta + I)\ddot{\theta} = 0 \tag{3–23}$$

where $I$ is the central moment of inertia of the lever and $m$ is the mass of the lever arm. Linearizing about $\theta = 0$ yields

$$-Kd^2\theta + mgd + Fd - (md^2 + I)\ddot{\theta} = 0 \tag{3–24}$$

from which the natural frequency is deduced as

$$\omega_n = \sqrt{\frac{Kd^2}{I + md^2}}. \tag{3–25}$$

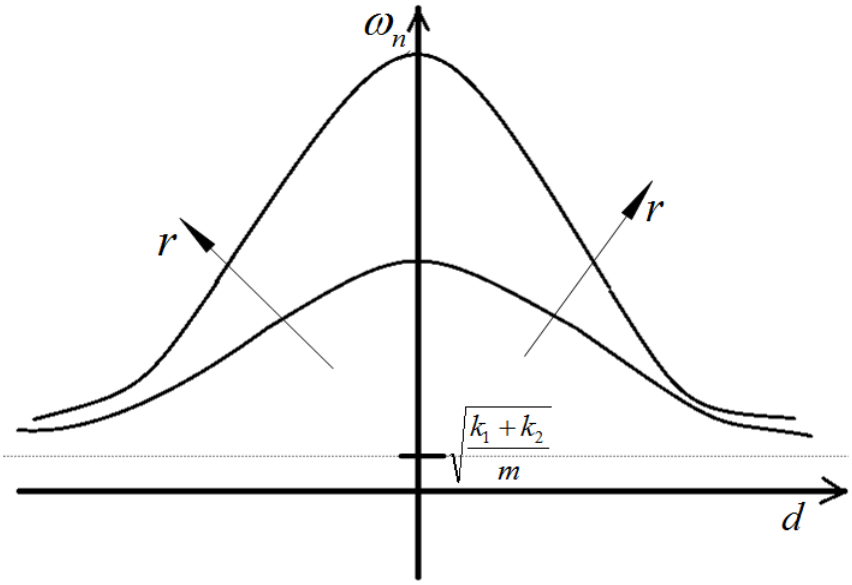


Figure 3-11. Natural frequency

Substituting the expression of $K$ from (3–10), the above becomes

$$\omega_n = \sqrt{\frac{k_1(L_1+d)^2 + k_2(L_2-d)^2}{I+md^2}}. \tag{3–26}$$

Figure 3-11 shows a plot of the natural frequency against the parameter $d$ over the aspect ratio $r$. The plot and (3–26) show that the maximum value occurs when $d = 0$ and the value is given by

$$\omega_{n_{max}} = \sqrt{\frac{k_1L_1^2 + k_2L_2^2}{I}}.$$

The practical interpretation of this observation is that the system behaves like a compound pendulum whose center of mass has a distance $L$ from the point of application of the force given by

$$L = \frac{k_1L_1^2 + k_2L_2^2}{mg}.$$

Also, as $d$ tends to infinity, the natural frequency asymptotically approaches $\sqrt{\frac{k_1+k_2}{m}}$, which is the resultant natural frequency of parallel connection of two simple springs of spring constants $k_1$ and $k_2$. Moreover, as shown in figure 3-11, the aspect ratio $r$

changes the shape of the natural frequency characteristic. The dome flattens out with reduced $r$.

# CHAPTER 4
# VARIABLE STIFFNESS SUSPENSION SYSTEM: PASSIVE CASE

Most semi-active suspension systems are designed to only vary the damping coefficient of the shock absorber while keeping the stiffness constant. Meanwhile, in suspension optimization, both the damping coefficient and the spring rate of the suspension elements are usually used as optimization arguments. Therefore, a semi-active suspension system that varies both the stiffness and damping of the suspension element could provide more flexibility in balancing competing design objectives. Suspension designs that exhibit variable stiffness phenomenon are few in literature considering the vast amount of researches that has been done on semi-active suspension designs. Knaap et. al[16, 29, 30] designed a variable geometry actuator for vehicle suspension called the Delft active suspension (DAS). Although, the intention of the design was not to vary the stiffness of the suspension system, the design used a variable geometry concept to vary the suspension force by effectively changing the stiffness of the suspension system. The basic idea behind the DAS concept is based on a wishbone which can be rotated over an angle and is connected to a pretensioned spring at a variable location. The spring pretension generates an effective actuator force, which can be manipulated by changing the position. This was achieved using an electric motor. Jerz[45] invented a variable stiffness suspension system which includes two springs connected in series. One of the springs is stiffer than the other. Under normal load conditions, the softer spring is responsible for keeping a good ride comfort. Upon the imposition of heavier load forces, the vehicle is supported more stiffly and primarily by the stronger spring. Conversion between the two conditions was done automatically by engagement under heavy load conditions of a pair of stop shoulders acting to limit the compression of the light spring. Similarly, upon excessive extension of the springs, an additional set of stop shoulders are engaged automatically to limit the amount of extension of the softer spring and causes the stiffer spring to resist further

extension. Kobori proposed a variable stiffness system to suppress buildings' responses to earthquakes[46]. The aim was to achieve a non-stationary and non-resonant state during earthquakes. Youn and Hac used an air spring in a suspension system to vary the stiffness among three discrete values[47]. Liu et. al proposed a suspension system which uses two controllable dampers and two constant springs to achieve variable stiffness and damping[48]. A Voigt element and a spring in series are used to control system stiffness. The Voigt element is comprised of a controllable damper and a constant spring. The equivalent stiffness of the whole system is changed by controlling the damper in the Voigt element.

The variation of stiffness concept used in this chapter uses "reciprocal actuation"[49] to effectively transfer energy between a vertical traditional strut and a horizontal oscillating control mass, thereby improving the energy dissipation of the overall suspension. Due to the relatively fewer number of moving parts, the concept can easily be incorporated into existing traditional front and rear suspension designs. An implementation with a double wishbone is shown in this chapter.

## 4.1 System Description

This section gives a detailed description of the variable stiffness concept, overall system, its incorporation in a vehicle suspension, and the resulting system dynamic model.

### 4.1.1 Variable Stiffness Concept

The variable stiffness mechanism concept is shown in Fig 4-1. The Lever arm OA, of length $L$, is pinned at a fixed point O and free to rotate about O. The spring AB is pinned to the lever arm at A and is free to rotate about A. The other end B of the spring is free to translate horizontally as shown by the double headed arrow. Without loss of generality, the external force $F$ is assumed to act vertically upwards at point A. $d$ is the horizontal distance of B from O. The idea is to vary the overall stiffness of the system by letting $d$ vary passively under the influence of a horizontal spring-damper system

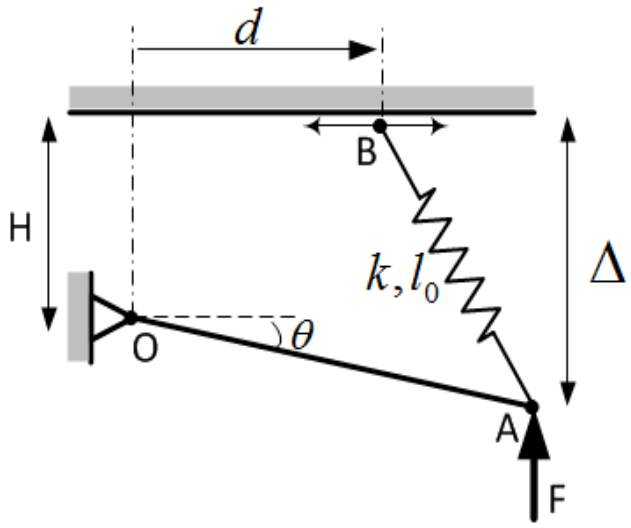


Figure 4-1. Variable stiffness mechanism

(not shown in the figure) . Let $k$ and $l_0$ be the spring constant and the free length of the spring AB respectively, and $\Delta$ the vertical displacement of the point A. The overall free length $\Delta_0$ of the mechanism is defined as the value of $\Delta$ when no external force is acting on the mechanism.

### 4.1.2 Mechanism Description

The suspension system considered is shown in Fig 4-2. The schematic diagram is shown in Fig 4-3. The model is composed of a quarter car body, wheel assembly, two spring-damper systems, road disturbance, lower and upper wishbones. The points O,A, and B are the same as shown in the variable stiffness mechanism of Fig 4-1. The horizontal control force $u$ controls the position $d$ of the control mass $m_d$ which, in turn, controls the overall stiffness of the mechanism. The tire is modeled as a linear spring of spring constant $k_t$.

The assumptions adopted in Fig 4-3 are summarized as follows:

1. The lateral displacement of the sprung mass is neglected, i.e only the vertical displacement $y_s$ is considered.
2. The wheel camber angle is zero at the equilibrium position and its variation is negligible throughout the system trajectory.

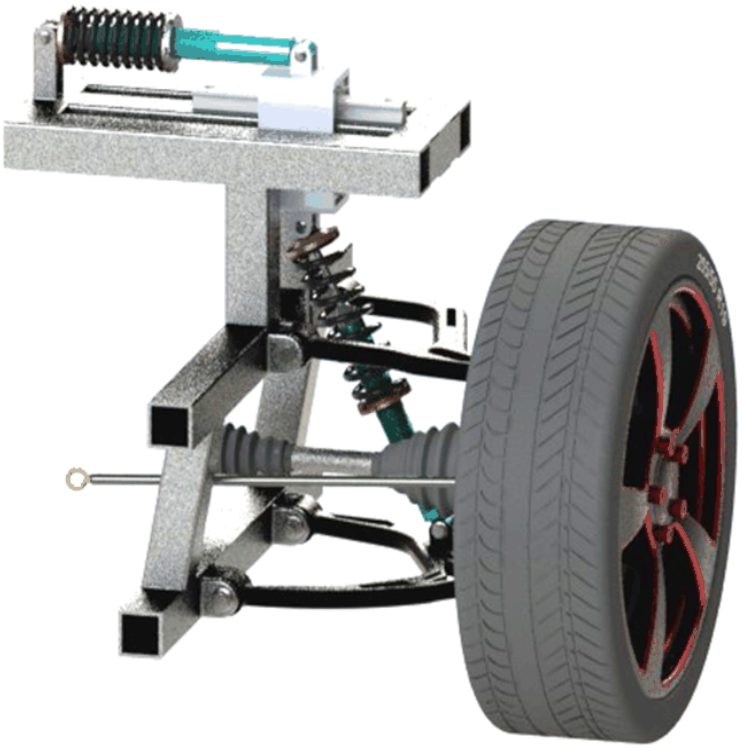

Figure 4-2. Variable stiffness suspension system

3. The springs and tire deflections are in the linear regions of their operating ranges.

### 4.1.3 Equations of Motion

Let

$$\mathbf{q} = \begin{bmatrix} y_s \\ \theta \\ d \end{bmatrix}, \tag{4–1}$$

be defined as the generalized coordinates. The equations of motion, derived using Lagrange's method, are then given by

$$\begin{aligned} M(\theta)\ddot{\mathbf{q}} + \mathbf{C}(\theta, \dot{\theta}) + B(\theta)\dot{\mathbf{q}} - \mathbf{K}(\mathbf{q}) + \mathbf{G}(\theta) \\ = \mathbf{e}_{3,3}u + W_d(\theta)\mathbf{d}_r \end{aligned} \tag{4–2}$$

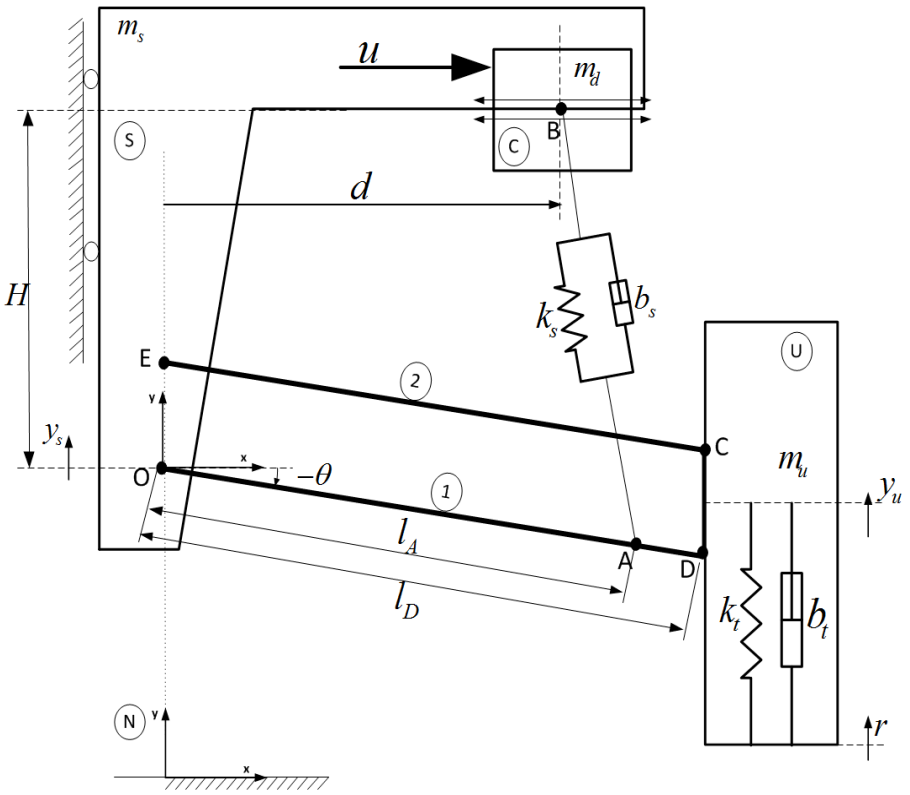


S: Sprung Mass (Chassis)
1: Lower Wishbone
2: Upper Wishbone
U: Unsprung Mass (Wheel Assembly)
C: Control Mass
N: Inertial Reference Frame

Figure 4-3. Quarter car model - passive case

where

$$M(\theta) = \begin{bmatrix} m_s + m_u + m_d & m_u l_D \cos\theta & 0 \\ m_u l_D \cos\theta & I_c + m_u l_D^2 \cos^2\theta & 0 \\ 0 & 0 & m_d \end{bmatrix},$$

$$\mathbf{C}(\theta, \dot{\theta}) = -m_u l_D \dot{\theta}^2 \sin\theta \mathbf{w}(\theta),$$

$$\mathbf{w}(\theta) = \begin{bmatrix} 1 \\ l_D \cos\theta \\ 0 \end{bmatrix},$$

$$B(\theta) = \begin{bmatrix} b_t & b_t l_D \cos\theta & 0 \\ b_t l_D \cos\theta & b_t l_D^2 \cos^2\theta + b_s g_\theta & \frac{b_s}{2} g_{d\theta} \\ 0 & \frac{b_s}{2} g_{d\theta} & b_s g_d \end{bmatrix},$$

$$g_d(d,\theta) = \frac{(d - l_A \cos\theta)^2}{H^2 + d^2 + l_A^2 - 2 l_A d \cos\theta - 2 H l_A \sin\theta},$$

$$g_{d\theta}(d,\theta) = \frac{2 l_A (d - l_A \cos\theta)(d \sin\theta - H \cos\theta)}{H^2 + d^2 + l_A^2 - 2 l_A d \cos\theta - 2 H l_A \sin\theta},$$

$$g_\theta(d,\theta) = \frac{l_A^2 (d \sin\theta - H \cos\theta)^2}{H^2 + d^2 + l_A^2 - 2 l_A d \cos\theta - 2 H l_A \sin\theta},$$

$$\mathbf{K}(\mathbf{q}) = \begin{bmatrix} k_t (\rho_t - 1)(y_s + l_D \sin\theta) \\ k_t (\rho_t - 1) l_D \cos\theta (y_s + l_D \sin\theta) \\ k_s(\rho_s - 1)(d - l_A \cos\theta) \end{bmatrix} + \begin{bmatrix} 0 \\ k_s (\rho_s - 1) l_A (d \sin\theta - H \cos\theta) \\ 0 \end{bmatrix},$$

$$\mathbf{G}(\theta) = \begin{bmatrix} m_s + m_u + m_d \\ m_u l_D \cos\theta \\ 0 \end{bmatrix} g,$$

$$W_d(\theta) = \begin{bmatrix} k_t(\rho_t - 1) & b_t \\ k_t l_D(\rho_t - 1)\cos\theta & b_t l_D \cos\theta \\ 0 & 0 \end{bmatrix},$$

$$\mathbf{d}_r = \begin{bmatrix} r \\ \dot{r} \end{bmatrix}.$$

$r(t)$ is the road displacement signal. It is a function of the road profile and the vehicle velocity. The terms $\rho_s$ and $\rho_t$ characterize the compression of the vertical strut and tire springs respectively. They are defined as the ratio of the free length and instantaneous length of the corresponding spring.

***Properties***: The following properties of the dynamics given in (4–2) are exploited in subsequent analyses:

1. The inertia matrix $M(\theta)$ is symmetric, positive definite. Also, since each element of $M(\theta)$ can be bounded below and above by positive constants, it follows that the eigenvalues, hence the singular values of $M(\theta)$ can also be bounded by constants. Thus, there exists $m_1, m_2 \in \mathcal{R}^+$ such that

$$m_1 \|\mathbf{x}\|^2 \leq \mathbf{x}^T M(\theta)\mathbf{x} \leq m_2 \|\mathbf{x}\|^2 \quad \text{and} \tag{4–3}$$

$$\frac{1}{m_2}\|\mathbf{x}\|^2 \leq \mathbf{x}^T M^{-1}(\theta)\mathbf{x} \leq \frac{1}{m_1}\|\mathbf{x}\|^2, \quad \forall \mathbf{x} \in \boldsymbol{\mathcal{R}}^2 \tag{4–4}$$

2. $\mathbf{C}(\theta, \dot{\theta})$ can be upper bounded as follows

$$\left\|\mathbf{C}(\theta, \dot{\theta})\right\| \leq c_1 \dot{\theta}^2, \quad c_1 \in \boldsymbol{\mathcal{R}}^+. \tag{4–5}$$

Also, there exist a matrix $V_m(\theta, \dot{\theta})$ such that $\mathbf{C}(\theta, \dot{\theta}) = V_m(\theta, \dot{\theta})\dot{\mathbf{q}}$ and

$$\mathbf{x}^T \left(\frac{1}{2}\dot{\mathbf{M}}(\theta) - V_m(\theta, \dot{\theta})\right)\mathbf{x} = 0, \quad \forall \mathbf{x} \in \boldsymbol{\mathcal{R}}^2 \tag{4–6}$$

The property in (4–6) is the usual skew symmetric property of the Coriolis/centripetal matrix of Lagrange dynamics [50].

3. The damping matrix $B(\theta)$ is symmetric and positive semi definite. Also, there exists positive definite matrices $\underline{B}$ and $\bar{B}$ such that

$$0 < \mathbf{x}^T \underline{B}\mathbf{x} \leq \mathbf{x}^T B(\theta)\mathbf{x} \leq \mathbf{x}^T \bar{B}\mathbf{x}, \quad \forall \mathbf{x} \in \mathcal{R}^2. \tag{4–7}$$

4. The stiffness vector $\mathbf{K}(\mathbf{q})$ is Lipschitz continuous, i.e there exists a positive constant $k_2$ such that

$$\|\mathbf{K}(\mathbf{q}_1) - \mathbf{K}(\mathbf{q}_2)\| \leq k_2 \|\mathbf{q}_1 - \mathbf{q}_2\|. \tag{4–8}$$

5. The unique static equilibrium point $\mathbf{q}_0 = \begin{bmatrix} y_{s_0} & \theta_0 & d_0 \end{bmatrix}^T$ of the undisturbed system is known and is given by

$$\mathbf{K}(\mathbf{q}_0) - \mathbf{G}(\theta_0) + \mathbf{e}_{3,3} u_0 = \mathbf{0}. \tag{4–9}$$

## 4.2 System Analysis

This section presents the finite-gain stability analysis of the system described in the previous section. The disturbance $\mathbf{d}_r$ in (4–2) is assumed to be unknown a priori but bounded in the sense that $\mathbf{d}_r \in \mathcal{L}_2$. As a result, robust optimal control is considered in which the gain of the system is optimized under worst excitations: [51–54]. The following definition describes the notion of stability used in the subsequent analyses.

**Definition 4.1** (Finite-Gain $\mathcal{L}$-Stable)**.** *([54]) Consider the nonlinear system*

$$\begin{aligned} \dot{\boldsymbol{x}} &= f(\boldsymbol{x}, \boldsymbol{w}) \\ \boldsymbol{z} &= h(\boldsymbol{x}) \end{aligned} \tag{4–10}$$

*where $\boldsymbol{x} \in \mathcal{R}^n$, $\boldsymbol{w} \in \mathcal{R}^p$, $\boldsymbol{z} \in \mathcal{R}^m$ are the state, input, and output vectors respectively. The system in (4–10), with the mapping $M_H : \mathcal{L}_e^p \to \mathcal{L}_e^m$, is said to be finite-gain $\mathcal{L}$-stable if there exist real constants $\gamma, \beta \geq 0$ such that*

$$\|M_H(\boldsymbol{w})\|_{\mathcal{L}} \leq \gamma \|\boldsymbol{w}\|_{\mathcal{L}} + \beta, \tag{4–11}$$

*where $\|.\|_{\mathcal{L}}$ denotes the $\mathcal{L}$ norm of a signal, and $\mathcal{L}_e^n$ is the extended $\mathcal{L}$ space defined as*

$$\mathcal{L}_e^n = \{\chi | \chi_\tau \in \mathcal{L}^n, \forall \tau \in [0, \infty)\} \tag{4–12}$$

*where $\chi_\tau$ is a truncation of $\chi$ given as*

$$\chi_\tau(t) = \begin{cases} \chi(t) & 0 \leq t \leq \tau \\ 0 & t > \tau. \end{cases} . \tag{4–13}$$

For the purpose of this paper, the $\mathcal{L}_2$-space is considered, hence the finite-gain $\mathcal{L}$-stability condition in (4–11) is rewritten as ([54])

$$\|M_H(\mathbf{w})\|_2 \leq \gamma \|\mathbf{w}\|_2 + \beta, \tag{4–14}$$

where $\|.\|_2$ denotes the $\mathcal{L}_2$ norm of a signal given by

$$\|\chi\|_2 = \left( \int_0^\infty \chi^T(t)\chi(t)dt \right)^{\frac{1}{2}}. \tag{4–15}$$

$\gamma^* = \inf \{\gamma | \, \|M_H(\mathbf{w})\|_2 \leq \gamma \|\mathbf{w}\|_2 + \beta\}$ is the gain of the system, and, in the case of linear quadratic problems, is the $H_\infty$ norm of the system. Given an attenuation level $\gamma > 0$, and the corresponding system dynamics, the objective is to show that (4–14) is satisfied for some $\beta > 0$. This solution is approached from the perspective of dissipative systems ([51, 54]). The following definition describes the concept of dissipativity with respect to the system in (4–10).

**Definition 4.2** (Dissipativity)**.** *The dynamics system* (4–10) *is dissipative with respect to a given supply rate $s(\boldsymbol{w}, \boldsymbol{z}) \in \mathcal{R}$, if there exists an energy function $V(\boldsymbol{x}) \geq 0$ such that, for all $\boldsymbol{x}(t_0) = \boldsymbol{x}_0$ and $t_f \geq t_0$,*

$$V(\boldsymbol{x}(t_f)) \leq V(\boldsymbol{x}(t_0)) + \int_{t_0}^{t_f} s(\boldsymbol{w}, \boldsymbol{z})dt, \quad \forall \boldsymbol{w} \in \mathcal{L}_2. \tag{4–16}$$

If the supply rate is taken as

$$s(\mathbf{w}, \mathbf{z}) = \gamma^2 \|\mathbf{w}\|^2 - \|\mathbf{z}\|^2, \tag{4–17}$$

then the dissipation inequality in (4–16) implies finite-gain $\mathcal{L}$-stability [54], and the system is said to be $\gamma$-dissipative. The dissipativity inequality is then written as

$$\dot{V} \leq \gamma^2 \|\mathbf{w}\|^2 - \|\mathbf{z}\|^2. \tag{4–18}$$

### 4.2.1 Performance Objective

As usual with suspension systems designs, the performance criterion is expressed in terms of the ride comfort, suspension deflection, and dynamic tire force. The performance vector

$$\mathbf{z} = \begin{bmatrix} \omega_1 y_{\text{cba}} \\ \omega_2 y_{\text{sd}} \\ \omega_3 y_{\text{dtf}} \end{bmatrix} \tag{4–19}$$

characterizes the ride comfort, suspension deflection, and road holding performances, where $\omega_1, \omega_2$, and $\omega_3$ are the respective user specified performance weights for car body acceleration $y_{\text{cba}}$, suspension deflection $y_{\text{sd}}$, and dynamic tire force $y_{\text{dtf}}$. The ride comfort is characterized by the car body acceleration $\ddot{y}_s$ which is approximated using the following high gain observer ([55]):

$$\begin{aligned} \varepsilon \dot{\boldsymbol{\eta}} &= A\boldsymbol{\eta} + \mathbf{b}\dot{y}_s, \;\; \boldsymbol{\eta}(0) = \mathbf{0} \\ y_{\text{cba}} &= \tfrac{1}{\varepsilon}\mathbf{c}^T\boldsymbol{\eta} \end{aligned} \tag{4–20}$$

where

$$A = \begin{bmatrix} -1 & 1 \\ -1 & 0 \end{bmatrix}, \;\; \mathbf{b} = \begin{bmatrix} 1 \\ 1 \end{bmatrix}, \;\; \mathbf{c} = \begin{bmatrix} 0 \\ 1 \end{bmatrix}.$$

The $\mathcal{L}_2$-norm of the car body acceleration can be upper bounded as ([55])

$$\|y_{\text{cba}}\|_2 \leq c_1 \|\dot{y}_s\|_2 \leq c_1 \|\dot{\mathbf{e}}\|_2, \tag{4–21}$$

where

$$c_1 = \frac{2\lambda_{\max}^2(P)\|\mathbf{b}\|_2\|\mathbf{c}\|_2}{\lambda_{\min}(P)}$$

and $P$ is the solution of the Lyapunov equation $PA + A^T P + I = 0$, which is obtained as

$$P = \frac{1}{\varepsilon}\begin{bmatrix} 1 & \frac{1}{2} \\ \frac{1}{2} & \frac{3}{2} \end{bmatrix}.$$

The suspension deflection is given as

$$\begin{aligned} y_{\text{sd}}(t) &= \sqrt{l_s^2(0) - l_s^2(t)} \\ &= \left\{ d(0)^2 - d(t)^2 - 2Hx\left(\sin\theta(0) - \sin\theta(t)\right)\right. \\ &\qquad \left. -2x\left(d(0)\cos\theta(0) - d(t)\cos\theta(t)\right)\right\}^{\frac{1}{2}} \qquad (4\text{–}22) \\ &\leq \begin{bmatrix} 0 & k_{41} & k_{42} \end{bmatrix} \begin{bmatrix} |y_{0_s} - y_s| \\ |\theta - \theta_0| \\ |d - d_0| \end{bmatrix}, \qquad (4\text{–}23) \end{aligned}$$

Using the Cauchy-Schwarz inequality, $y_{\text{sd}}(t)$ can be upper bounded as

$$y_{\text{sd}}(t) \leq k_4\|\mathbf{e}\|, \qquad (4\text{–}24)$$

where $k_{41}, k_{42},$ and $k_4$ are positive constants, and $k_4 \geq \sqrt{k_{41}^2 + k_{42}^2}$.

The dynamic tire force is characterized using the tire deflection and is given by

$$\begin{aligned} y_{\text{dtf}}(t) &= y_u(0) - y_u(t) \\ &= y_{0_s} - y_s + l_D(\sin\theta_0 - \sin\theta) \qquad (4\text{–}25) \\ &\leq \begin{bmatrix} 1 & k_5 & 0 \end{bmatrix} \begin{bmatrix} |y_{0_s} - y_s| \\ |\theta - \theta_0| \\ |d - d_0| \end{bmatrix}, \qquad (4\text{–}26) \end{aligned}$$

where $k_5$ is a positive constant. Using the Cauchy-Schwarz inequality, $y_{\text{dtf}}(t)$ can be upper bounded as

$$y_{\text{dtf}} \leq \sqrt{1 + k_5^2}\, \|\mathbf{e}\| = k_6 \|\mathbf{e}\|. \tag{4–27}$$

Finally, the $\mathcal{L}_2$-norm of the performance vector in (4–19) can be upper bounded as

$$\|\mathbf{z}\|_2 \leq \phi_1 \|\dot{\mathbf{e}}\|_2 + \phi_2 \|\mathbf{e}\|_2 \tag{4–28}$$

where

$$\phi_1 = \omega_1 c_1$$

$$\phi_2 = \omega_2 k_4 + \omega_3 k_6.$$

### 4.2.2 Constant Stiffness Case

Now, consider the constant stiffness case in which the control mass is locked at a given position $d$. As a result, the overall stiffness is constant for the entire trajectory of the system. For this case, the dynamics in (4–2) reduces to

$$M_1(\theta)\ddot{\mathbf{q}}_1 + \mathbf{C}_1(\theta, \dot{\theta}) + B_1(\theta)\dot{\mathbf{q}}_1 - \mathbf{K}_1(\mathbf{q}_1) + \mathbf{G}_1(\theta) = \mathbf{w}, \tag{4–29}$$

where

$$M_1 = M_{1:2,1:2}, \mathbf{C}_1 = \mathbf{C}_{1:2},$$

$$\mathbf{K}_1 = \mathbf{K}_{1:2}, B_1 = B_{1:2,1:2},$$

$$\mathbf{w} = W_{d_1}\mathbf{d}_r, W_{d_1} = W_{d_{1:2,1:2}}$$

Here, the corresponding dynamics of the control mass has been eliminated.

Let

$$\mathbf{e}_1 = \mathbf{q}_1 - \mathbf{q}_{0_1} \tag{4–30}$$

where

$$\mathbf{q}_{0_1} = \begin{bmatrix} y_{s_0} \\ \theta_0 \end{bmatrix} \tag{4–31}$$

be the equilibrium value of the reduced state vector $\mathbf{q}_1$. After using the Mean Value Theorem, the closed-loop dynamics in (4–29) is expressed as

$$M_1\ddot{\mathbf{e}}_1 + V_{m_1}\dot{\mathbf{e}}_1 + K_1\mathbf{e}_1 + B_1\dot{\mathbf{e}}_1 = \mathbf{w} \tag{4–32}$$

where

$$K_1 = -\left.\frac{\partial \mathbf{K}_1}{\partial \mathbf{q}_1}\right|_{\mathbf{q}_1=\zeta_1} + \left.\frac{\partial \mathbf{G}_1}{\partial \mathbf{q}_1}\right|_{\mathbf{q}_1=\zeta_2} \zeta_1, \zeta_2, \in \mathcal{L}_s(\mathbf{q}_{0_1}, \mathbf{q}_1).$$

**Lemma 1.** *The matrix*

$$P = \begin{bmatrix} I & m_1 I \\ m_1 I & M_1 \end{bmatrix} \tag{4–33}$$

*is positive definite, where* $m_1^2 < \lambda_{min}\{M_1\}$.

*Proof.* Let $\lambda$ be an eigenvalue of $P$. It follows that $\lambda \in \mathcal{R}$, since $P$ is symmetric. The characteristic polynomial of $P$ is given by

$$p(\lambda) = det\{\lambda I - P\} \tag{4–34}$$

$$= det\left\{(\lambda - 1)(\lambda I - M) - m_1^2 I\right\} \tag{4–35}$$

Now, $\lambda = 1 \Rightarrow p(\lambda) = m_1^4$, which implies that $\lambda = 1$ is NOT an eigenvalue of $P$. Suppose without loss of generality that $\lambda \neq 1$, then

$$p(\lambda) = (\lambda - 1)^2 \, det\left\{\frac{\lambda^2 - \lambda - m_1^2}{\lambda - 1} I - M\right\}. \tag{4–36}$$

Thus there exists an eigenvalue $\lambda_m$ of $M$ such that

$$\frac{\lambda^2 - \lambda - m_1^2}{\lambda - 1} = \lambda_m, \tag{4–37}$$

which implies that

$$\lambda = \frac{1}{2}\left(1 + \lambda_m \pm \sqrt{(1+\lambda_m)^2 - 4\left(\lambda_m - m_1^2\right)}\right), \tag{4–38}$$

from which it follows that $\lambda > 0$. Since $P$ is symmetric, the conclusion follows. □

**Remark 4.1.** *It follows from Rayleigh-Ritz Inequality that*

$$p_1 \|\boldsymbol{\chi}\|^2 \leq \boldsymbol{\chi}^T P \boldsymbol{\chi} \leq p_2 \|\boldsymbol{\chi}\|^2, \tag{4–39}$$

*where* $p_1 = \lambda_{min}\{P\}$, *and* $p_2 = \lambda_{max}\{P\}$.

**Theorem 4.1.** *If the matrix*

$$H_1 = \frac{1}{2}\begin{bmatrix} -\hat{K}_1 - \hat{K}_1^T & -K_1^T - m_1 M_1^{-1} B_1 \\ -K_1 - m_1\left(M_1^{-1} B_1\right)^T & -2\hat{B}_1 \end{bmatrix}, \tag{4–40}$$

*where*

$$\hat{K}_1 = m_1 M_1^{-1} K_1 - \frac{c_1 \|\dot{\boldsymbol{e}}\|}{2} I \tag{4–41}$$

$$\hat{B}_1 = B_1 - \left(m_1 + \frac{c_1 \|\dot{\boldsymbol{e}}\|}{2}\right) I, \tag{4–42}$$

*is negative definite along the entire trajectory of the closed-loop error system in* (4–32), *then the* $\mathcal{L}_2$*-norm of the performance vector in* (4–19) *can be upper bounded as*

$$\|\boldsymbol{z}\|_2 \leq \gamma_1 \|\boldsymbol{w}\|_2 + \beta_1, \tag{4–43}$$

*where*

$$\gamma_1 = \frac{\phi \sigma p_2}{p_1 h_1}, \tag{4–44}$$

$$\beta_1 = \frac{\sqrt{2}\phi p_2}{\sqrt{p_1 h_1}}, \tag{4–45}$$

*and*

$$\phi = \max\{\phi_1, \phi_2\} \tag{4–46}$$

$$\sigma = \sigma_{max}\left\{\begin{bmatrix} m_1 M_1^{-1} \\ I \end{bmatrix}\right\} \tag{4–47}$$

$$h_1 = |\lambda_{min}\{H_1\}|. \tag{4–48}$$

*Proof.* Consider the energy function

$$V(\mathbf{e}_1, \dot{\mathbf{e}}_1) = \frac{1}{2}\boldsymbol{\chi}_1^T P \boldsymbol{\chi}_1, \tag{4–49}$$

where

$$\boldsymbol{\chi}_1 = \begin{bmatrix} \mathbf{e}_1 \\ \dot{\mathbf{e}}_1 \end{bmatrix}. \tag{4–50}$$

Taking time derivative of (5–33) and using the skew symmetric property in (4–6) yields

$$\begin{aligned} \dot{V} = &-\dot{\mathbf{e}}_1^T (B_1 - m_1 I)\dot{\mathbf{e}}_1 - \dot{\mathbf{e}}_1{}^T K_1 \mathbf{e}_1 + \dot{\mathbf{e}}_1^T \mathbf{w} + m_1 \mathbf{e}_1^T M_1^{-1} \mathbf{w} \\ &- m_1 \mathbf{e}_1^T M_1^{-1} V_m \dot{\mathbf{e}}_1 - m_1 \mathbf{e}_1^T M_1^{-1} B_1 \dot{\mathbf{e}}_1 - m_1 \mathbf{e}_1^T M_1^{-1} K_1 \mathbf{e}_1. \end{aligned} \tag{4–51}$$

Using the property in (4–5) yields

$$\dot{V} \leq \boldsymbol{\chi}_1^T H_1 \boldsymbol{\chi}_1 + \boldsymbol{\chi}_1^T \begin{bmatrix} m_1 M_1^{-1} \\ I \end{bmatrix} \mathbf{w}, \tag{4–52}$$

which after using the negative definiteness of $H_1$ yields

$$\dot{V} \leq -h_1 \|\boldsymbol{\chi}_1\|^2 + \sigma \|\boldsymbol{\chi}_1\| \|\mathbf{w}\|. \tag{4–53}$$

Take $W(t) = \sqrt{V(\boldsymbol{\chi}_1)}$. When $V(\boldsymbol{\chi}_1) \neq 0$, $\dot{W} = \dot{V}/(2\sqrt{V})$ yields

$$\dot{W} \leq -\frac{h_1}{2p_2} W + \frac{\sigma}{2\sqrt{p_1}} \|\mathbf{w}\|. \tag{4–54}$$

When $V(\boldsymbol{\chi}_1) = 0$, it can be verified ([55]) that

$$D^+ W \leq \frac{\sigma}{2\sqrt{p_1}} \|\mathbf{w}\|, \tag{4–55}$$

where $D^+$ denotes the upper right hand differentiation operator. Hence

$$D^+ W \leq -\frac{h_1}{2p_2} W + \frac{\sigma}{2\sqrt{p_1}} \|\mathbf{w}\| \tag{4–56}$$

for all values of $V(\boldsymbol{\chi}_1)$. Next using comparison (Lemma 3.4, [55]) yields

$$\begin{aligned} W(t) \leq W(0) \exp\left(-\frac{h_1 t}{2p_2}\right) \\ + \frac{\sigma}{2\sqrt{p_1}} \int_0^t \|\mathbf{w}\| \exp\left(-\frac{h_1(t-\tau)}{2p_2}\right) d\tau, \end{aligned} \tag{4–57}$$

which implies that

$$\begin{aligned} \|\boldsymbol{\chi}_1(t)\| \leq \sqrt{\frac{p_2}{p_1}} \|\boldsymbol{\chi}_1(0)\| \exp\left(-\frac{h_1 t}{2p_2}\right) \\ + \frac{\sigma}{2p_1} \int_0^t \|\mathbf{w}\| \exp\left(-\frac{h_1(t-\tau)}{2p_2}\right) d\tau. \end{aligned} \tag{4–58}$$

Thus

$$\|\boldsymbol{\chi}_1(t)\|_2 \leq \frac{\sigma p_2}{p_1 h_1} \|\mathbf{w}\|_2 + \frac{\sqrt{2} p_2}{\sqrt{p_1 h_1}} \|\boldsymbol{\chi}_1(0)\|.$$

Lastly, after using the inequality in (4–28), the $\mathcal{L}_2$-norm of the performance vector can be upper bounded as

$$\|\mathbf{z}\|_2 \leq \frac{\phi\sigma p_2}{p_1 h_1} \|\mathbf{w}\|_2 + \frac{\sqrt{2}\phi p_2}{\sqrt{p_1 h_1}} \|\boldsymbol{\chi}_1(0)\|. \tag{4–59}$$

□

**Remark 4.2.** *The $\mathcal{L}_2$-gain of the system decreases with increasing $h_1$. This means that the more the negative definiteness of $H_1$, the more the disturbance rejection achievable by the system.*

The following theorem gives the bounds on achievable $\gamma$.

**Theorem 4.2.** *Given an attenuation level $\gamma$, and provided that the performance weights are selected to satisfy the sufficient condition*

$$\phi = \max\{\phi_1, \phi_2\} < \sqrt{h_1}, \tag{4–60}$$

*then the closed loop error system in (4–32) is $\gamma$-dissipative with respect to the supply rate*

$$s(\boldsymbol{w}, \boldsymbol{z}) = \gamma^2 \|\boldsymbol{w}\|^2 - \|\boldsymbol{z}\|^2 \tag{4–61}$$

*if*

$$\gamma \geq \frac{0.5\sigma}{\sqrt{h_1 - \phi^2}}. \tag{4–62}$$

*Proof.* Consider the energy storage function in (5–33). Taking first time-derivate, and adding and subtracting the supply rate yields

$$\begin{aligned}
\dot{V} &\leq \boldsymbol{\chi}^T H_1 \boldsymbol{\chi} + \boldsymbol{\chi}^T L \mathbf{w} \\
&\leq \gamma^2 \|\mathbf{w}\|^2 - \|\mathbf{z}\|^2 + \boldsymbol{\chi}^T H_1 \boldsymbol{\chi} \\
&\qquad - \gamma^2 \left\| \mathbf{w} - \frac{L^T \boldsymbol{\chi}}{2\gamma^2} \right\|^2 + \frac{1}{4\gamma^2} \boldsymbol{\chi}^T L L^T \boldsymbol{\chi} + \phi^2 \|\boldsymbol{\chi}\|^2 \\
&\leq \gamma^2 \|\mathbf{w}\|^2 - \|\mathbf{z}\|^2 + \boldsymbol{\chi}^T \left( H_1 + \left( \phi^2 + \frac{\sigma^2}{4\gamma^2} \right) I \right) \boldsymbol{\chi} \\
&\leq \gamma^2 \|\mathbf{w}\|^2 - \|\mathbf{z}\|^2 - \left( h_1 - \phi^2 - \frac{\sigma^2}{4\gamma^2} \right) \|\boldsymbol{\chi}\|^2
\end{aligned} \tag{4–63}$$

After using the inequality in (4–62)

$$\dot{V} \leq \gamma^2 \|\mathbf{w}\|^2 - \|\mathbf{z}\|^2, \tag{4–64}$$

which implies that the closed loop error system in (4–32) is $\gamma$-dissipative. □

**Remark 4.3.** *The inequality in (4–62) shows that the level of performance achievable is limited by the amount of damping and stiffness available in the system. It will be shown in subsequent sections that this limit can be pushed further by using a variable stiffness*

*architecture. The lower bound in* (4–62) *is termed "**best-case-gain**". It defines the smallest gain achievable by the system.*

*The stiffness and damping matrices* $K_1$*, and* $B_1$ *contain bounded functions of state and uncertain dynamic parameters which range between bounded values. Thus the best-case gain of the system with constant stiffness can be lower bounded as*

$$\underline{\gamma}_1 \geq \frac{0.5\sigma}{\sqrt{h_1^* - \phi^2}}. \tag{4–65}$$

*where* $h_1^*$ *is the smallest positive number larger than the smallest singular value of* $H_1$*, and* $\underline{\gamma}_1$ *is termed the "**robust best-case gain**".*

### 4.2.3 Passive Variable Stiffness Case

Here, the control mass is allowed to move under the influence of a restoring spring and damper forces. There is no external force generator added to the system. As a result, the system response is purely passive. Let $k_u$ and $b_u$ be the spring constant and damping coefficient of the restoring spring and damper respectively. The control force $u$ is then given by

$$u = -b_u \dot{d} - k_u(d - l_{0_d}), \tag{4–66}$$

and the resulting dynamics of the control mass is given by

$$\begin{aligned} m_d \ddot{d} + b_u \dot{d} + k_u(d - l_{0_d}) + k_s(\rho_s - 1)(d - x\cos\theta) \\ + \frac{b_s}{2} g_{d\theta} \dot{\theta} + b_s g_d \dot{d} = 0, \end{aligned} \tag{4–67}$$

and the static equilibrium equation for the control mass is given by

$$k_u(d_0 - l_{0_d}) + k_s(\rho_{s_0} - 1)(d_0 - x\cos\theta_0) = 0, \tag{4–68}$$

where $d_0$ is the equilibrium position of the control mass, and $l_{0_d}$ is the free length of the restoring spring. Let

$$e_d = d - d_0 \tag{4–69}$$

be the displacement of the control mass from its equilibrium position. Substituting (4–69) into (4–67) and using the Mean Value Theorem yields

$$m_d \ddot{e}_d + \mathbf{B}_d^T \dot{\mathbf{e}} + \mathbf{K}_d^T \mathbf{e} = 0, \tag{4–70}$$

where

$$\mathbf{e} = \begin{bmatrix} \mathbf{e}_1 \\ e_d \end{bmatrix}, \tag{4–71}$$

$$\mathbf{B}_d = \begin{bmatrix} 0 \\ \frac{b_s}{2} g_{d\theta} \\ b_s g_d + b_u \end{bmatrix}, \tag{4–72}$$

$$\mathbf{K}_d = \begin{bmatrix} 0 \\ k_s \frac{\partial(\rho_s - 1)(d - x\cos\theta)}{\partial\theta}\Big|_{\theta \in \mathcal{L}_s(\theta_0, \theta)} \\ k_u + k_s \frac{\partial(\rho_s - 1)(d - x\cos\theta)}{\partial d}\Big|_{d \in \mathcal{L}_s(d_0, d)} \end{bmatrix}. \tag{4–73}$$

Now, consider the energy function

$$V_2(\mathbf{e}, \dot{\mathbf{e}}) = .\boldsymbol{\chi}_2^T P_2 \boldsymbol{\chi}_2, \tag{4–74}$$

where,

$$\boldsymbol{\chi}_2 = \begin{bmatrix} \mathbf{e} \\ \dot{\mathbf{e}} \end{bmatrix}, \tag{4–75}$$

and

$$P_2 = \begin{bmatrix} I & mI \\ mI & M \end{bmatrix} \tag{4–76}$$

is positive definite, with $m^2 < \lambda_{\min}\{M\}$. Taking the first time derivative of (4–74), and following a similar procedure as in the constant stiffness case in the previous section yields

$$\dot{V}_2 \leq \gamma^2 \|\mathbf{w}\|^2 - \|\mathbf{z}\|^2 + \boldsymbol{\chi}_2^T H_2 \boldsymbol{\chi}_2, \tag{4–77}$$

where

$$H_2 = \frac{1}{2}\begin{bmatrix} -\hat{K} - \hat{K}^T & -K^T - mM^{-1}B \\ -K - m\left(M^{-1}B\right)^T & -2\hat{B} \end{bmatrix}, \tag{4–78}$$

$$\hat{K} = mM^{-1}K - \frac{c_1\|\dot{\mathbf{e}}\|}{2}I, \tag{4–79}$$

$$\hat{B} = B - \left(m_1 + \frac{c_1\|\dot{\mathbf{e}}\|}{2}\right)I, \tag{4–80}$$

and

$$K = -\left.\frac{\partial \mathbf{K}}{\partial \mathbf{q}}\right|_{\mathbf{q}=\zeta} + \left.\frac{\partial \mathbf{G}}{\partial \mathbf{q}}\right|_{\mathbf{q}=\zeta_2}, \zeta_1, \zeta_2, \in \mathcal{L}_s(\mathbf{q}_0, \mathbf{q}). \tag{4–81}$$

Now, the robust best-case gain of the system with a passive variable stiffness is given by

$$\underline{\gamma}_2 \geq \frac{0.5\sigma}{\sqrt{h_2^* - \phi^2}}. \tag{4–82}$$

where $h_2^*$ is the smallest positive number larger than smallest singular value of $H_2$. Here, the spring constant $k_u$, and the damping coefficient $b_u$ of the control mass restoring spring-damper system can be chosen such that $\underline{\gamma}_2 < \underline{\gamma}_1$. **Thus, a better performance can be achieved just by letting the stiffness vary naturally using a spring-damper**

**system. This claim is supported subsequently by experimental and simulation results**. This is a very appealing result due to its practicability. No additional electronically controlled or force generating device is required, only mechanical elements like the spring and damper are used.

### 4.2.4 Experiment

The experimental setup is shown in Fig. 4-4. It is a quarter car test rig scaled down to about a ratio of 1:10 compared to an average passenger car in 2004 [56]. The quarter car body is allowed to translate up-and-down along a rigid frame. This was made possible through the use of two pairs of linear motion ball-bearing carriages, with each pair on separate parallel guide rails. The guide rails are fixed to the rigid frame and the carriage is attached to the quarter car frame. The quarter car frame is made of 80/20 aluminium framing and then loaded with a solid steel cylinder weighing approximately 80lbs. The horizontal and vertical struts are 2011 Honda PCX scooter front suspensions. The road generator is a simple slider-crank mechanism actuated by Smartmotor® SM3440D geared down to a ratio of 49:1 using CMI® gear head P/N 34EP049 . Three accelerometers are attached one each to the quarter car frame, the wheel hub, and the road generator. Data acquisition is done using the MATLAB data acquisition toolbox via a NI USB-6251. Experiments were performed for the passive case, where the horizontal strut is just a passive spring-damper system, and also for the fixed stiffness case, where the top of the vertical strut is locked in a fixed position. This position is the equilibrium position of the passive case when the system is not excited.

Two tests were carried out; Sinusoidal, and drop test. For the Sinusoidal test, the road generator is actuated by a constant torque from the DC motor. As a result, the quarter car frame moves up and down in a sinusoidal fashion. For the drop test, the suspension system was dropped from a fixed height. The resulting quarter car body acceleration and tire deflection accelerations were recorded. The tire deflection

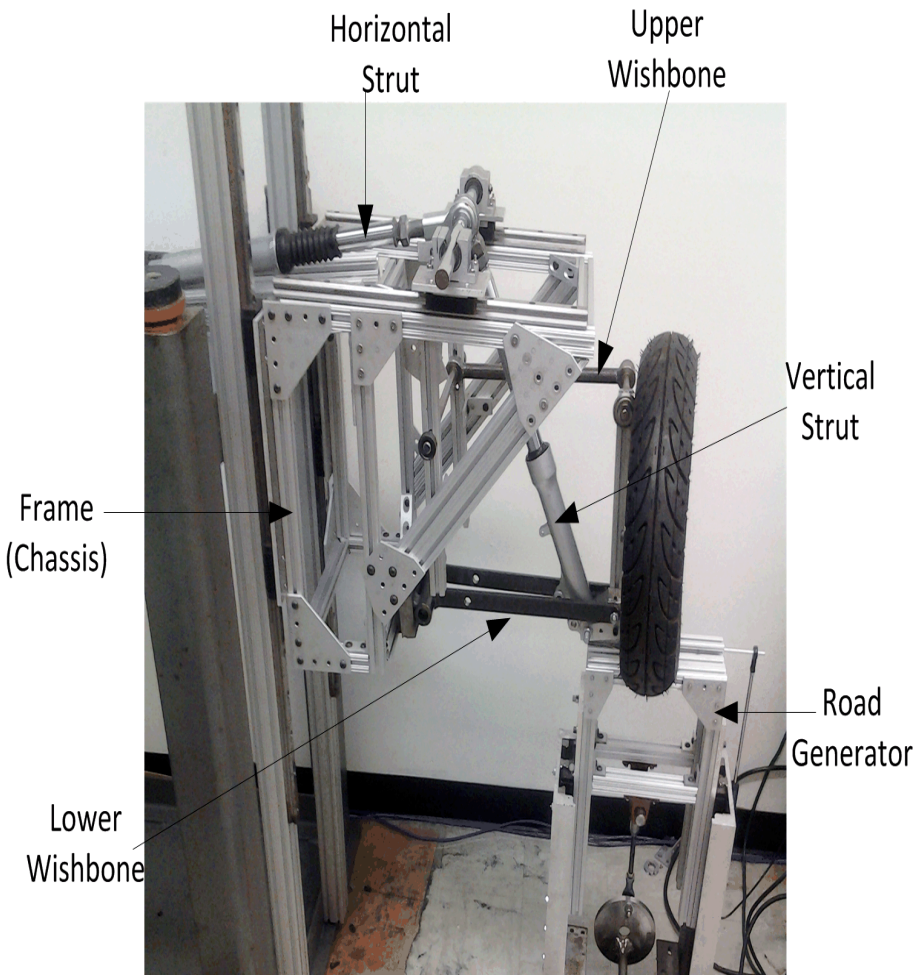


Figure 4-4. Quarter car experimental setup

Table 4-1. RMS gain values of experimental results
CBA: car body acceleration. TDA: tire deflection acceleration

| | | Fixed | Passive |
|---|---|---|---|
| Drop | CBA (g) | 0.6206 | 0.5864 |
| | TDA (g) | 0.9759 | 0.9685 |
| Sinusoidal | CBA (g) | 0.6181 | 0.5240 |
| | TDA (g) | 1.3152 | 1.0460 |

acceleration is obtained as the difference between the wheel acceleration and the road generator acceleration.

Figure 4-5 and Figure 4-6 shows the results of the sinusoidal test for the fixed and passive cases respectively. The results are not plotted together because of the

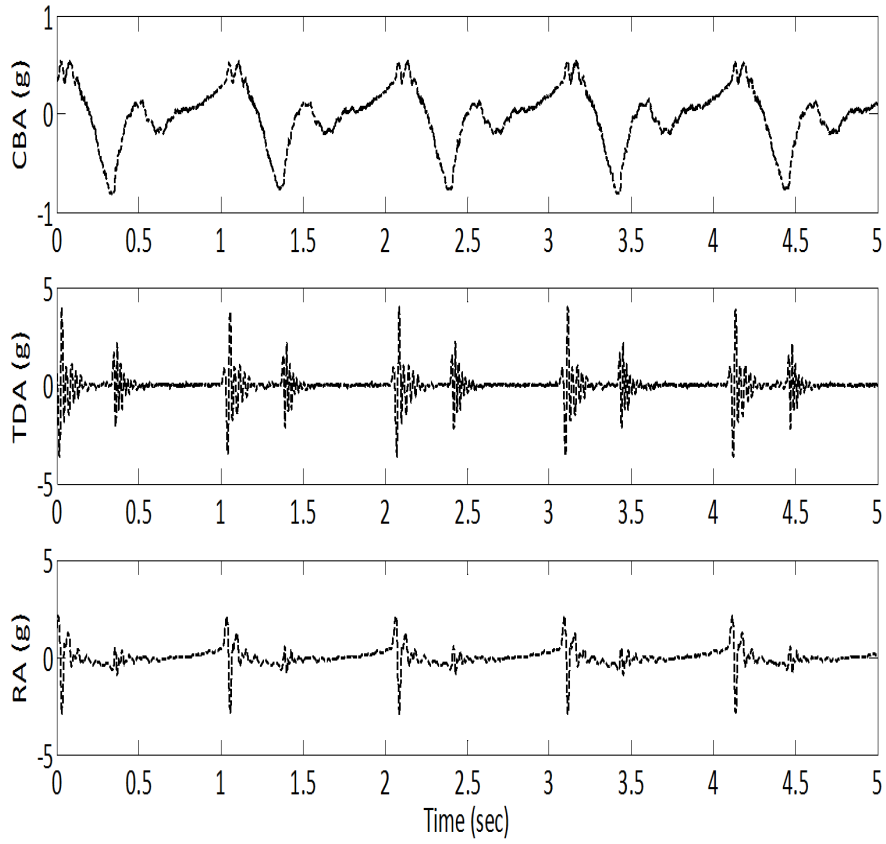


Figure 4-5. Sinusoidal test - fixed case
CBA: car body acceleration, TDA: tire deflection accleration.
RA: road acceleration

difference in the road acceleration for both cases, even as the DC motor was run at the same constant torque for both cases. One of several reasons for this observed phenomenon is the interaction and energy transfer between the horizontal and vertical struts for the passive case. To facilitate a good comparison of the observations, the “rms gain” of the system for a given response is computed as

$$\text{rms gain} = \frac{\text{rms value of the response signal}}{\text{rms value of the road acceleration signal}}. \tag{4–83}$$

Table 5-1 shows the rms gains for the sinusoidal and the drop test. However, for the drop test, the responses for the fixed and passive cases are plotted together because the DC motor was not used and the apparatus was dropped from the same height for both

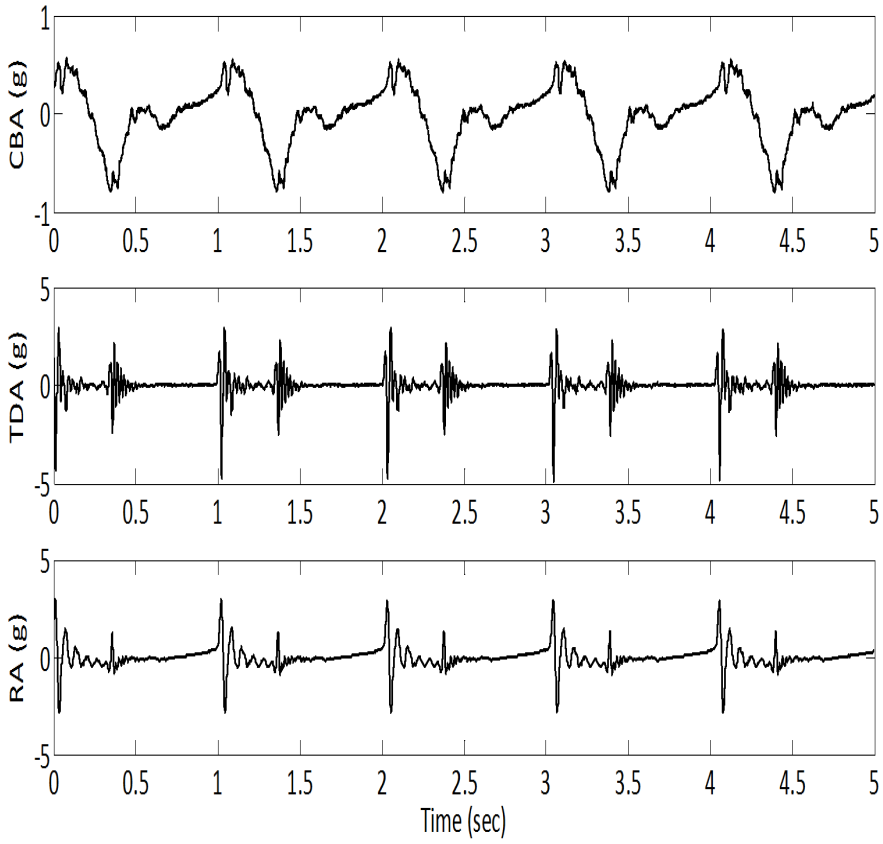


Figure 4-6. Sinusoidal test: passive case
CBA: car body acceleration, TDA: tire deflection accleration.
RA: road acceleration

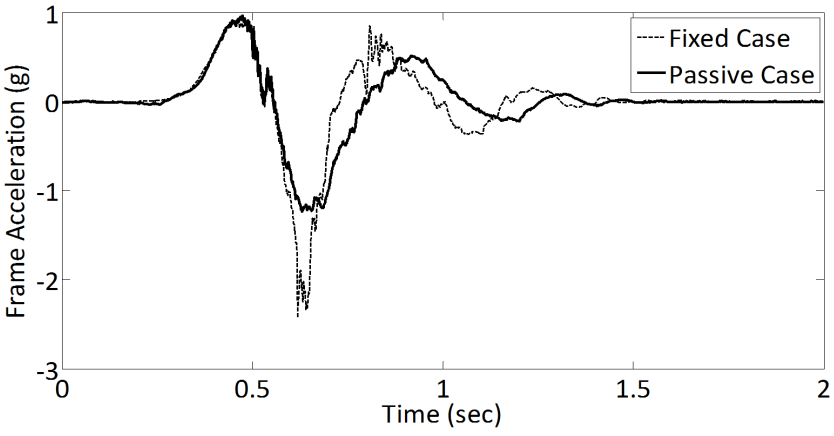


Figure 4-7. Drop test - car body acceleration

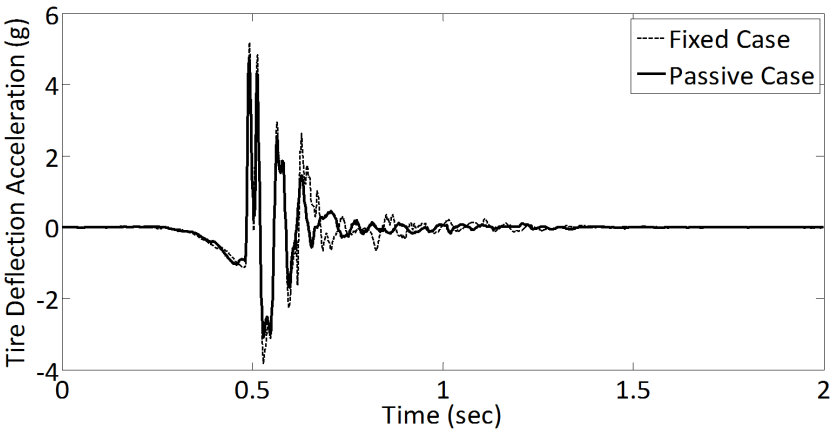


Figure 4-8. Drop test - tire deflection acceleration

cases. Figure 4-7 and Figure 4-8 shows the car body acceleration responses and tire deflection acceleration responses for the fixed and active cases.

### 4.2.5 Simulation

In order to study the behavior of the quarter car system at full scale as well as responses like suspension deflection, which are difficult to measure experimentally, and excitation scenarios that are difficult to implement experimentally, realistic simulations were carried out using MATLAB Simmechanics Second Generation. First, the system was modeled in Solidworks as shown in Fig. 4-9. Next, a Simmehanics model was developed. The mass/inertia properties used are the ones generated from the Solidworks model. The vertical strut and tire damping and stiffness used are the ones given in the “Renault Mégane Coupé” model [43]. The values are given in Table 2-1.

#### 4.2.5.1 Time Domain Simulation

In the time domain simulation, the vehicle traveling at a steady horizontal speed of $40mph$ is subjected to a road bump of height $8cm$. The Car Body Acceleration, Suspension Deflection, and Tire Deflection responses are compared between the constant stiffness and the passive variable stiffness cases. For the constant stiffness case, the control mass was locked at three different locations ($d = 40cm$, $d = 45.56cm$ and $d = 50cm$). The value $d = 45.56cm$ is the equilibrium position of the

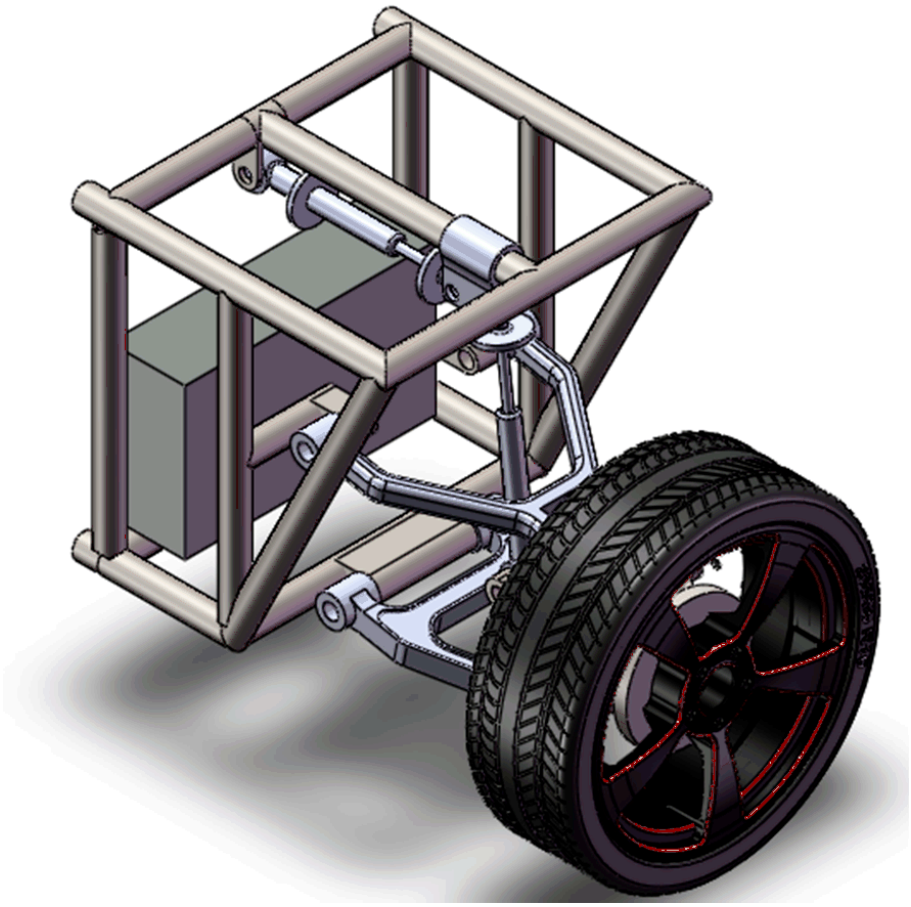

Figure 4-9. Solidworks quarter car model

control mass. Next, a simulation is performed for the passive case. The results are reported in Figures 4-10, 4-11, and 4-12 which are the the car body acceleration, suspension deflection, and tire deflection responses, respectively. Figure 4-13 shows the position history of the control mass for both the passive variable stiffness case.

#### 4.2.5.2 Frequency Domain Simulation

For the frequency domain simulation, an approximate frequency response from the road disturbance input to the performance vector given in (4–19), is computed using the

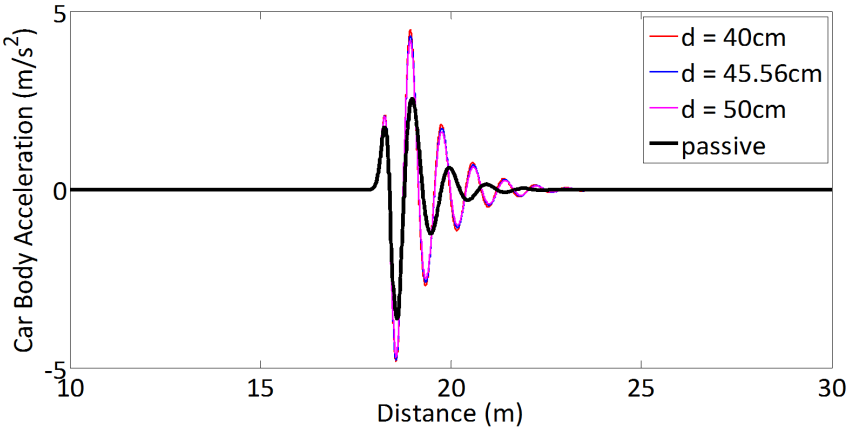


Figure 4-10. Time domain simulation - car body acceleration

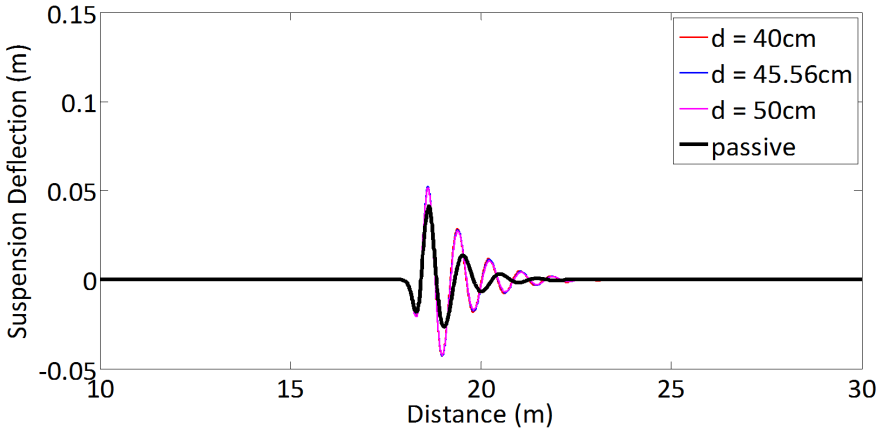


Figure 4-11. Time domain simulation - suspension deflection

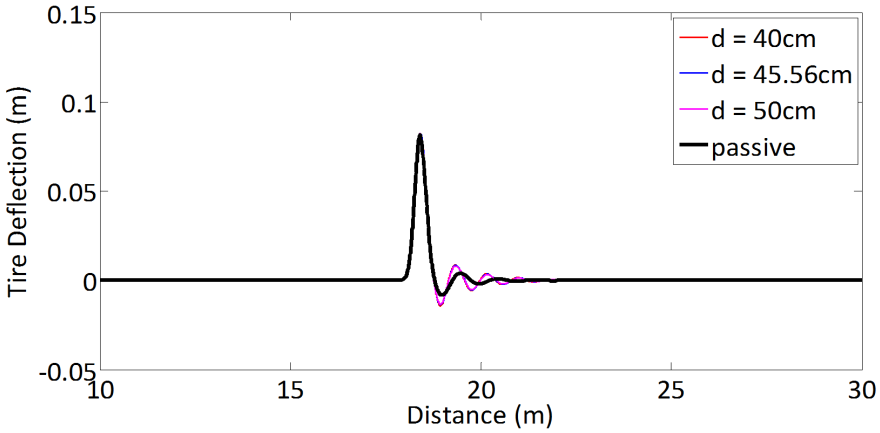


Figure 4-12. Time domain simulation: tire deflection

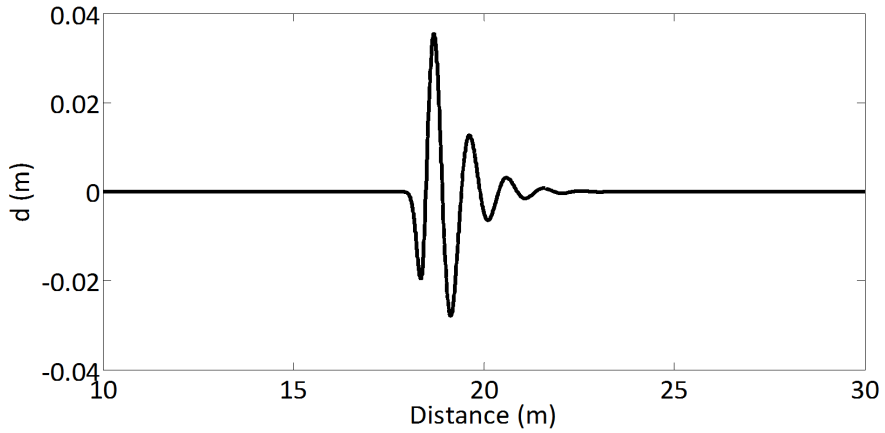


Figure 4-13. Time domain simulation - control mass position

notion of variance gain[57, 58]. The approximate variance gain is given by

$$G(j\omega) = \sqrt{\frac{\int_0^{2\pi N/\omega} z^2 \, dt}{\int_0^{2\pi N/\omega} A^2 \sin^2(\omega t) \, dt}}, \tag{4–84}$$

where $z$ denotes the performance measure of interest which is taken to be car body acceleration, suspension deflection, and tire deflection. The closed loop system is excited by the sinusoid $r = A\sin(\omega t), \;\; t \in [0, \;\; 2\pi N/\omega]$, where $N$ is an integer big enough to ensure that the system reaches a steady state. The corresponding output signals were recorded and the approximate variance gains were computed using (5–3). Figures 4-14, 4-15, and 4-16 show the variance gain plots for the car body acceleration, suspension deflection, and tire deflection respectively. The figures show that the variable stiffness suspension achieves better vibration isolation in the human sensitive frequency range [59](4-8Hz), and better handling beyond the tire hop frequency [19] ($>$59Hz).

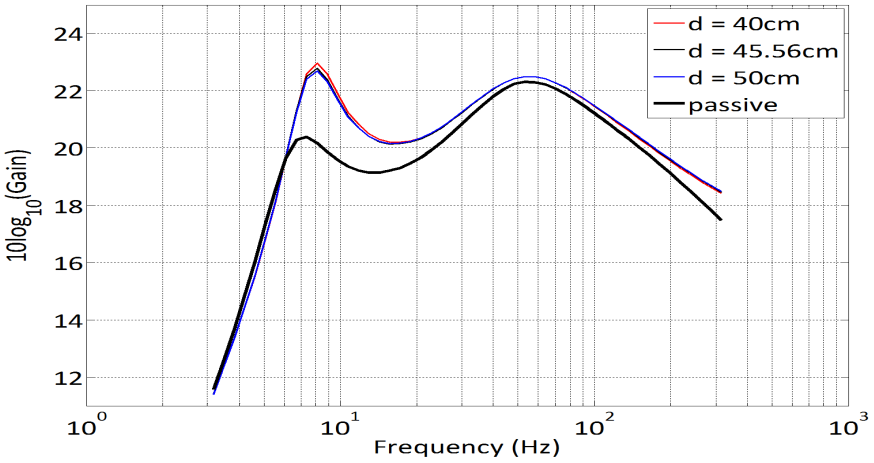


Figure 4-14. Frequency domain simulation - car body acceleration

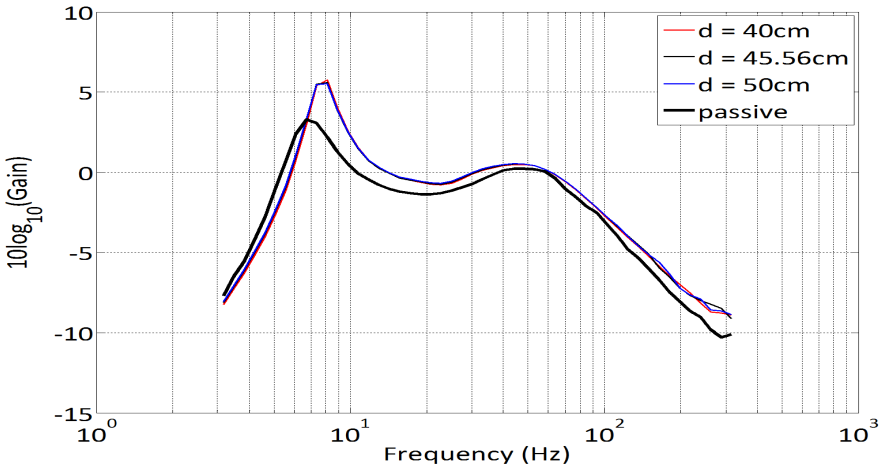


Figure 4-15. Frequency domain simulation - suspension deflection

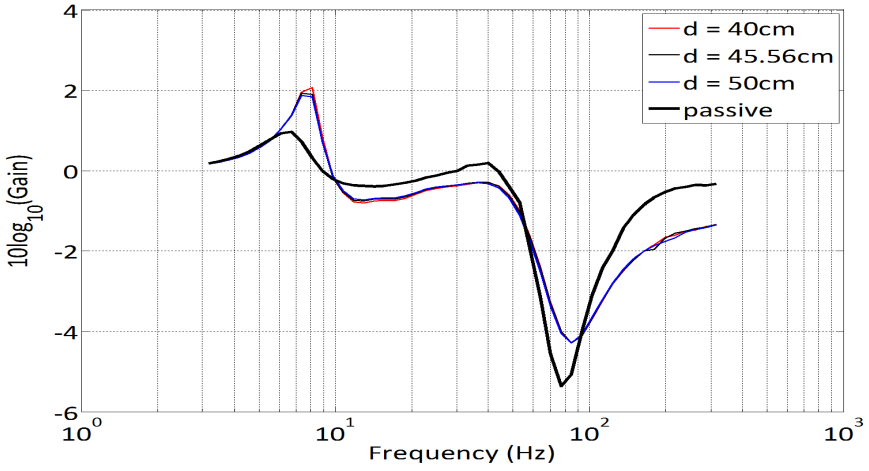


Figure 4-16. Frequency domain simulation - tire deflection

# CHAPTER 5
# VARIABLE STIFFNESS SUSPENSION SYSTEMS USING NONLINEAR ENERGY SINKS: ACTIVE AND SEMI-ACTIVE CASES

Nonlinear energy sinks (NES) are essentially nonlinear damped oscillators which are attached to a primary system[1] for the sake of vibration absorption and mitigation. Such attachments have been used extensively in engineering applications, particularly in vibration suppression or aeroelastic instability mitigation. The vibration of systems with essential (strongly or weakly) coupled nonlinearity has been studied extensively in literature[60–64]. It was shown in [61] that such attachments can be designed to act as a sink for unwanted vibrations generated by external impulsive excitations. The underlying dynamical phenomenon governing the passive energy pumping from a primary vibrating system to the attached nonlinear energy sink has be shown to be a resonance capture on a 1:1 manifold[64–69]. It was shown[68–70] that under certain conditions, vibration energy gets passively pumped from directly excited primary system to the nonlinear secondary system in a one-way irreversible fashion. Nonlinear passive absorbers can be designed with far smaller additional masses than the linear absorbers[62], thanks to the energy pumping phenomenon. This corresponds to a controlled one-way channeling of the vibration energy to a passive nonlinear structure where it localizes and diminishes in time due to damping dissipation. This allows nonlinear energy pumping to be used in coupled mechanical systems, where the essential nonlinearity of the attached absorber enables it to resonate with any of the linearized modes of the substructure[64].

In the previous chapter, “reciprocal actuation” concept was used to design a variable stiffness suspension system for isolating a car body from road disturbance[71]. The system is essentially a passive vibration isolation system in which the motion of the

[1] This refers to the main system whose vibration is intended to be absorbed

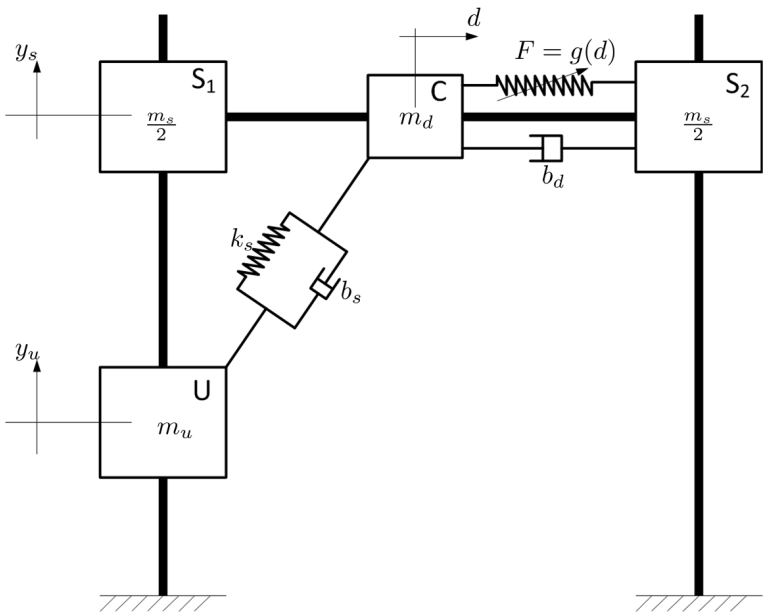


Figure 5-1. Orthogonal nonlinear energy sink (NES)

secondary linear attachment is made orthogonal to the primary system. The primary and secondary systems are coupled through the traditional suspension system. In this chapter, the concept is extended by using active and semi-active linear generators, controlled to mimic the behavior of nonlinear energy sinks, to drive the orthogonal secondary system[2] . The motivation for the use of NES is primarily due to their proven capability to achieve one-way irreversible energy pumping from the linear primary system to the nonlinear attachment. The goal therefore is to achieve a one-way irreversible energy pumping of the road disturbance to the secondary system whose vibration is orthogonal to the car body motion. A fairly general nonlinear function is used in this work, instead of cubic nonlinearity that is generally used.

## 5.1 Orthogonal Nonlinear Energy Sink

Fig. 5-1 shows the NES considered in this work. The term orthogonal NES is used to describe the concept because the direction of motion of the secondary system

[2] This refers to the vibration absorber or isolator

is orthogonal to the primary system. This is suitable, structurally, for the application in question. The subsystems $S_1$, $C$, and $S_2$ constitute the primary subsystem, and are allowed to slide vertically together as a unit of total sprung mass $m_s + m_d$. The subsystem $C$ is termed the control mass (or control subsystem). It, together with the nonlinear spring and the dashpot of damping coefficient $b_d$, constitute the secondary subsystem. The nonlinear function is defined as

$$F = g(d) = -k_1(l_{0_d} - d) - k_2 \sinh(\alpha_1(l_{0_d} - d)), \tag{5–1}$$

where $l_{0_d}$ is the free length of the idealized nonlinear spring. The nonlinear function used is fairly more general compared to the pure cubic nonlinearity that have been used in the past[72]. The Taylor series expansion is

$$F = -k_1(l_{0_d} - d) - k_2 \sum_{i=1}^{\infty} k_{2i-1}(\alpha_1)(l_{0_d} - d)^{2i-1}, \;\; k_{2i-1}(\alpha_1) > 0 \tag{5–2}$$

from which the generality obvious. The mass labeled $U$ is the unsprung mass, whose displacement $y_u$ is used as the source of disturbance to the system.

An approximate frequency response from the input $y_u$ to the sprung mass acceleration $\ddot{y}_s$ and the rattle space deflection $y_s - y_u$, is computed using the notion of variance gain ([57, 58]). The approximate variance gain is given by

$$G(j\omega) = \sqrt{\frac{\int_0^{2\pi N/\omega} z^2 \, dt}{\int_0^{2\pi N/\omega} A^2 \sin^2(\omega t) \, dt}}, \tag{5–3}$$

where $z$ denotes the performance measure of interest (sprung mass acceleration and rattle space deflection in this case). The system is excited by the sinusoid $r = A\sin(\omega t), \;\; t \in [0, \;\; 2\pi N/\omega]$, where $N$ is an integer big enough to ensure that the system reaches a steady state. The corresponding output signals were recorded and the approximate variance gains were computed using (5–3). The resulting variance

gain responses are shown in Figs. 5-2A, and 5-2B for the constant stiffness suspension (CSS)[3] , the variable stiffness suspension with linear energy sink (VSS:LES)[4] , and the variable stiffness suspension with nonlinear energy sink (VSS:NES) . The figures show that the variable stiffness suspension achieves better vibration isolation, with a significant improvement from the linear energy sink case to the nonlinear energy sink case. As shown in Fig. 5-2B, the improvement gained in vibration isolation results in a corresponding performance degradation in the rattle space deflection. However, when compared with the improvement in the vibration isolation, there is an overall improvement in performance associated with the use of the variable stiffness suspension with nonlinear energy sink. This agrees with the usual trade-off in suspension design [19]. The performance improvement can further be increased by transitioning from LES in low frequency range ($< 8Hz$) to NES in high frequency range ($> 8Hz$).

## 5.2 Active Case

In the active case, a hydraulic actuator is used to drive the control mass. The quarter car model of the suspension system considered is shown in Fig 5-3. It is composed of a quarter car body, wheel assembly, two spring-damper systems, road disturbance, and lower and upper wishbones. The points O,A, and B are the same as shown in the variable stiffness mechanism of Fig 4-1. The horizontal control force, exerted by the hydraulic actuator H, controls the position $d$ of the control mass $m_d$ which, in turn, controls the overall stiffness of the mechanism. The control force is

[3] Here, the position of the control mass is fixed. This corresponds to the traditional constant stiffness suspension system

[4] In this case, the control mass is allowed to move under the influence of a linear horizontal spring and damper. This is the case reported in [71]

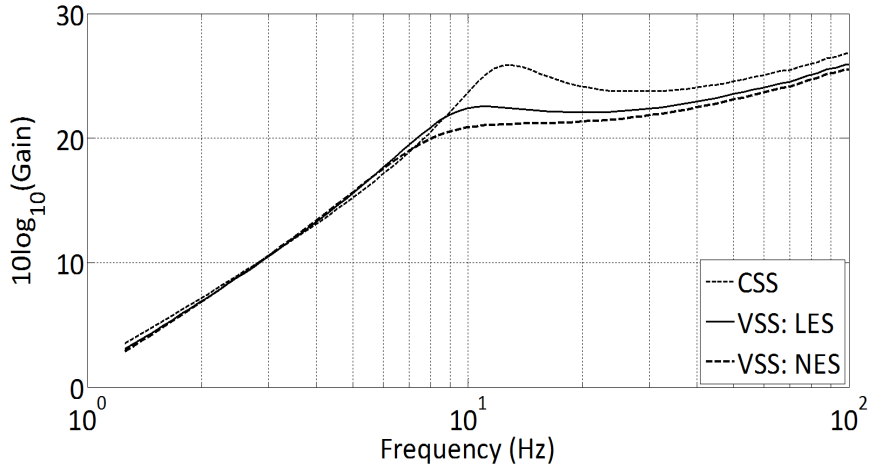


A Car body acceleration

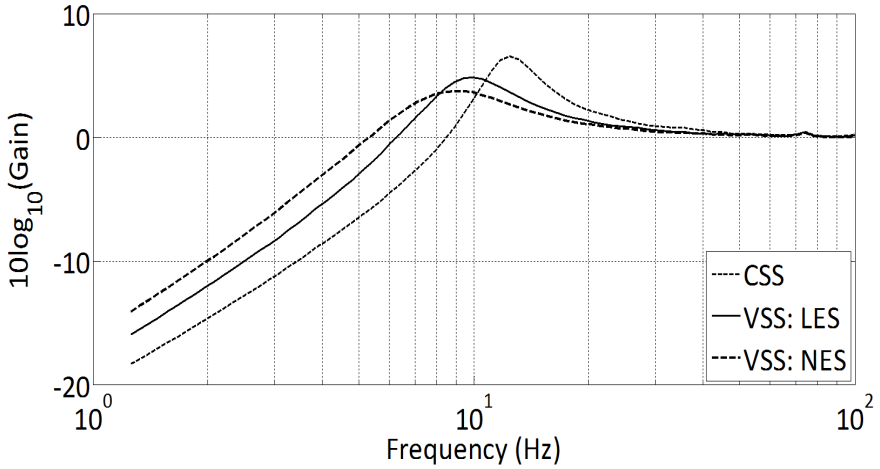


B Rattle space displacement

Figure 5-2. Variance Gain

designed in subsequent sections to mimic the orthogonal NES introduced in the previous section. The tire is modeled as a linear spring of spring constant $k_t$.

The assumptions adopted in Fig 5-3 are summarized as follows:

1. The lateral displacement of the sprung mass is neglected, i.e only the vertical displacement $y_s$ is considered.
2. The wheel camber angle is zero at the equilibrium position and its variation is negligible throughout the system trajectory.
3. The springs and tire deflections are in the linear regions of their operating ranges.

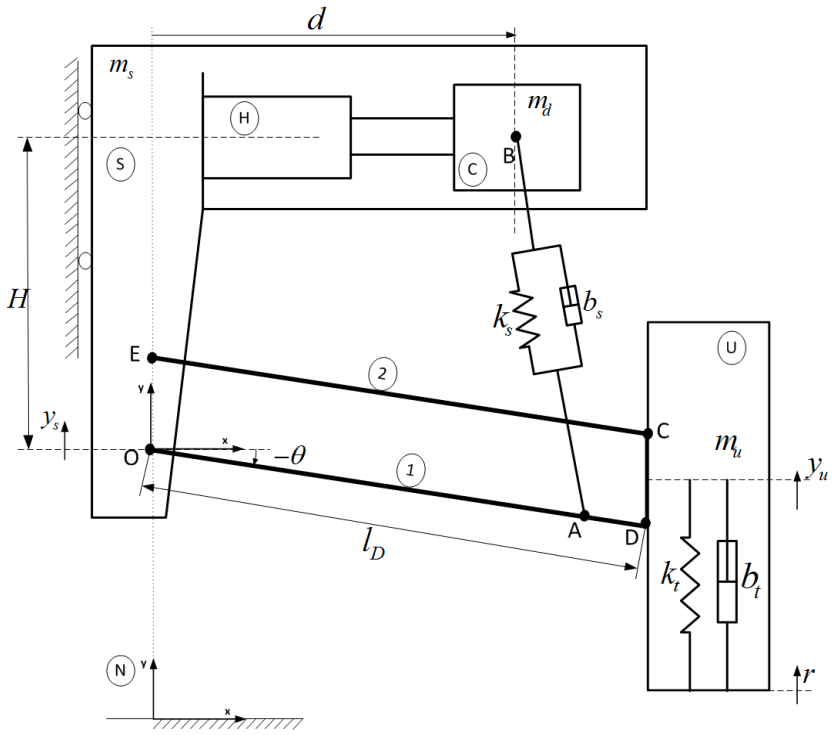


Figure 5-3. Quarter car model - active case

### 5.2.1 Control Masses and Actuator Dynamics

The dynamics of of the hydraulic actuator is given by[73, 74]

$$\dot{P}_L = -\alpha A v_p - \beta P_L + \gamma x_v \sqrt{P_s - sgn(x_v) P_L}, \tag{5–4}$$

$$\dot{x}_v = -\frac{1}{\tau} x_v + \frac{K}{\tau} u, \tag{5–5}$$

$$F = A P_L, \tag{5–6}$$

where $A$ is the pressure area in the actuator, $P_L$ is the load pressure, $v_p = \dot{d}$ is the actuator piston velocity, $F$ is the output force of the actuator, $\alpha, \beta,$ and $\gamma$ are positive parameters depending on the actuator pressure area, effective system oil volume,

effective oil bulk modulus, oil density, hydraulic load flow, total leakage coefficient of the cylinder, discharge coefficient of the cylinder, and servo valve area gradient, $x_v$ is the spool valve position, $\tau$ is the actuator electrical time constant, $K$ is the DC gain of the four-way spool valve, and $u$ is the input current to the servo valve.

### 5.2.2 Control Development

In terms of the Force,$F$ exerted by the actuator, the actuator dynamics in (6–75) is written as

$$\dot{F} = -\beta F - \alpha A^2 \dot{d} + \gamma A \bar{u}, \tag{5–7}$$

where

$$\bar{u} = x_v \sqrt{P_s - \text{sgn}(x_v)\frac{F}{A}} \tag{5–8}$$

is a fictitious control variable, from which the slow component (or envelop) of the control is obtained, after singular perturbation of the valve dynamics. Let the actuator force tracking error be defined as

$$e = F - F_d, \tag{5–9}$$

where

$$F_d = -k_1(l_{0_d} - d) - k_2 \sinh(\alpha(l_{0_d} - d)) - b_d \dot{d}, \tag{5–10}$$

is the desired force to be tracked by the actuator force dynamics in (5–45). Taking the derivative of (5–9) yields the actuator force tracking error dynamics

$$\dot{e} = -\beta F \alpha A^2 \dot{d} + \gamma A \bar{u} - \dot{F}_d \tag{5–11}$$

$$= -\beta e - \widetilde{\dot{F}}_d + \alpha A \left( \bar{u} - \frac{\alpha A}{\gamma} \dot{d} - \frac{\beta}{\gamma A} F_d - \frac{1}{\gamma A} \hat{\dot{F}}_d \right) \tag{5–12}$$

$$= -\beta e - \widetilde{\dot{F}}_d + \alpha A \left( \bar{u} - Y^T \Theta \right), \tag{5–13}$$

where the regression matrix $Y$ and the unknown parameter vector $\Theta$ are given by

$$Y = \begin{bmatrix} \dot{d} & F_d & \hat{\dot{F}}_d \end{bmatrix}^T, \tag{5–14}$$

$$\Theta = \begin{bmatrix} \frac{\alpha A}{\gamma} & \frac{\beta}{\gamma A} & \frac{1}{\gamma A} \end{bmatrix}^T, \tag{5–15}$$

and $\hat{\dot{F}}_d$ is an approximation of the desired force $\dot{F}_d$ obtained using the high gain observer [55]

$$\varepsilon_2 \dot{\mathbf{p}} = A_{hg}\mathbf{p} + \mathbf{b}_{hg} F_d \tag{5–16}$$

$$\hat{\dot{F}}_d = \left( \frac{1}{\varepsilon_2} \mathbf{c}_{hg}^T \mathbf{p}, a, b \right) \tag{5–17}$$

where the saturation function $(\ldots)$ is given by

$$(\chi, a, b) = \begin{cases} a, & \text{if } \chi < a \\ \chi & \text{if } a \leq \chi \leq b \\ b & \text{if } \chi > b, \end{cases} \tag{5–18}$$

and

$$A_{hg} = \begin{bmatrix} -1 & 1 \\ -1 & 0 \end{bmatrix}, \mathbf{b}_{hg} = \begin{bmatrix} 1 \\ 1 \end{bmatrix}, \mathbf{c}_{hg} = \begin{bmatrix} 0 \\ 1 \end{bmatrix}, \varepsilon_2 \ll 1.$$

The is done because , as can be seen in (5–10), $\dot{F}_d$ contains unmeasurable signal $\ddot{d}$. It can be shown (see [55]) that the estimation error, $\tilde{\dot{F}}_d = \dot{F}_d - \hat{\dot{F}}_d$ decays, in the fast time scale, to the ball $|\tilde{\dot{F}}_d| < O(\varepsilon_2)$. The saturation function is used to overcome the peaking phenomenon associated with high gain observers[55]. The fictitious control $\bar{u}$ is then designed as follows

$$\bar{u} = Y^T \hat{\Theta} - k_1 e - c_1 \operatorname{sgn}(e), \tag{5–19}$$

where $\hat{\Theta}$ is an adaptive estimate of $\Theta$ – the adaptation law will be designed in the subsequent sections, $k_1$ and $c_1$ are control gains. Thus the closed loop error dynamics,

obtained by substituting (6.4.2) into (5–13), is given by

$$\dot{e} = -(\beta + k_1\gamma A)\, e - \widetilde{\dot{F}}_d - c_1\gamma A \,\mathrm{sgn}(e) - \gamma A Y^T \widetilde{\Theta}, \tag{5–20}$$

where the parameter estimation error $\widetilde{\Theta}$ is given by

$$\widetilde{\Theta} = \Theta - \hat{\Theta}. \tag{5–21}$$

In order to simplify the controller design for the actuators, the spool valve dynamics is reduced, using a singular perturbation technique [75]. The control input is designed as

$$u = -K_f x_v + \frac{1 + KK_f}{K} u_s, \tag{5–22}$$

where $u_s$ is a slow control in time and $K_f$ is a positive design control gain. Consequently, the valve psuedo-closed loop dynamics is given by

$$\varepsilon \dot{x}_v + x_v = u_s, \tag{5–23}$$

where

$$\varepsilon = \frac{\tau}{1 + KK_f} \tag{5–24}$$

is the perturbation constant. The pseudo-closed loop in (6–111) has a quasi-steady state solution, $x_{v_i}(\varepsilon = 0) \triangleq \bar{x}_{v_i}$, given by

$$\bar{x}_v = u_s. \tag{5–25}$$

Using the fast time scale $\nu = \frac{t}{\varepsilon}$ and Tichonov's Theorem [75], the valve dynamics is decomposed into fast and slow time scales as follows

$$x_v = \bar{x}_v + \eta + O(\varepsilon), \tag{5–26}$$

$$\frac{d\eta}{d\nu} = -\eta, \tag{5–27}$$

where $\eta(\nu)$ is a boundary layer correction term. It is seen that $\eta(\nu)$ decays exponentially in the fast time scale. Typically, the time constant $\tau$ in the actual system is designed to satisfy $0 < \varepsilon \ll 1$ [76]. Therefore, by choosing the control gain $K_f$ large enough, the perturbation constant can be made as small as possible. As a result, $\eta + O(\varepsilon)$ becomes negligibly small, and the fictitious control becomes

$$\bar{u} = u_s \sqrt{P_s - \text{sgn}(u_s)\frac{F}{A}}. \tag{5–28}$$

Assuming sufficient pressure for the hydraulic pump, the term inside the square root operator is taken as positive. Thus

$$\text{sgn}(\bar{u}) = \text{sgn}(u_s), \tag{5–29}$$

which implies that

$$u = \bar{u}\left(P_s - \text{sgn}(\bar{u})\frac{F}{A}\right)^{-\frac{1}{2}}. \tag{5–30}$$

### 5.2.3 Stability Analysis

This section presents the Lyapunov based stability analysis of the closed loop error dynamics in (5–20). The adaptation law for the parameter estimation is designed. It is also shown that if the control gains are chosen to satisfy certain sufficient conditions, then the actuator force tracking error will approach zero asymptotically .

**Theorem 5.1.** *Given the adaptive update law*

$$\dot{\hat{\Theta}} = -\Gamma Y e, \tag{5–31}$$

*where $\Gamma$ is a positive definite adaptation gain matrix. If the control gain $c_1$ is chosen to satisfy the following sufficient conditions*

$$c_1 \geq \frac{|O(\varepsilon_2)|}{\gamma A} \geq \frac{|\widetilde{\dot{F}}_d|}{\gamma A}, \tag{5–32}$$

*then the actuator tracking error in* (5–9) *approaches zero asymptotically. i.e*

$$e(t) \to 0, \ \textit{as} \ t \to \infty.$$

*Proof.* Consider the following positive definite Lyapunov function candidate

$$V = \frac{1}{2}e^2 + \frac{\gamma A}{2}\widetilde{\Theta}^T \Gamma^{-1} \widetilde{\Theta}, \tag{5–33}$$

Taking the first time derivative and substituting the closed loop error dynamics in (5–20) yields

$$\dot{V} = e\dot{e} - \gamma A \widetilde{\Theta}^T \Gamma^{-1} \dot{\hat{\Theta}} \tag{5–34}$$

$$= e\left(-\left(\beta + k_1 \gamma A\right) e - \widetilde{\dot{F}}_d - c_1 \gamma A \, \mathrm{sgn}(e) - \gamma A Y^T \widetilde{\Theta}\right) - \gamma A \widetilde{\Theta}^T \Gamma^{-1} \dot{\hat{\Theta}}, \tag{5–35}$$

which, after applying the update laws in (5–31), becomes

$$\dot{V} \leq -\left(\beta + k_1 \gamma A\right) e^2 + |\widetilde{\dot{F}}_d||e| - c_1 \gamma A |e|. \tag{5–36}$$

Using the sufficient condition in (5–32), the inequality in (5–36) yields

$$\dot{V} \leq -\left(\beta + k_1 \gamma A\right) e^2 \leq 0. \tag{5–37}$$

From (5–33) and (5–37), it follows that $V(t)$ is bounded, which also implies that $e(t),$ and $\widetilde{\Theta}(t)$ are bounded. Using the boundedness of $\hat{\dot{F}}_d(t)$ , from (5–17), it follows from (5–20) that $\dot{e}(t)$ is bounded, which implies that the signal $e(t)$ is uniformly continuous. Integrating (5–37) yields

$$\lim_{t \to \infty} \int_0^t e(t)^2 dt = \frac{V(0) - V(\infty)}{\beta + k_1 \gamma A} \in \mathcal{L}_\infty. \tag{5–38}$$

Thus, using Barbalat's Lemma (Section 8.3, [55]), it can be shown that

$$e(t) \to 0, \ \text{as} \ t \to \infty.$$

□

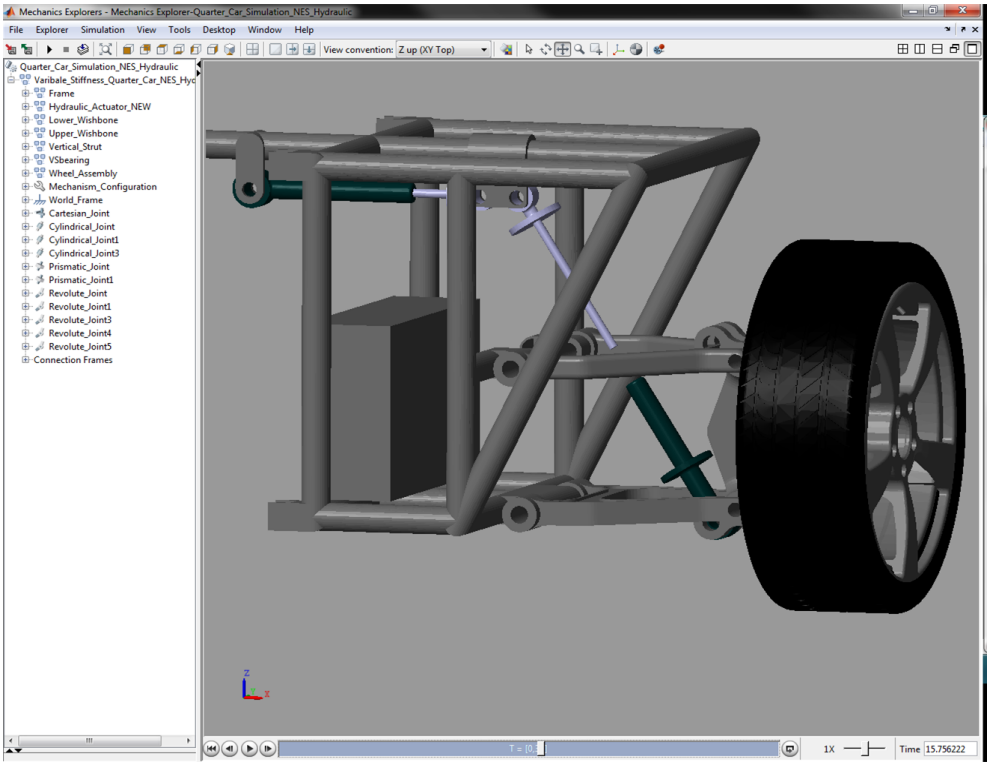


Figure 5-4. Simmechanic model

Table 5-1. Dynamic parameter values

| Parameter | Value |
|---|---|
| $m_s$ | 315 $kg$ |
| $m_u$ | 37.5 $kg$ |
| $b_s$ | 1500 $N/m/s$ |
| $k_s$ | 29500$N/m$ |
| $k_t$ | 210000 $N/m$ |

### 5.2.4 Simulation

In order to study the behavior of the quarter car system to different road excitation scenarios, as well as measure responses like suspension deflection, realistic simulations were carried out using MATLAB Simmechanics. First, the system was modeled in Solidworks, and then translated to a Simmechanic model (Fig. 5-4). The vertical strut and tire damping and stiffness used are the ones given in the “Renault Mégane Coupé” model ([43]). The values are given in Table 5-1. The values of the hydraulic parameters were obtained emperically in [73], and are given in Table 5-4.

Table 5-2. Hydraulic parameter values

| Parameter | Value |
|---|---|
| $\alpha$ | $4.515 \times 10^{13}\ N/m^5$ |
| $\beta$ | $1\ sec^{-1}$ |
| $\gamma$ | $1.545 \times 10^{9}\ N/m^{5/2}kg^{1/2}$ |
| $\tau$ | $1/30\ sec$ |
| $P_s$ | $10342500\ Pa$ |
| $A$ | $3.35 \times 10^{-4}\ m^2$ |

In the simulation, the vehicle traveling at a steady horizontal speed of $40mph$ is subjected to a road bump of height $10cm$. The Car Body Acceleration, Suspension Travel, and Tire Deflection responses are measured. The suspension travel is defined as the vertical distance between the centers of mass of the sprung and unsprung masses, and the tire deflection as the difference between the center of mass of the unsprung mass and the road height. Simulations were carried out for the constant stiffness and the variable stiffness suspension systems. For the constant stiffness suspension, the control mass was locked at a fixed position corresponding to the equilibrium position of the control mass for the variable stiffness system. Moreover, for each stiffness type, both passive and active cases were considered. The passive case of the constant stiffness suspension is the traditional passive suspension, while in the active case, the passive springdamper is replaced with a hydraulic actuator controlled to track a skyhook[31] suspension force. On the other hand, the passive case of the variable stiffness suspension corresponds to the LES, while the active case corresponds to the NES. The results obtained are reported in Figures 5-5, through 5-9. Table 5-3 shows the variance gains for the different responses. Fig 5-5 shows the car body acceleration, which is used here to describe the ride comfort. The lower the car body acceleration, the better the ride comfort. As seen in the figure, the NES is the most ”ride friendly” suspension, outperforming the skyhook control. As shown in Fig 5-6, associated with this improvement is a corresponding degradation in the suspension travel. This agrees with the observation made in earlier sections, as well as the well know trade off between

Table 5-3. Variance gain values

| | Constant Stiffness Passive | Constant Stiffness Active | Variable Stiffness Passive | Variable Stiffness NES |
|---|---|---|---|---|
| Car Body Acceleration ($s^{-1}$) | 109.0389 | 64.2818 | 65.6127 | 42.9737 |
| Suspension Defelction | 80.8817 | 80.8725 | 84.3834 | 82.6723 |
| Tire Travel | 1.0562 | 1.0100 | 1.0188 | 1.0152 |

ride comfort and suspension deflection. Fortunately, the degradation in suspension deflection is not as much as the improvement gained in the ride comfort, resulting in an overall better performance. Moreover, the suspension travel performance can be improved by designing the a gain scheduled controller, using an observed frequency of the sprung mass as the scheduling variable. AS a result, the NES can be turned on and off depending on the frequency, as described previously. Figure 5-8 shows the position history of the control mass for the variable stiffness suspension, from which the boundedness of the motion of the control mass is seen. The maximum displacement of the control mass from the equilibrium position is about 7cm. This implies that the space requirement for the control mass is small, which further demonstrates the practicality of the system. Fig 5-7 shows that there is no significant reduction in the tire deflection. Thus, the suspension systems are approximately equally ”road friendly”. It is also seen, in Fig 5-9, that the hydraulic force from the NES is about $60\%$ of that from the skyhook counterpart. This translates to a lower power requirement for the proposed system.

### 5.3 Semi-active Case

In the semi-active case two semi-active devices are used; a vertical, mounted along the vertical strut, and a horizontal, mounted along the horizontal strut, semi-active devices. The semi-active device considered is the MR-damper.

The quarter car model of the suspension system considered is shown in Fig 5-10. It is composed of a quarter car body, wheel assembly, two spring- MR damper systems,

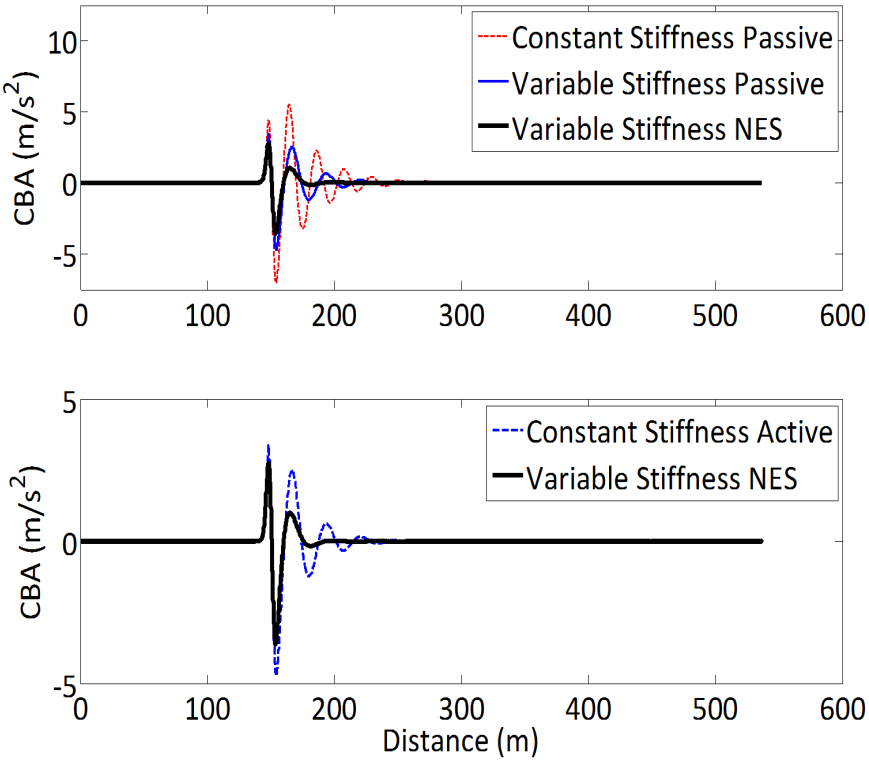


Figure 5-5. Car body acceleration (CBA)

road disturbance, and lower and upper wishbones. The points O,A, and B are the same as shown in the variable stiffness mechanism of Chapter 3. The motion of the control mass, which in turns determine the effective stiffness of the suspension system, is influenced by the MR1. The MR1 damper force is designed in subsequent sections to mimic the orthogonal NES introduced in the previous section and the MR2 damper force is designed to mimic the traditional skyhook[31] damping force. The tire is modeled as a linear spring of spring constant $k_t$.

The assumptions adopted in Fig 5-10 are summarized as follows:

1. The lateral displacement of the sprung mass is neglected, i.e only the vertical displacement $y_s$ is considered.
2. The wheel camber angle is zero at the equilibrium position and its variation is negligible throughout the system trajectory.

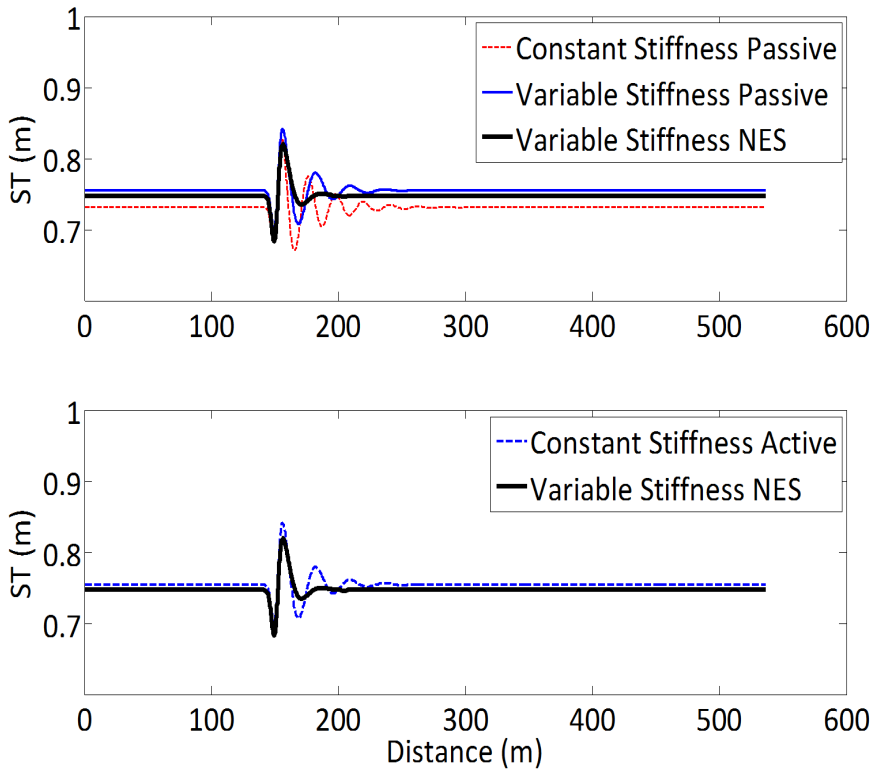


Figure 5-6. Suspension travel (ST)

3. The springs and tire deflections are in the linear regions of their operating ranges. The damping characteristics f the considered semi-active device can be changed by a control current. However, there is no corresponding energy input into the system as a result of the control current. This implies a passivity constraint on the MR-damper model. The control current is designed to mimic a desired force as close as possible, while enforcing the passivity constraint. This approach has been used in the past for semi-active control design [9, 10, 77].

### 5.3.1 MR-damper Modeling

The relationship between the MR-damper control current and the damping force exhibit a nonlinear phenomenon, and as a result, MR-damper based vibration control is a challenging tasks. Different damper models have been developed to capture the behavior of MR-dampers. Generally, the approaches that exists in literature can be

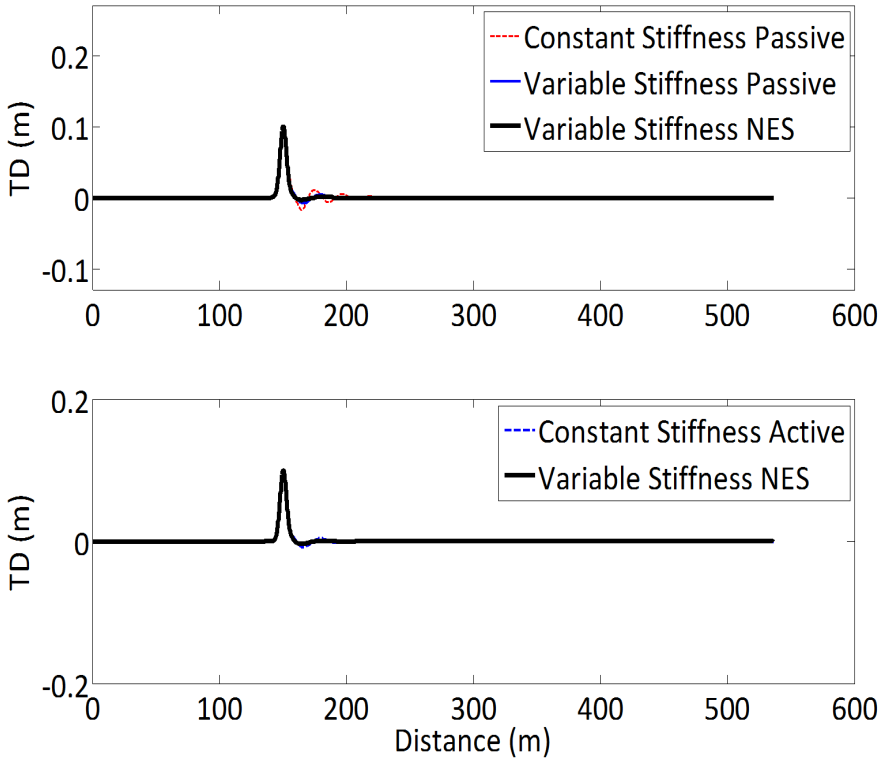


Figure 5-7. Tire deflection(TD)

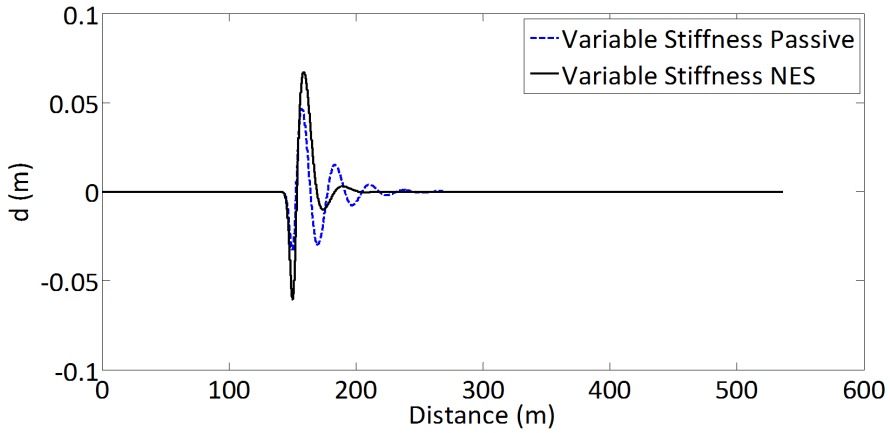


Figure 5-8. Control mass displacement

grouped into parametric and nonparametric [78, 79]. The parametric modeling technique characterizes the MR-damper device as a collection of (linear and/or nonlinear) springs, dampers, and other physical elements. A number of studies have addressed the

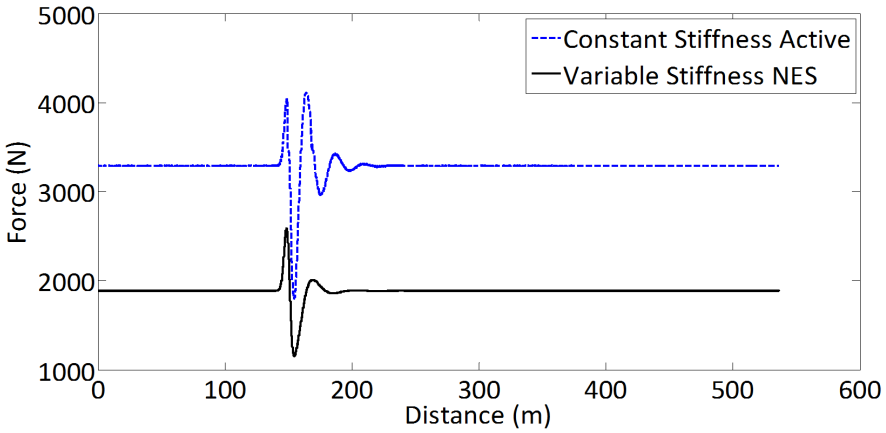


Figure 5-9. Actuator forces

parametric modeling of MR-dampers. One of the early models is Bouc-Wen model [80] which was derived from a Markov-vector formulation to model nonlinear hysteric systems. Later, the Bingham viscoelastic-plastic model was described by Shames and Cozzarelli [81]. Spencer and co-workers [26] developed a phenomenological model that accurately portrays the response of an MR-damper in response to cyclic excitations. This is a modified Bouc-Wen model governed by ordinary differential equations. Bouc-Wen based models in semi-active seismic vibration control have proven to be easy to use and numerically amenable. Other authors have studied parametric model of MR-dampers, emphasizing the difference between the pre-yield viscoelastic region and the post-yield viscous region as a key aspect of the damper. One of such model is given in [38], where the damper force is modeled using the nonlinear static semi-active damper model. The allows fulfilling the passivity constraint of MR-damper.

On the other hand, nonparametric modeling employs analytical expressions to describe the characteristics of the modeled device based on both testing data analysis and device working principle [78]. Although parametric models effectively characterizes the MR-dampers at fixed values of the control current, they do not include the magnetic field saturation that is inherent in MR-dampers. The representation of the magnetic field saturation is crucial in accurately using the MR-damper model for design analysis

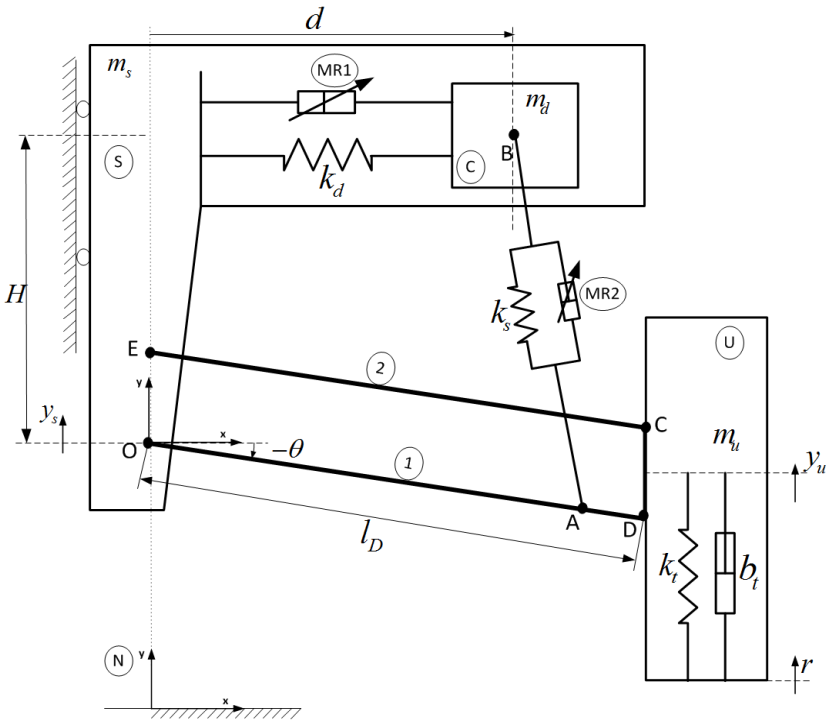


Figure 5-10. Quarter car model - Semi-active case

and control development. Recently, Song et. al [78] proposed a nonparametric model where the characteristics of a commercial MR-damper are represented by a series of continuous functions and differential equations, which are tractable using numerical simulation techniques. This model was used in [77] and will also be used in this work to represent the dynamics of the MR-damper. The nonparametric model is shown schematically in Figure 5-11. The input to the model is the relative velocity, $v(t)$, across the damper terminals, and the output is the damper force, $F(t)$. The modeled aspect of the MR-damper are:

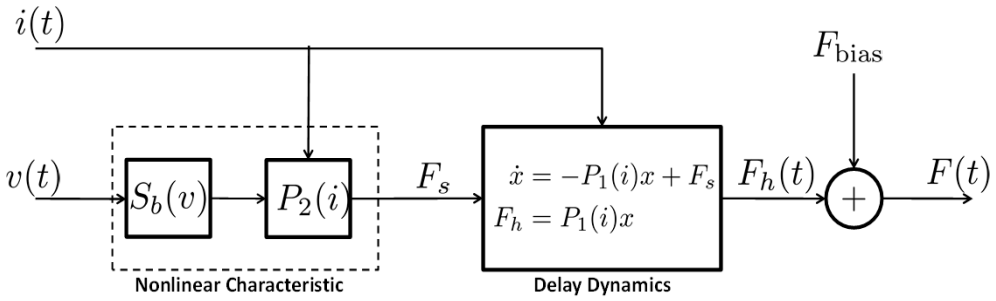


Figure 5-11. Nonparametric MR-damper model

**Maximum Damping Force,** $P_2(i(t))$

This is described using a polynomial function of the control current, $i(t)$, as

$$P_2(i) = A_0 + A_1 i + A_2 i^2 + A_3 i^3 + A_4 i^4, \tag{5–39}$$

where $A_j, j = 0 - 4$ are the polynomial coefficients with appropriate units.

**Shape Function** $S_b(v(t))$

This is used to preserve the wave-shape correlation between the damper force and the relative velocity across the damper, and is given by

$$S_b(v) = \frac{(b_0 + b_1|v_r|)^{b_2 v_r} - (b_0 + b_1|v_r|)^{-b_2 v_r}}{b_0^{b_2 v_r} + b_0^{-b_2 v_r}}, \tag{5–40}$$

where

$$v_r = v - v_0, \tag{5–41}$$

and $b_0 > 0, b_1 > 0, b_2 > 0, v_0$ are constants.

**Delay Dynamics** $G(s, i(t))$

A first-order filter is used to create the hysteresis loop observed in experimental data. It is given in state space form as

$$\begin{aligned} \dot{x} &= -P_1(i)x + F_s = -P_1(i)x + P_2(i)S_b(v) \\ F_h &= P_1(i)x, \end{aligned} \tag{5–42}$$

where $x$ is the internal state of the filter and $P_1(i(t))$ is a polynomial function of the control current given by

$$P_1(i) = h_0 + h_1 i + h_2 i^2, \tag{5–43}$$

where $h_j, j = 0 - 2$ are polynomial coefficients with appropriate units. It is worth noting that the condition

$$P_1(i) > 0 \tag{5–44}$$

is imposed on $P_1(i(t))$ in order to guarantee a decaying solution.

**Offset Function, $F_{\text{bias}}$**

In some cases, the damping force is not centered at zero because of the effect of the gas-charged accumulator in the damper. The force bias $F_{\text{bias}}$ is included in the model to capture this effect, and as result, the overall damper force is given by

$$F(t) = F_h + F_{\text{bias}}. \tag{5–45}$$

Table 5-4 shows the optimal values of the MR-damper model obtained from experimental data via an optimization process [78]. In terms of the input $v(t)$ and output $F(t)$, the overall dynamics of the MR-damper is given by

$$\dot{F}_h = -P_1(i)F_h + P_1(i)S_b(v)P_2(i) \tag{5–46}$$

$$F(t) = F_h + F_{\text{bias}} \tag{5–47}$$

### 5.3.2 Control Development

The schemes used for the desired damper forces are the NES, and skyhook based control forces

$$f_{d_H} = k_1 \sinh(\alpha_1(l_{0_d} - d)), \tag{5–48}$$

$$f_{d_V} = b_{\text{sky}}\dot{y}_s, \tag{5–49}$$

Table 5-4. MR-damper parameter values

| Parameter | Value |
|---|---|
| $A_0$ | 164.8 |
| $b_0$ | 5.8646 |
| $h_2$ | 566 |
| $A_1$ | 1316.5 |
| $b_1$ | 0.0060 |
| $v_0$ | 0.6248 |
| $A_2$ | 1407.8 |
| $b_2$ | 0.2536 |
| $F_{\text{bias}}$ | 0 |
| $A_3$ | -1562.8 |
| $h_0$ | 299.7733 |
| $A_4$ | 388.8 |
| $h_1$ | -210.32 |

where $f_{d_i}, i = \{H, V\}$ are the corresponding horizontal and vertical desired forces respectively, $k_1$ and $\alpha_1$ are positive constants used to tune the performance of the NES control, and $b_{\text{sky}}$ is the damping coefficient of the skyhook damper[5] .

#### 5.3.2.1 Open Loop Tracking Error Development

Although the MR damper parameter values given in Table 5-4 were determined experimentally, they can change over time due to usage and other causes. As a result, an adaptive tracking control for the MR damping force is developed. To this effect, it is assumed that the coefficients of the polynomial $P_2(i)$ are unknown. Also, the desired control force may not generally satisfy the passivity constraint at a given instant. At the instances when the passivity constraint is violated, the desired damping force lies outside the "trackable" passivity region of the MR damper. In order to ensure a valid tracked desired damping force, the force $f_{d_i}$ given in (5–48) is "clipped" in the passivity region. Using the Final Value Theorem, the steady state MR damper force, from (5–46),

[5] a vertical fictitious damper between the sprung mass and inertial frame

is given by

$$F_{ss} = S_b(v)P_2(i). \tag{5–50}$$

Thus, the tracked desired damper force is obtained by "clipping" $f_d$ as follows

$$F_d(f_{d_i}, v) = \begin{cases} S_b(v)\underline{P}_2 & \text{if} \quad v_r f_d \leq v_r S_b(v)\underline{P}_2 \\ f_{d_i} & \text{if} \quad v_r S_b(v)\underline{P}_2 < v_r f_d < v_r S_b(v)\overline{P}_2 \\ S_b(v)\overline{P}_2 & \text{if} \quad v_r f_d \geq v_r S_b(v)\overline{P}_2 \end{cases} \tag{5–51}$$

where

$$\underline{P}_2 = \min_{[0 \quad i_{\max}]} \{P_2(i)\} \tag{5–52}$$

$$\overline{P}_2 = \max_{[0 \quad i_{\max}]} \{P_2(i)\}, \tag{5–53}$$

and $i_{\max}$ is the maximum current that can be sent to the MR damper. Now, let

$$e = F - F_d \tag{5–54}$$

be the tracking error of the damper force, Taking the first time derivative of (5–54) yields

$$\dot{e} = \dot{F} = -P_1 F + S_b P_1 P_2 \tag{5–55}$$

$$= -P_1(e + F_d) + S_b P_1 P_2. \tag{5–56}$$

The response of MR dampers are very fast compared to the vibrating mechanical system [26, 82]. Hence, the commanded desired force $F_d(\mathbf{e}, \dot{\mathbf{e}}, v)$ is assumed to be fairly constant compared to the dynamics of the MR damper. Adding and subtracting the term $P_1(-F_d + S_b\hat{P}_2)$ yields the open loop error system

$$\dot{e} = -P_1 e + P_1 S_b(P_2 - \hat{P}_2) + P_1\alpha(i), \tag{5–57}$$

where

$$\alpha(i) = -F_d + S_b \hat{P}_2, \tag{5–58}$$

and $\hat{P}_2$ is an adaptive estimate of the polynomial $P_2(i)$. The update law is designed subsequently.

#### 5.3.2.2 Closed Loop Error System Development

First, a close approximation of the polynomial $P_2(i)$ is given within the operating interval. Given the bounds $\underline{P}_2$ and $\overline{P}_2$, the polynomial $P_2(i)$ is approximated in the interval $[0 \quad i_{max}]$ as

$$P_2(i) = \underline{P}_2 + \frac{i}{i_{max}} \left( \overline{P}_2 - \underline{P}_2 \right) + \beta(i), \tag{5–59}$$

where

$$\beta(i) = i(i - i_{max}) \left( \theta_0 + i\theta_1 + i^2\theta_2 \right), \tag{5–60}$$

is chosen to satisfy the constraints $\beta(0) = \beta(i_{max}) = 0$, which implies that $P_2(0) = \underline{P}_2$ and $P_2(i_{max}) = \overline{P}_2$. The approximation is largely dependent on the monotonicity and the onto properties of $P_2(i)$.

**Lemma 2.** *There exists unique ideal parameters $\underline{P}_2, \overline{P}_2, \theta_0, \theta_1,$ and $\theta_2$ such that the approximated polynomial given in* (5-12) *matches the original polynomial in* (5–39) *exactly.*

*Proof.* The approximated polynomial is written in an expanded form as follows

$$P_2(i) = \underline{P}_2 + i \left( \frac{\overline{P}_2 - \underline{P}_2}{i_{max}} - \theta_0 i_{max} \right) + i^2 \left( \theta_0 - \theta_1 i_{max} \right) + i^3 \left( \theta_1 - \theta_2 i_{max} \right) + i^4 \theta_2. \tag{5–61}$$

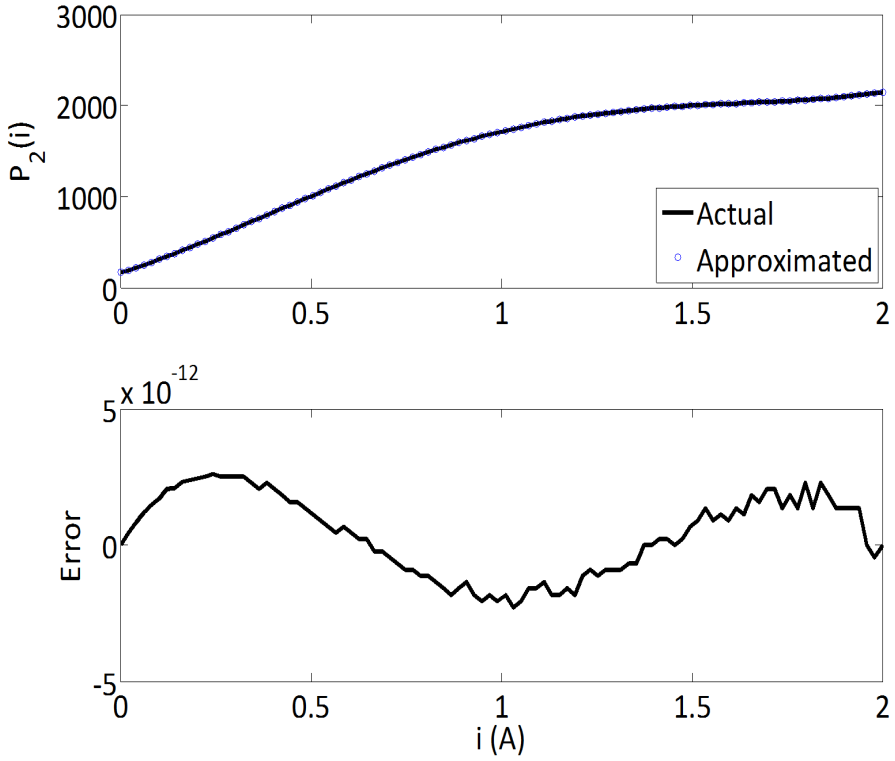


Figure 5-12. Polynomial approximation

Comparing (5–61) with (5–39) yields the system of linear equation

$$\begin{bmatrix} 1 & 0 & 0 & 0 & 0 \\ 1 & -1 & -i_{\max}^2 & 0 & 0 \\ 0 & 0 & 1 & -i_{\max} & 0 \\ 0 & 0 & 0 & 1 & -i_{\max} \\ 0 & 0 & 0 & 0 & 1 \end{bmatrix} \begin{bmatrix} \underline{P}_2 \\ \overline{P}_2 \\ \theta_0 \\ \theta_1 \\ \theta_2 \end{bmatrix} = \begin{bmatrix} A_0 \\ A_1 i_{\max} \\ A_2 \\ A_3 \\ A_4 \end{bmatrix}. \tag{5–62}$$

The determinant of the coefficient matrix in (5–62) is $-1$, which implies that the coefficient matrix is full ranked. As, a result, there exists a unique vector $\begin{bmatrix} \underline{P}_2 & \overline{P}_2 & \theta_0 & \theta_1 & \theta_2 \end{bmatrix}^T$ that satisfies (5–62). □

Fig 5-12 shows the plot of the actual and the approximated polynomials with $\theta_0, \theta_1, \theta_2$ determined using least square method, given $\underline{P}_2$ and $\overline{P}_2$. The Polynomial in

(5–59) is linear in the unknown parameters $\theta_j, j = 0 - 2$. Thus (5–57) becomes

$$\dot{e} = -P_1 e + S_b P_1 Y^T \left(\Theta - \hat{\Theta}\right) + P_1 \alpha(i) \tag{5–63}$$

$$= -P_1 e + S_b P_1 Y^T \tilde{\Theta} + P_1 \alpha(i), \tag{5–64}$$

where

$$\Theta = \begin{bmatrix} \theta_0 & \theta_1 & \theta_2 \end{bmatrix}^T \tag{5–65}$$

is the parameter vector to be estimated, with a corresponding parameter estimation error vector

$$\tilde{\Theta} = \Theta - \hat{\Theta}, \tag{5–66}$$

$$Y = i(i - i_{\max}) \begin{bmatrix} 1 \\ i \\ i^2 \end{bmatrix}^T \tag{5–67}$$

is the current dependent regression matrix, and

$$\hat{P}_2(i) = \underline{P}_2 + \frac{i}{i_{\max}} \left(\overline{P}_2 - \underline{P}_2\right) + Y(i)^T \hat{\Theta}. \tag{5–68}$$

The following lemma is used to guarantee the existence of a valid control current in the interval $[0 \quad i_{\max}]$.

**Lemma 3.** *If the parameter update law is designed such that the estimate $\hat{\Theta}$ is continuous, then the polynomial $\alpha(i)$ given in (5–58) has at least one root in the operating interval $[0 \quad i_{max}]$.*

*Proof.* From (5–51), it is seen that the clipped desired damping force satisfies the following passivity constraint

$$(v - v_0)S_b(v)\underline{P}_2 \leq (v - v_0)F_d(u, v) \leq (v - v_0)S_b(v)\overline{P}_2. \tag{5–69}$$

Also, from (5–40), it can be shown that the term $(v - v_0)S_b(v)$ is positive. Thus dividing through by $(v - v_0)S_b(v)$ in (5–69) yields

$$\underline{P}_2 \leq \frac{F_d(f_d, v)}{S_b(v)} \leq \overline{P}_2, \tag{5–70}$$

which implies that

$$\frac{F_d(f_d, v)}{S_b(v)} \in [\underline{P}_2 \quad \overline{P}_2]. \tag{5–71}$$

Since $\hat{\Theta}$ is continuous by the hypothesis, it implies that $\hat{P}_2(i)$ is continuous. Also, since $\hat{P}_2(0) = \underline{P}_2$ and $\hat{P}_2(i_{\max}) = \overline{P}_2$ , using the Intermediate Value Theorem, it follows that there exists at least one $i_c \in [0 \quad i_{\max}]$ such that

$$\hat{P}_2(i_c) = \frac{F_d(f_d, v)}{S_b(v)}, \tag{5–72}$$

which implies that

$$\alpha(i_c) = F_d(f_d, v) - S_b(v)\hat{P}_2(i_c) = 0. \tag{5–73}$$

Thus $i_c \in roots(\alpha(i))$ and, since $i_c \in [0 \quad i_{\max}]$, the proof is complete. □

Next, Suppose that $\hat{\Theta}$ is continuous, then, using Lemma 3, it follows that there exists a control current $i_c \in [0 \quad i_{\max}]$ such that $\alpha(i_c) = 0$. Consequently, the closed loop error system is given by

$$\dot{e} = -P_1 e + S_b P_1 Y(i_c)^T \tilde{\Theta}. \tag{5–74}$$

### 5.3.3 Stability Analysis

**Theorem 5.2.** *Given the update law*

$$\dot{\hat{\Theta}} = LeS_b(v)Y(i_c), \quad \Theta(0) = \Theta_0, \tag{5–75}$$

*where $L$ is a positive constant adaptation gain, and the control law*

$$i_c = \arg \min_{[0 \;\; i_{max}]} roots(\alpha(\tau)), \tag{5–76}$$

*the closed-loop error dynamics in (5–74) is stable, and the tracking error $e(t)$ approaches zero asymptotically. Also, the parameter estimate $\hat{\Theta}$ is continuous, thus satisfying the hypothesis of Lemma 3.*

*Proof.* Consider the positive definite Lyapunov candidate function

$$V_L = \frac{1}{2}e^2 + \frac{1}{2}\tilde{\Theta}^T\tilde{\Theta}. \tag{5–77}$$

Taking the first time derivative of (5–77) along the closed loop trajectory in (5–74) yields

$$\dot{V}_L = e\dot{e} - \tilde{\Theta}\dot{\hat{\Theta}} \tag{5–78}$$

$$= e\left(-P_1 e + S_b P_1 Y(i_c)^T\tilde{\Theta}\right) - \tilde{\Theta}^T\dot{\hat{\Theta}}. \tag{5–79}$$

Substituting the update law in (5–75) yields

$$\dot{V}_L = -P_1 e^2. \tag{5–80}$$

Since $P_1(i) > 0$, it implies that $\dot{V}_L$ is negative semi-definite, and since $V_L$ is positive definite, it follows that $V_L \in \mathcal{L}_\infty$. From (5–77), it follows that $e, \tilde{\Theta} \in \mathcal{L}_\infty$, which also implies that $\hat{\Theta} \in \mathcal{L}_\infty$-since $\Theta$ is a constant. Integrating (5–80) yields

$$V_L - V_L(0) \leq -\int_0^t P_1(i(\tau))e(\tau)^2 d\tau, \tag{5–81}$$

from which it follows that $e \in \mathcal{L}_2$. Also from (5–74), it follows that $\dot{e} \in \mathcal{L}_\infty$ which implies that $e$ is uniformly continuous. Thus, since $e \in \mathcal{L}_2$ and uniformly continuous, it can be shown using Barbalat's lemma[55] that $e(t) \to 0$ asymptotically. □

**Remark 5.1.** *The following algorithm summarizes the control and update laws developed in the last two sections:*

***Algorithm 5.3.1:*** CONTROL/UPDATE$(f_d, v, \hat{\Theta})$

***comment:*** *Clipped Desired Force*

$F_d \leftarrow F_d(f_d, v)$

***comment:*** *Compute tracking error*

$e \leftarrow F - F_d$

***comment:*** *Compute control current*

$i_c = \min_{[0 \quad i_{max}]} roots\left(-F_d + S_b(v)\hat{P}_2(i)\right)$

***comment:*** *Parameter Update*

$\dot{\hat{\Theta}} \leftarrow L \int_0^t e(\tau) S_b(v) Y(i_c) d\tau + \hat{\Theta}_0$

***return*** $(i_c, \hat{\Theta})$

### 5.3.4 Simulation Results

The simulation is setup as described in the previous section, the vehicle traveling at a steady horizontal speed of $40mph$ is subjected to a road bump of height $10cm$. The Car Body Acceleration, Suspension Travel, and Tire Deflection responses are measured. The suspension travel is defined as the vertical displacement of the center of mass of the sprung mass with respect to the unsprung mass, and the tire deflection as the vertical displacement of the unsprung mass with respect to the road level. Simulations were carried out for the constant stiffness and the variable stiffness

suspension systems. For the constant stiffness suspension, the control mass was locked at a fixed position corresponding to the equilibrium position of the control mass for the variable stiffness system. The results obtained are reported in Figures 5-13, through 5-19. Table 5-5 shows the variance gains for the different responses. Fig 5-13 shows the car body acceleration, which is used here to describe the ride comfort. The lower the car body acceleration, the better the ride comfort. As seen in the figure, the variable stiffness suspension is a more ”ride friendly” suspension, outperforming the traditional vertical skyhook control. As shown in Fig 5-14, associated with this improvement is a corresponding degradation in the suspension travel. This agrees with the observation made in earlier sections, as well as the well known trade off between ride comfort and suspension deflection. Fortunately, the $12\%$ degradation in suspension deflection is not as much as the $30\%$ improvement gained in the ride comfort, resulting in an overall better performance. Figure 5-16 shows the position history of the control mass for the variable stiffness suspension, from which the boundedness of the motion of the control mass is seen. The maximum displacement of the control mass from the equilibrium position is less than 15cm. This implies that the space requirement for the control mass is small, which further demonstrates the practicality of the system. Fig 5-15 shows that there is no significant reduction in the tire deflection. Thus, the suspension systems are approximately equally ”road friendly”. Fig. 5-17 shows the parameter estimates. The upper sub-figure shows that the parameters are not updated in the control of the horizontal MR damper. This is because the corresponding control current is bang-bang, switching from $i_c = 0$ to $i_c = i_{\max}$. As a result, the elements of the regression matrix given in (5–67) are zeros, which further implies, from (5–75), that $\dot{\hat{\Theta}} = \mathbf{0}$. Thus the parameter estimate will remain constant. Fig. 5-19 shows the horizontal and vertical damper forces.

Table 5-5. Variance gain values

| | Constant Stiffness | Variable Stiffness |
|---|---|---|
| CBA ($s^{-1}$) | 50.7306 | 35.5151 |
| ST | 99.9988 | 112.1389 |
| TD | 1.0669 | 1.0450 |

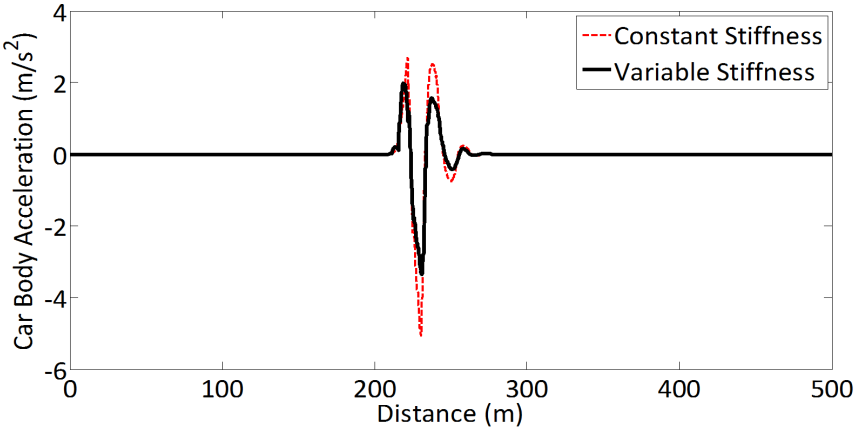


Figure 5-13. Car body acceleration (CBA) - semi-active case

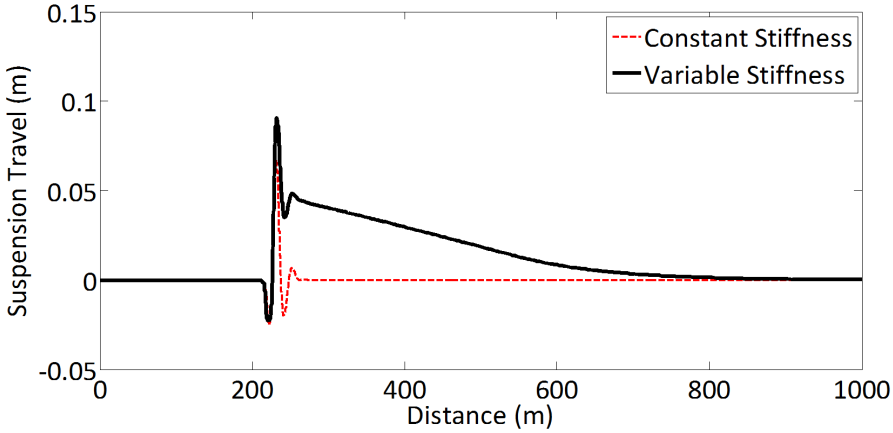


Figure 5-14. Suspension travel (ST) - semi-active case

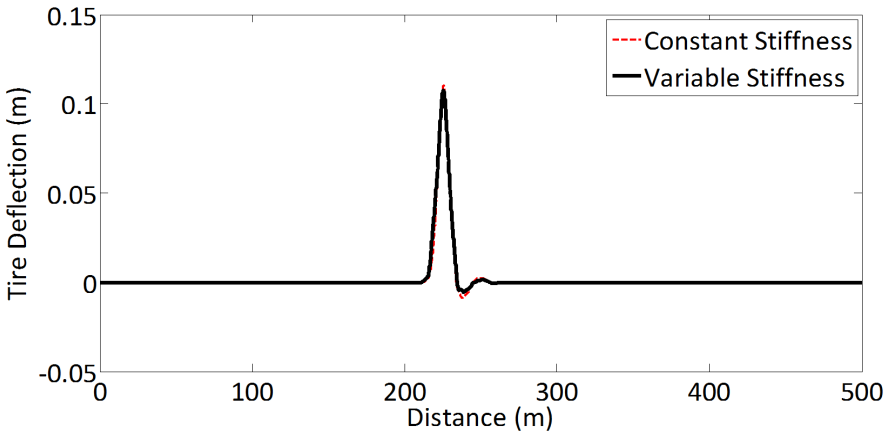


Figure 5-15. Tire deflection(TD) - semi-active Case

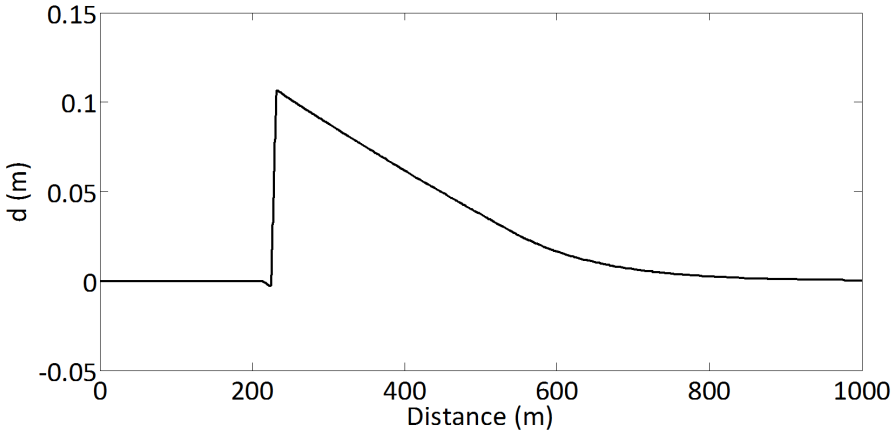


Figure 5-16. Control mass displacement - semi-active case

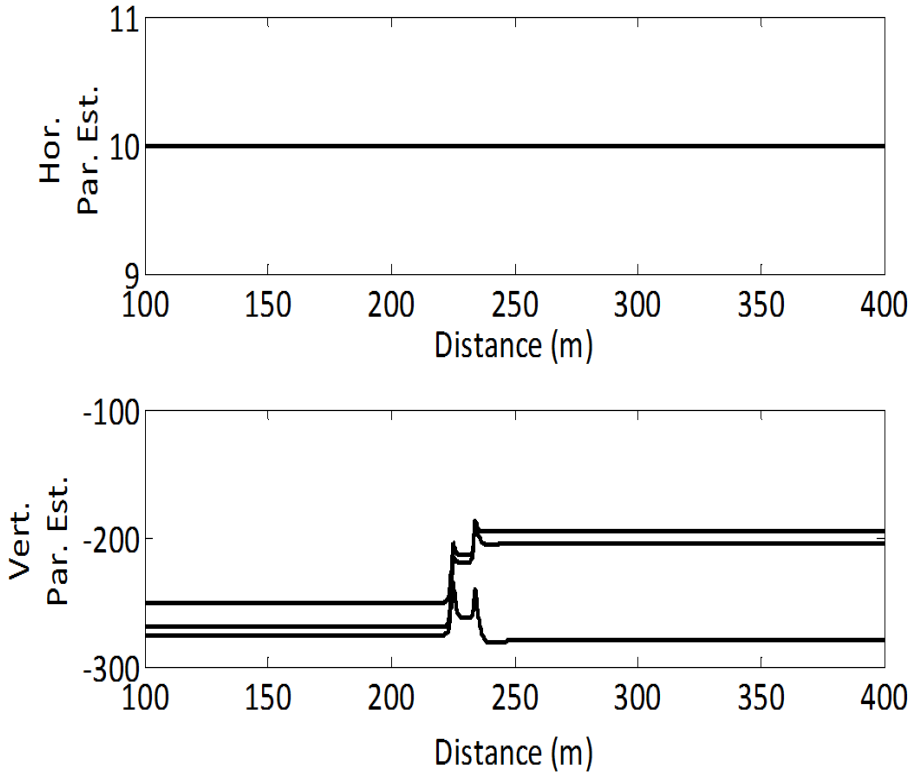


Figure 5-17. Parameter estimates - semi-active case

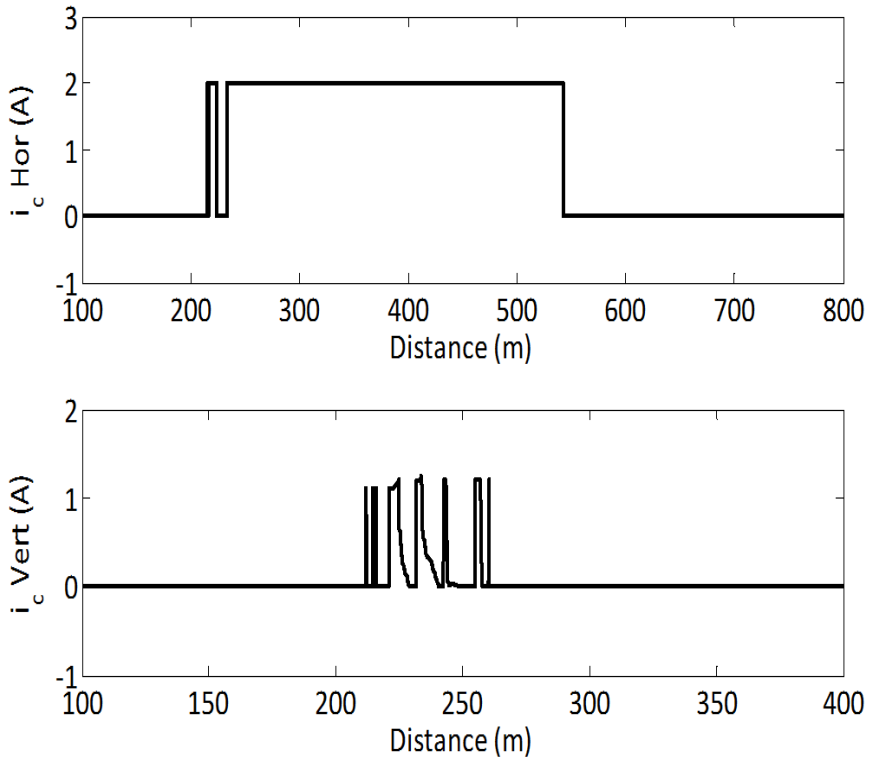


Figure 5-18. Control currents

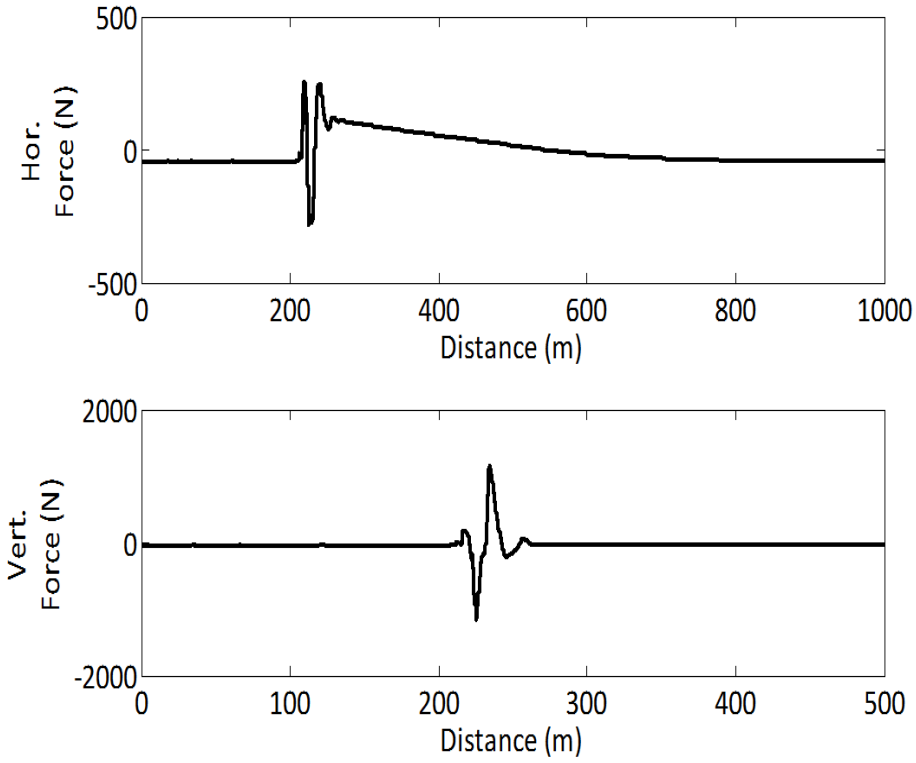


Figure 5-19. MR-damper forces

# CHAPTER 6
# ROLL STABILIZATION ENHANCEMENT USING VARIABLE STIFFNESS SUSPENSION

In this chapter, a variable stiffness architecture is used in the suspension system to counteract the body roll moment, thereby enhancing the roll stability of the vehicle. The proposed system can be used in conjunction with existing methods that do not interfere with the suspension system. First, a kinematic control using the position of the control masses as the control input is designed. Then, a fully actuated system featuring hydraulic actuators is considered. The lateral dynamics of the system is developed using a bicycle model. The accompanying roll dynamics are also developed and validated using experimental data. The positions of the left and right control masses are optimally allocated to reduce the effective body roll and roll rate. Simulation results show that the resulting variable stiffness suspension system has more than 50% improvement in roll response over the traditional constant stiffness counterparts. The simulation scenarios examined are; the fishhook maneuver and the ISO 3888-2 double lane change maneuvers.

Roll dynamics is critical to the stability of road vehicles. A loss of roll stability results in a rollover accident. Typically, vehicle rollovers are very dangerous. Research by the National Highway Traffic Safety Administration (NHTSA) shows that rollover accidents are the second most dangerous form of accidents in the United States, after head-on collision [83]. In 2000, approximately 9,882 people were killed in the United States in a rollover accident involving light vehicles[83]. Rollover crashes kill more than 10,000 occupants of passenger vehicles each year. As part of its mission to reduce fatalities and injuries, since model year 2001, the National Highway Traffic Safety Administration (NHTSA) has included rollover information as part of its New Car Assessment Program (NCAP) ratings. One of the primary means of assessing rollover risk is the static stability factor (SSF), a measurement of a vehicle's resistance to rollover [84]. The higher the SSF, the lower the rollover risk. Roll stability, on the other hand, refers to the capability

of a vehicle to resist overturning moments generated during cornering, that is to avoid rollover [85]. Several factors contribute to roll stability, among which are Static Stability Factor (SSF), kinematic and compliance properties of the suspension system etc.

A number of rollover prevention and roll stability enhancement methods exist in literature that are based on one or more of differential braking, steer-by-wire, differential drive torque distribution, and active steering. In [86], an optimal rollover prevention system using a combination of steer-by-wire and differential braking was presented. A differential braking based anti-rollover control algorithm based on the Time-To-Rollover metric was proposed for Sport Utility Vehicles in [87] and evaluated using human-in-the-loop simulations. In [88], the authors discuss some of the problems rellated to commercial vehicle stability in general, and proposed a solution for detecting and avoiding rollover using existing sensors and actuators of the electronic brake system (EBS). The author in [89] proposed a method of identifying real-time predictive lateral load transfer ratio for rollover prevention systems.

Moreover, engineers have invented mechanical/electromechanical systems to improve the roll stability of road vehicles. One of the earliest basic invention is the anti-roll bar (or sway bar or stabilizer bar). A sway bar is usually in the form of a torsional bar connecting opposite (left/right) wheels together. It generally helps in resisting vehicle body roll motions during fast cornering or road irregularities by increasing the suspension's roll stiffness, independent of the vertical spring constants. The first sway bar patent was awarded to S.L.C Coleman on April 22, 1919 [90]. After then, some more inventions have been geared towards vehicle roll stabilization. These anti-roll systems are either passive [91, 92], semi-active [93], or active [94–98] by design.

## 6.1 Mechanism Description

The schematic diagram of the half car model of the variable stiffness suspension system is shown in Fig 6-1. The model is composed of a half car body (sprung mass), two identical wheel assemblies (unsprung masses), two vertical spring-damper systems,

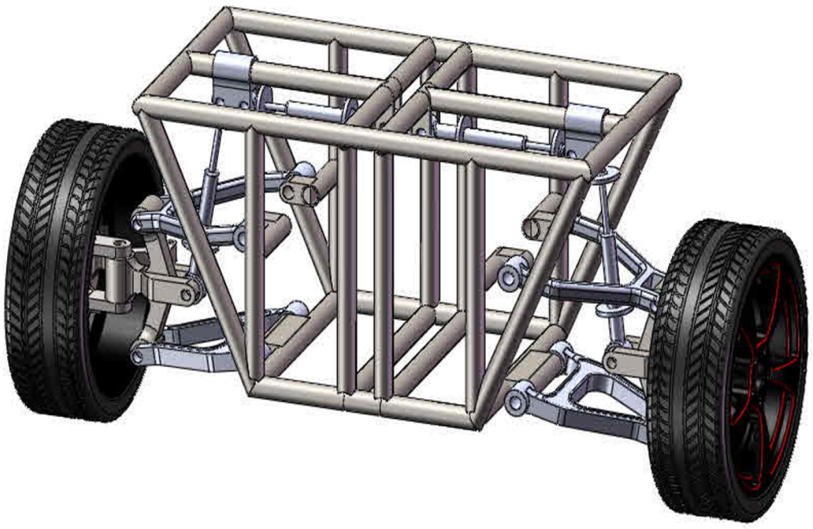

Figure 6-1. Half car model

left and right lower and upper wishbones, and control masses. The main idea of the design is to vary the effective vertical reactive forces of the left and right suspensions to counteract the body roll moments. This is achieved by an appropriately designed control for the variation of the point of attachment of the top end of the suspension struts to the car body. During cornering, a vehicle experiences a radially outwards lateral acceleration acting at the center of mass, as well as corresponding lateral tire forces acting at the tire/road contacts. This results in a roll moment which causes the vehicle to lean outwards. To counteract this roll moment, the outside suspension should become stiffer while the inside suspension should become softer. This generates a counter moment to improve the stability of the roll dynamics.

## 6.2 Modeling

Fig. 6-2 shows a schematic of the modeling aspects of the system. Each block in the schematic is further expatiated in the subsequent subsections.

### 6.2.1 Yaw Dynamics

The yaw dynamics of a vehicle may be effectively decoupled from the roll dynamics by modeling it as a rigid bicycle in a planar motion as shown in Fig. 6-3. The model has three degrees of freedom. As a result, the yaw dynamics are given by a set of

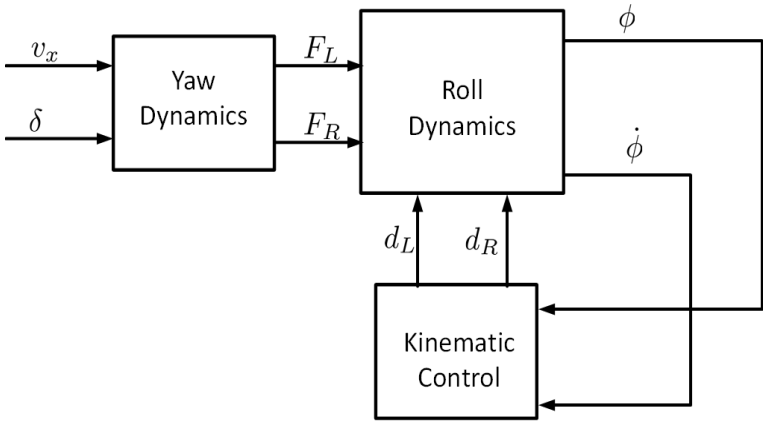


Figure 6-2. Modeling schematics

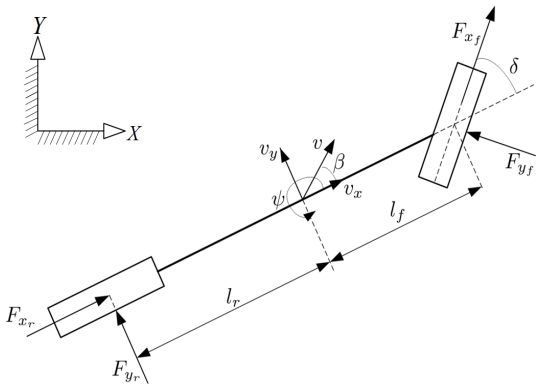


Figure 6-3. Bicycle model

three coupled first order ordinary differential equations [99–101]. However, since the manuevers considered in this paper are constant speed maneuvers, the corresponding forward velocity dynamic is remove and the remaining yaw dynamics are given as follows:

$$\dot{x} = v_x \cos\psi - v_y \sin\psi \tag{6–1}$$

$$\dot{y} = v_x \sin\psi + v_y \cos\psi \tag{6–2}$$

$$\dot{\psi} = r \tag{6–3}$$

$$\dot{v}_y = \frac{1}{m}\left(F_{xf}\sin\delta + F_{yf}\cos\delta + F_{yr}\right) - v_x r \tag{6–4}$$

$$\dot{r} = \frac{1}{I_z}\left(I_f\left(F_{xf}\sin\delta + F_{yf}\cos\delta\right) - I_r F_{yr}\right), \tag{6–5}$$

The term in these equations are defined in the nomenclature section of the paper. To capture the effect of the nonlinear tire forces at large slip angles, the well known Pacejka "Magic Formula" [102] is used to model the tire lateral forces. The lateral forces are expressed as

$$F_{yj} = -\mu\mu_{yj}F_{zj}, \quad (j = f, r), \tag{6–6}$$

where $\mu$ is the maximum friction coefficient of the road surface, $F_{zj}$ is the normal load at each tire, and $\mu_{yj}$ is the tire-road interaction coefficient given by the Magic Formula

$$\mu_{yj} = MF(s_{yj}) = \sin\left(C\tan^{-1}\left(Bs_{yj}\right)\right), \tag{6–7}$$

where $s_yj$ are the lateral slip ratios, given respectively for the front and rear tires as

$$s_{yf} = \frac{v_y\cos\delta - v_x\sin\delta + rl_f\cos\delta}{v_x\cos\delta + v_y\sin\delta + rl_f\sin\delta} \tag{6–8}$$

$$s_{yr} = \frac{v_y - l_r r}{v_x}. \tag{6–9}$$

Here, $v_x$ is the constant vehicle forward speed. In order to keep the total tire forces from exceeding the maximum frictional force, the friction cone constraint is enforced as follows

$$F_{xj}^2 + F_{yj}^2 = \mu^2 F_{zj}^2, \tag{6–10}$$

which implies that

$$F_{xj} = \mu\mu_{xj}F_{zj} \tag{6–11}$$

$$\mu_{xj} = \sqrt{1 - \mu_{yj}^2}. \tag{6–12}$$

The effect of longitudinal load transfer is captured by summing forces in the vertical direction, and taking moments about the body lateral axis, while neglecting pitch

dynamics, as follows

$$F_{zf} + F_{zr} = mg \tag{6–13}$$

$$l_f F_{zf} - l_r F_{zr} = h\left(F_{xf}\cos\delta - F_{yf}\sin\delta + F_{xr}\right), \tag{6–14}$$

where $h$ is the height of the body center of mass from the ground. After some algebraic manipulations, and using (6–6) and (6–11), Equations (6–13) and (6–14) yield the expressions for the respective normal laods at the front and rear tires as

$$F_{zf} = \frac{mg\left(l_r + h\mu\mu_{xr}\right)}{l_f + l_r - h\mu\left(\mu_{xf}\cos\delta + \mu_{yf}\sin\delta - \mu_{xr}\right)} \tag{6–15}$$

$$F_{zr} = \frac{mg\left(l_f - h\mu\left(\mu_{xf}\cos\delta + \mu_{yf}\sin\delta - \mu_{xr}\right)\right)}{l_f + l_r - h\mu\left(\mu_{xf}\cos\delta + \mu_{yf}\sin\delta - \mu_{xr}\right)}. \tag{6–16}$$

### 6.2.2 Roll Dynamics

The free body diagram of an idealized half car model of the system is shown in Fig. 6-4, where the suspension forces have been replaced with their horizontal components, $M_L$, $M_R$, and vertical components $N_L$, $N_R$. The assumptions adopted for

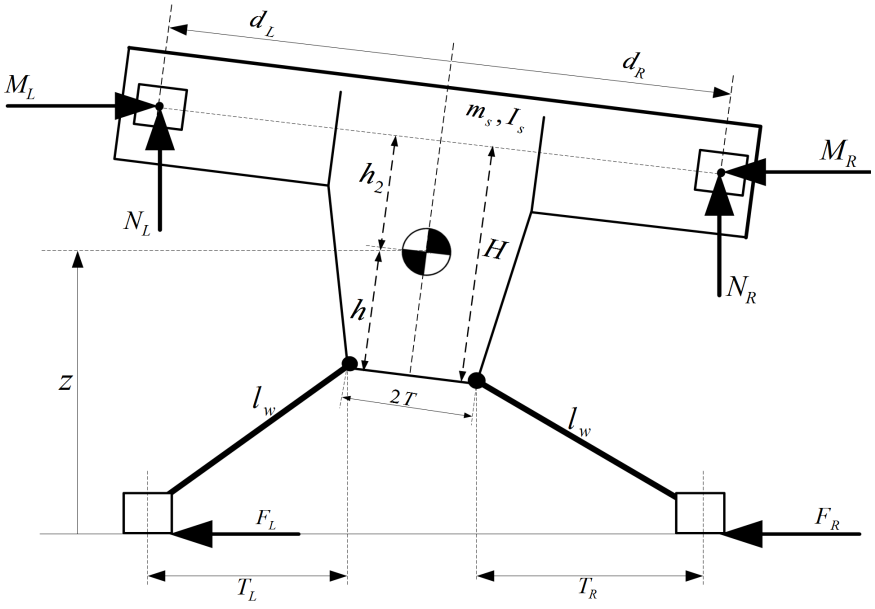


Figure 6-4. Idealized half car model for roll dynamics modeling

the subsequent dynamic model are summarized as follows:

1. The half car body is symmetric about the mid-plane, and as a result the center of mass is located on the mid-plane at a height $h$ above the base of the chassis.

2. The road is level and the points of contact of the tires are on the same horizontal plane.

3. The springs and damper forces are in the linear regions of their operating ranges.

4. The compliance effects in the joints are negligible.

The instantaneous lengths, $l_L$ and $l_R$ of the left and right suspensions respectively, are given as

$$l_L^2 = (T\cos\phi - d_L\cos\phi - H\sin\phi + T_L)^2 + (z - d_L\sin\phi + h_2\cos\phi)^2\,, \tag{6–17}$$

$$l_R^2 = (-T\cos\phi + d_R\cos\phi - H\sin\phi - T_R)^2 + (z + d_R\sin\phi + h_2\cos\phi)^2\,, \tag{6–18}$$

and the corresponding suspension forces are given by

$$F_{s_L} = k_s\,(l_{0_s} - l_L) - b_s\dot{l}_L \tag{6–19}$$

$$F_{s_R} = k_s\,(l_{0_s} - l_R) - b_s\dot{l}_R. \tag{6–20}$$

Thus the horizontal and vertical components of the left, and right suspension forces are given by

$$M_L = \frac{F_{s_L}}{l_L}\,(T\cos\phi - d_L\cos\phi - H\sin\phi + T_L)\,, \tag{6–21}$$

$$M_R = \frac{F_{s_R}}{l_R}\,(-T\cos\phi + d_R\cos\phi - H\sin\phi - T_R)\,, \tag{6–22}$$

$$N_L = \frac{F_{s_L}}{l_L}\,(z - d_L\sin\phi + h_2\cos\phi)\,, \tag{6–23}$$

$$N_R = \frac{F_{s_R}}{l_R}\,(z + d_R\sin\phi + h_2\cos\phi)\,. \tag{6–24}$$

Following the assumptions above, and neglecting the lateral dynamics, the equations of motion of the system are given by the following set of differential algebraic equations:

$$N_L + N_R - m_s g - m_s \ddot{z} = 0, \tag{6–25}$$

$$M_c - I_s \ddot{\phi} = 0, \tag{6–26}$$

$$T_L^2 + (z - T\sin\phi - h\cos\phi)^2 - l_w^2 = 0, \tag{6–27}$$

$$T_R^2 + (z + T\sin\phi - h\cos\phi)^2 - l_w^2 = 0, \tag{6–28}$$

where

$$\begin{aligned} M_c =& g_L(N_L, M_L, \phi) d_L + g_R(N_R, M_R, \phi) d_R \\ & - ((N_L + N_R)\sin\phi + (M_L + M_R)\cos\phi)\, h_2 + F_{yj} z, \end{aligned} \tag{6–29}$$

and

$$g_L(N_L, M_L, \phi) = -N_L\cos\phi + M_L\sin\phi \tag{6–30}$$

$$g_R(N_R, M_R, \phi) = N_R\cos\phi - M_R\sin\phi. \tag{6–31}$$

Here, the total ground force $F_L + F_R$ is equivalent to the lateral tire forces $F_{yj}$ from the yaw dynamics.

### 6.3 Kinematic Control

The purpose of this section is to design the desired trajectory for the control masses to generate the appropriate counter roll moment, given the physical constraints of the suspension kinematics. And, using the simulation results, to understand how the motion of the control masses affect roll stability. In the subsequent section, hydraulic actuators will be used to drive the control masses along the desired trajectory designed in this section, while imposing the physical saturation limits on the actuator.

Since only kinematic control is considered in this section, the dynamics of the control masses are neglected. Their positions $d_L$, and $d_R$ are used as control inputs to

adjust the effective anti-roll moment generated by the suspensions, thereby controlling the roll dynamics of the half car. A control-oriented reduced-order roll dynamics of the half car is then given by:

$$I_s\ddot{\phi} = M_c. \tag{6–32}$$

Adding the stiffness and damping term $k_1\phi + k_2\dot{\phi}$ to both sides of Equation (6–32) yields

$$\begin{aligned} &I_s\ddot{\phi} + k_2\dot{\phi} + k_1\phi - \widetilde{F}_{yj}z + u \\ &\quad + ((N_L + N_R)\sin\phi + (M_L + M_R)\cos\phi)\,\widetilde{h}_2 = e_d, \end{aligned} \tag{6–33}$$

where

$$\begin{aligned} e_d =& g_L d_L + g_R d_R + k_1\phi + k_2\dot{\phi} + u \\ &- ((N_L + N_R)\sin\phi + (M_L + M_R)\cos\phi)\,\hat{h}_2 + \hat{F}_{yj}z, \end{aligned} \tag{6–34}$$

$\hat{F}_{yj}$ and $\hat{h}_2$ are estimates of the lateral tire force $F_{yj}$ and the height $h_2$ respectively with the corresponding estimation errors given by

$$\widetilde{F}_{yj} = F_{yj} - \hat{F}_{yj} \tag{6–35}$$

$$\widetilde{h}_2 = h_2 - \hat{h}_2, \tag{6–36}$$

and $u$ is an auxiliary control which is designed in the subsequent section. Here, it is assumed that the lateral tire force estimation error can be upper bounded by a known positive constant as follows

$$0 \leq |\widetilde{F}_{yj}| \leq C. \tag{6–37}$$

The components $N_L$, $N_R$, $M_L$, $M_R$ of the spring forces are also assumed to be measurable using force sensors. The control gains $k_1$ and $k_2$ are designed to minimize

$$J = \int_0^\infty \left(\omega_1^2\phi(t)^2 + \omega_2^2\dot{\phi}(t)^2 + \left(k_1\phi(t) + k_2\dot{\phi}(t)\right)^2\right)dt \tag{6–38}$$

subject to

$$\begin{aligned} I_s\ddot{\phi} + k_2\dot{\phi} + k_1\phi = 0 \\ \phi(0) = \phi_0 \\ \dot{\phi}(0) = 0, \end{aligned} \tag{6–39}$$

where $\omega_1,$ and $\omega_2$ are performance weights used to penalize the performance index with respect to roll and roll rate respectively. The performance index in (6–81) is chosen to ensure fast smooth and bounded roll dynamics of the vehicle body, with the performance weights specifying a trade-off between achieved boundedness (controlled by $k_1$) and smoothness (controlled by $k_2$) of the ride. The solution to the LQR problem above is obtained as

$$k_1 = \omega_1 \tag{6–40}$$

$$k_2 = \sqrt{2I_s k_1 + \omega_2^2}. \tag{6–41}$$

### 6.3.1 Control Allocation

A control allocation approach is generally used when different possible control choices can produce the same result. This usually happens when the number of effectors exceeds the state dimension, as is the case in this paper. The general control allocation problem, as well as existing solution methods, are well expounded upon in [103, 104].

To this effect, let

$$d_L = d_0 + \Delta_L \tag{6–42}$$

$$d_R = d_0 + \Delta_R, \tag{6–43}$$

where $d_0$ is the equilibrium position of the control masses, with $\Delta_L$ and $\Delta_R$ being their desired displacements respectively. Then

$$e_d = g_L\Delta_L + g_R\Delta_R - f, \tag{6–44}$$

where

$$f = -\left(g_L + g_R\right) d_0 - k_1\phi - k_2\dot{\phi} - u \tag{6–45}$$

$$+ \left(\left(N_L + N_R\right)\sin\phi + \left(M_L + M_R\right)\cos\phi\right)\hat{h}_2 - \hat{F}_{yj}z. \tag{6–46}$$

The control law is therefore defined as

$$\Delta_L, \Delta_R = \arg\min\left\{|e_d| : \underline{d} \leq \Delta_L, \Delta_R \leq \bar{d}\right\}, \tag{6–47}$$

where $\underline{d}$ and $\bar{d}$ are physical limits on the position of the control masses. Due to the special form of (6–44), the solution to (6–95) is obtained sequentially as follows

$$\Delta_L = \text{clip}\left(\frac{f}{g_L}, \underline{d}, \bar{d}\right) \tag{6–48}$$

$$\Delta_R = \text{clip}\left(\frac{f - g_L\Delta_L}{g_R}, \underline{d}, \bar{d}\right), \tag{6–49}$$

where the saturation function, clip(...), is defined as

$$\text{clip}\left(x, a, b\right) \triangleq \begin{cases} a, & \text{if } x < a \\ x, & \text{if } a \leq x \leq b \\ b, & \text{if } x > b \end{cases} \tag{6–50}$$

$$= \min\left\{\max\left\{a, x\right\}, b\right\}. \tag{6–51}$$

### 6.3.2 Stability Analysis

Let $\epsilon$ be the residual error of the optimization in (6–95), and let a signal $r(t)$ be defined as

$$r(t) = \dot{\phi}(t) + \alpha\phi(t), \tag{6–52}$$

where $\alpha$ is a positive gain constant. The closed loop roll dynamics is then given by

$$I_s \dot{r} = \epsilon - (k_2 - \alpha I_s)\, r - (k_1 - \alpha\,(k_2 - \alpha I_s))\,\phi + \widetilde{F}_{yj} z + u - Y\widetilde{h}_2, \tag{6–53}$$

where the regression signal $Y$ is given by

$$Y = (N_L + N_R)\sin\phi + (M_L + M_R)\cos\phi. \tag{6–54}$$

The parenthesized arguments have been dropped unless otherwise required for clarity.

**Theorem 6.1.** *Given the auxiliary control and the adaptive update law*

$$u = -C\,\mathit{sgn}(r)|z| \tag{6–55}$$

$$\dot{\hat{h}}_2 = -\eta\hat{h}_2 + \gamma Y r, \;\; \hat{h}_2(0) = h_0; \tag{6–56}$$

*where $\gamma > 0$ is an adaptation gain constant. If the control gains are chosen to satisfy the following sufficient conditions*

$$k_2 - \alpha I_s = \rho_1 + \rho_2 \tag{6–57}$$

$$k_1 - \alpha\,(k_2 - \alpha I_s) = \rho_3, \tag{6–58}$$

$$\rho_1, \rho_2, \rho_3 > 0,$$

*then the closed loop roll dynamics in* (6–53) *is uniformly ultimately bounded*[1] *with respect to the closed ball*

$$B(r) = \left\{ \boldsymbol{\chi} : \|\boldsymbol{\chi}\| \leq \sqrt{\frac{\lambda_2}{\lambda_1}} r + \frac{1}{\sqrt{\lambda_1 \lambda}} \sqrt{\frac{\epsilon^2}{4\rho_2} + \frac{\eta h_2^2}{2\gamma}} \right\}, \tag{6–59}$$

[1] A signal $\mathbf{x}(t)$ is uniformly ultimately bounded (UUB) with respect to a closed ball $B(r)$ if for all $r > 0$, there exists $T(r)$ such that $\|\mathbf{x}(t_0)\| \leq r$ implies that $\mathbf{x}(t) \in B(r),\ \forall t > t_0 + T$

*where*

$$\lambda = \min\left\{\frac{\rho_1}{I_s}, \alpha, \frac{\eta}{2}\right\},$$
$$\lambda_1 = \min\left\{I_s, \rho_3, \frac{1}{\gamma}\right\},$$
$$\lambda_2 = \max\left\{I_s, \rho_3, \frac{1}{\gamma}\right\}.$$

*Proof.* Consider the following positive definite candidate Lyapunov function

$$V = \frac{1}{2}I_s r^2 + \frac{1}{2}\rho_3\phi^2 + \frac{\widetilde{h}_2^2}{2\gamma}. \tag{6–60}$$

Taking the first time-derivative and using the sufficient conditions in (6–140) and (6–141) yields

$$\begin{aligned}\dot{V} = r\left(\epsilon - (\rho_1+\rho_2)r - \rho_3\phi + \widetilde{F}_{yj}z + u - Y\widetilde{h}_2\right) \\ + \rho_3\phi\left(r - \alpha\phi\right) - \frac{\widetilde{h}_2\dot{\hat{h}}_2}{\gamma},\end{aligned} \tag{6–61}$$

which after substituting the auxiliary control and the adaptive update law yields

$$\begin{aligned}\dot{V} &\leq -\rho_1 r^2 + r(\epsilon - \rho_2 r) - \alpha\rho_3\phi^2 + \frac{\eta\widetilde{h}_2\hat{h}_2}{\gamma} \\ &\leq -\rho_1 r^2 - \rho_2\left(r - \frac{\epsilon}{2\rho_2}\right)^2 + \frac{\epsilon^2}{4\rho_2} - \alpha\rho_3\phi^2 - \frac{\eta\widetilde{h}_2^2}{2\gamma} + \frac{\eta h_2^2}{2\gamma} \\ &\leq \rho_1 r^2 - \alpha\rho_3\phi^2 - \frac{\widetilde{h}_2^2}{2\gamma} + \frac{\epsilon^2}{4\rho_2} + \frac{\eta h_2^2}{2\gamma} \\ &\leq -2\lambda\left(\frac{1}{2}I_s r^2 + \frac{1}{2}\rho_3\phi^2 + \frac{1}{2\gamma}\widetilde{h}_2^2\right) + \frac{\epsilon^2}{4\rho_2} + \frac{\eta h_2^2}{2\gamma} \\ &= -2\lambda V + \frac{\epsilon^2}{4\rho_2} + \frac{\eta h_2^2}{2\gamma}.\end{aligned} \tag{6–62}$$

Using the Comparison Lemma (Lemma 3.4, [55]), it follows that

$$V(t) \leq V(0)e^{-2\lambda t} + \frac{1}{2\lambda}\left(\frac{\epsilon^2}{4\rho_2} + \frac{\eta h_2^2}{2\gamma}\right)\left(1 - e^{-2\lambda t}\right), \tag{6–63}$$
$$\leq V(0)e^{-2\lambda t} + \frac{1}{2\lambda}\left(\frac{\epsilon^2}{4\rho_2} + \frac{\eta h_2^2}{2\gamma}\right), \tag{6–64}$$

which implies that

$$\frac{\lambda_1}{2}\|\boldsymbol{\chi}(t)\|^2 \leq \frac{\lambda_2}{2}\|\boldsymbol{\chi}(0)\|^2 e^{-2\lambda t} + \frac{1}{2\lambda}\left(\frac{\epsilon^2}{4\rho_2} + \frac{\eta h_2^2}{2\gamma}\right), \tag{6–65}$$

where

$$\boldsymbol{\chi} = \begin{bmatrix} r \\ \phi \\ \widetilde{h}_2 \end{bmatrix}. \tag{6–66}$$

Taking the square roots and using the inequality $\sqrt{a^2+b^2} \leq a+b$ for nonnegative numbers $a$ and $b$ yields

$$\|\boldsymbol{\chi}(t)\| \leq \sqrt{\frac{\lambda_2}{\lambda_1}}\|\boldsymbol{\chi}(0)\| e^{-\lambda t} + \frac{1}{\sqrt{\lambda_1 \lambda}}\left(\frac{\epsilon^2}{4\rho_2} + \frac{\eta h_2^2}{2\gamma}\right) \tag{6–67}$$

$$\leq \sqrt{\frac{\lambda_2}{\lambda_1}}\|\boldsymbol{\chi}(0)\| + \frac{1}{\sqrt{\lambda_1 \lambda}}\left(\frac{\epsilon^2}{4\rho_2} + \frac{\eta h_2^2}{2\gamma}\right). \tag{6–68}$$

Therefore, $\|\boldsymbol{\chi}(0)\| \leq r \;\; \Rightarrow \boldsymbol{\chi}(t) \in B(r) \;\; \forall t > 0$ □ □

**Remark 6.1.** *It can be easily verified that the sufficient conditions in* (6–140) *and* (6–141) *are satisfied by the control gains in* (6–40) *and* (6–41) *if the performance weights are selected as*

$$\omega_1 = \rho_3 + \alpha\left(\rho_1 + \rho_2\right) \tag{6–69}$$

$$\omega_2 = \sqrt{\left(\rho_1 + \rho_2\right)^2 + \alpha^2 l_s^2 - 2 l_s \rho_3}, \tag{6–70}$$

*given* $\alpha, \rho_1, \rho_2, \rho_3 > 0$.

### 6.3.3 Simulation

The performance of the proposed control is examined via simulation, using the NTSHA fish hook and double lane change maneuvers. First, the parameters of the roll dynamics are estimated so that the resultant roll dynamics matches experimental data. The vehicle used for the data collection is a 2007 Toyota Highlander Hybrid equipped with an Inertial Measurement Unit, shown in Fig. 6-5 during one of the maneuvers.


Figure 6-5. Snap shot during data collection process

Two sets of data were collected. The first is termed the Snake Data, in which the car is driven around equidistant cones arranged on a straight line in a snake-like fashion. The second is termed the Eight Data. Here, the vehicle is driven several times along an eight-shaped path. The data collected for each experiment includes the longitudinal and lateral velocities, lateral acceleration, roll angle and roll rate. The parameters of the model are estimated using the trust-region-reflective method in MATLAB. Figs. 6-6A and 6-6C show validations of the estimated parameters against a new Snake Dataset which was not used for the estimation process. Figs. 6-6B and 6-6D show similar plots for the Eight Dataset.

The values of the control gains used for the subsequent simulations are given $k_1 = 5000, k_2 = 1565.2, \alpha = 2, \gamma = 10, \eta = 10, C = 5$.

#### 6.3.3.1 Fish hook Maneuver

The Fish hook maneuver, by NHTSA, is a very useful test maneuver in the context of rollover, in that it attempts to maximize the roll angle under transient conditions. The procedure is outlined as follows, with an entrance speed of 50 mph $(22.352 m/s)$:

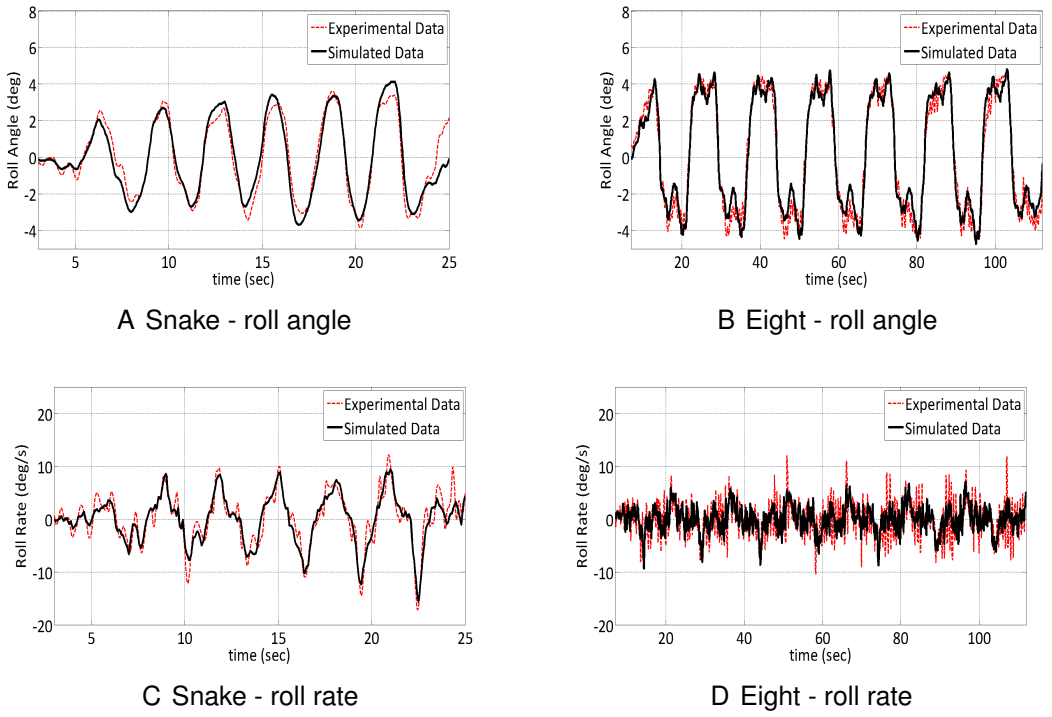


Figure 6-6. Parameter estimation validation - snake data

1. The steering angle is increased at a rate of 720 deg/s up to $6.5\delta_{stat}$, where $\delta_{stat}$ is the steering angle which is necessary to achieve 0.3g stationary lateral acceleration at 50mph
2. This value is held for 250ms
3. The steering wheel is turned in the opposite direction at a rate of 720deg/s up to $-6.5\delta_{stat}$

The steering angle for the fish hook maneuver is shown in Fig. 6-7.

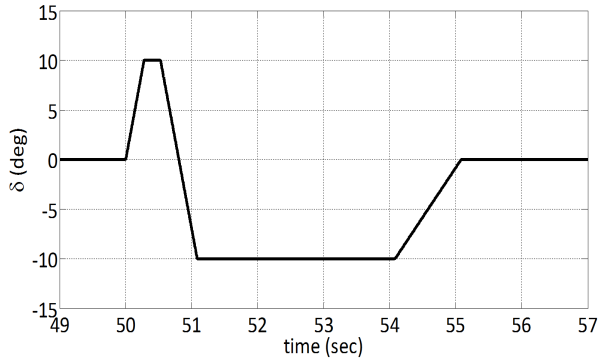


Figure 6-7. Fishhook - steering command

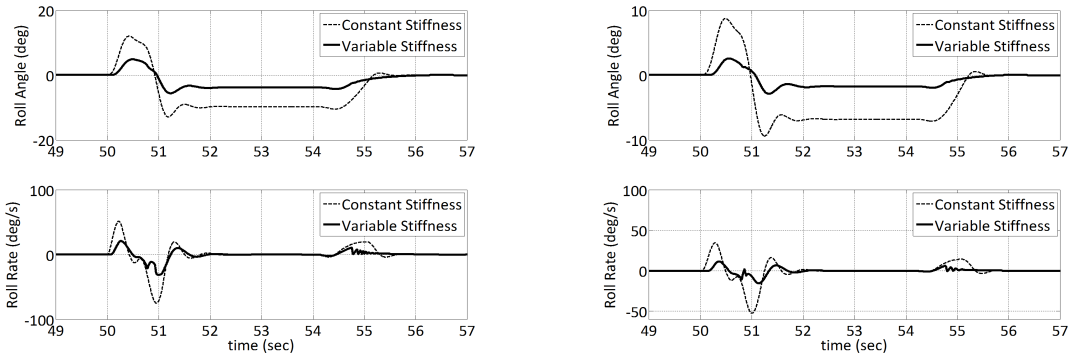


A Front axle B Rear axle

Figure 6-8. Fishhook - roll response

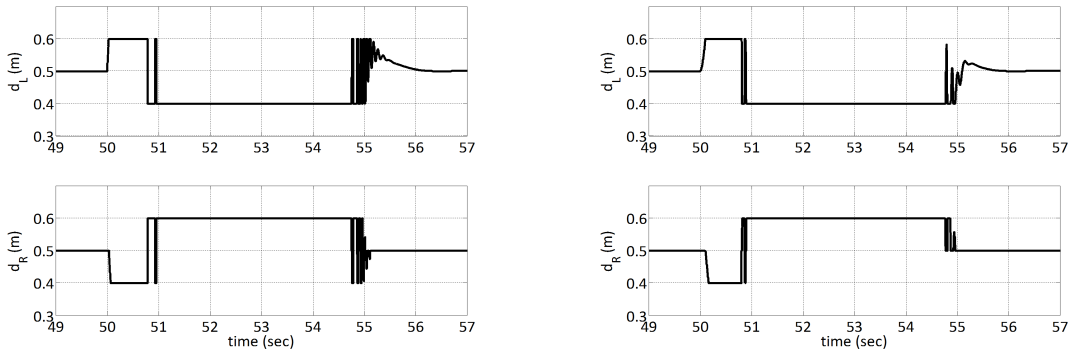


A Front axle B Rear axle

Figure 6-9. Fishhook - control mass displacement

Figs. 6-15A and 6-8B show the roll dynamics for the front and rear axles respectively, where the constant and variable stiffness cases are plotted together for comparison. These results show that by using the variable stiffness mechanism together with the kinematic control developed in the previous sections, the roll angle and roll rates are reduced by more than 50%.

The associated displacements of the left and right control masses are shown in Figs. 6-16A and 6-9B for the front and rear axles respectively. It is seen also that the control allocation exhibit some ganging phenomenon.

#### 6.3.3.2 Double Lane Change Maneuver

The ISO 3888 Part 2 Double Lane Change course was developed to observer the way vehicles respond to hand wheel inputs drivers might use in an emergency situation. The course requires the driver to make a sudden obstacle avoidance steer to the left(or right lane), briefly establish position in the new lane, and then rapidly return to the original lane[105]. The steering command to the wheels is shown in Fig. 6-10. The corresponding roll responses and control authorities are shown in Figs. 6-11A through 6-12B, from which it is also seen that the variable stiffness systems shows much better behavior during the severe obstacle avoidance maneuver.

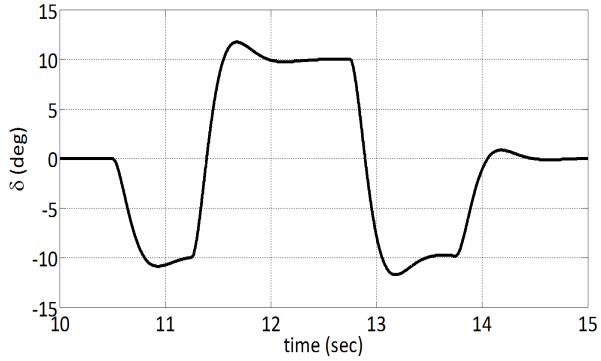


Figure 6-10. Double lane change - steering command

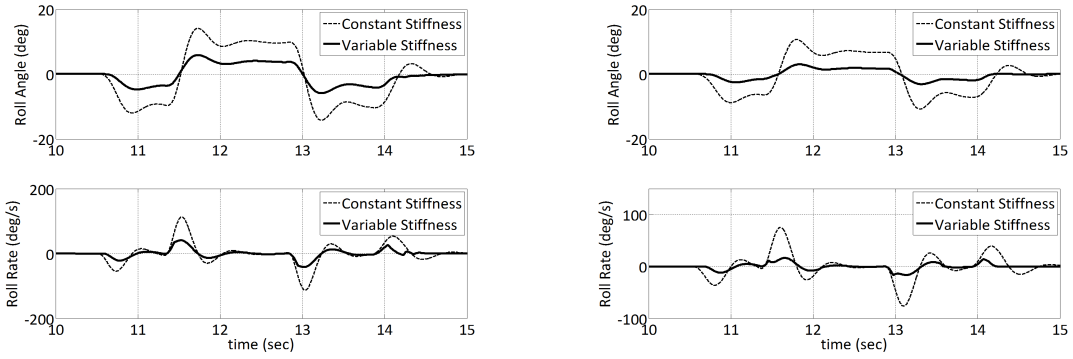


A Front axle B Rear axle

Figure 6-11. Double lane change - roll response

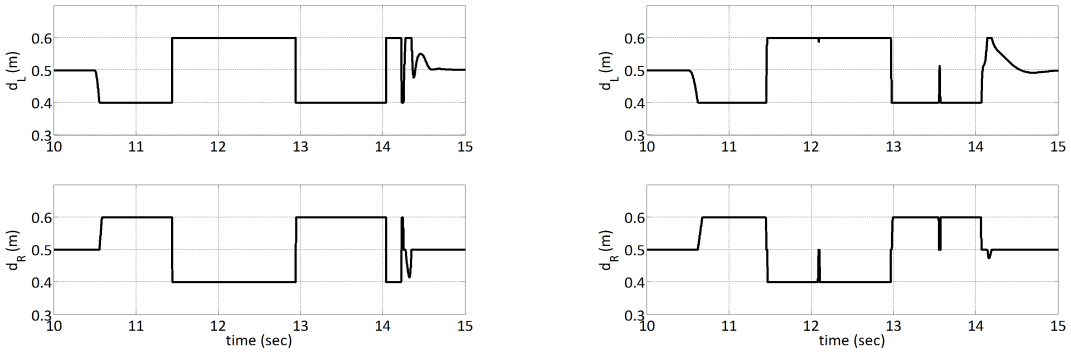


A Front axle B Rear axle

Figure 6-12. Double lane change - control mass displacement

## 6.4 Dynamic Control

In this section, the full dynamics of the control masses are taken into consideration, as well as the actuator model. The schematic diagram of the half car model of the

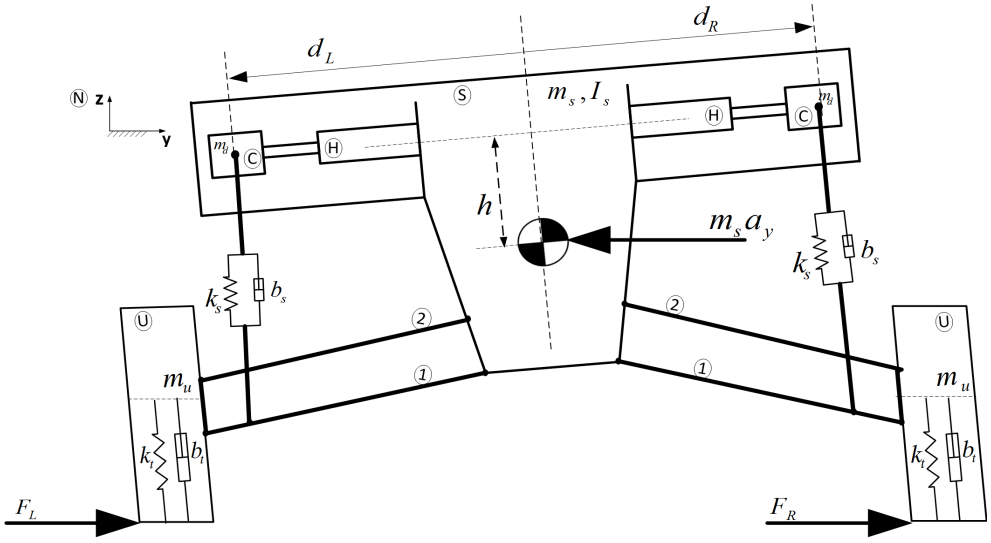


S: Sprung Mass (Chassis)
1: Lower Wishbone
2: Upper Wishbone
U: Unsprung Mass (Wheel Assembly)
C: Control Mass
H: Hydraulic Actuator
N: Inertial Reference Frame

Figure 6-13. Half car model

variable stiffness suspension system is shown in Fig 6-13. The model is composed of

a half car body (sprung mass), two identical wheel assemblies (unsprung masses), two vertical spring-damper systems, left and right lower and upper wishbones, hydraulic actuators. The main idea of the design is to vary the effective vertical reactive forces of the left and right suspensions to counteract the body roll moments. This is achieved by an appropriately designed control for the hydraulic actuators.

### 6.4.1 Control Masses and Actuator Dynamics

Similarly to previous chapter, the dynamics of of the hydraulic actuator is given by[73, 74]

$$\dot{P}_L = -\alpha v_p - \beta P_L + \gamma x_v \sqrt{P_s - sgn(x_v) P_L}, \tag{6–71}$$

$$\dot{x}_v = -\frac{1}{\tau} x_v + \frac{K}{\tau} u, \tag{6–72}$$

$$F^a = A P_L, \tag{6–73}$$

where $A$ is the pressure area in the actuator, $P_L$ is the load pressure, $v_p$ is the actuator piston velocity, $F^a$ is the output force of the actuator, $\alpha, \beta,$ and $\gamma$ are parameters depending on the actuator pressure area, effective system oil volume, effective oil bulk modulus, oil density, hydraulic load flow, total leakage coefficient of the cylinder, discharge coefficient of the cylinder, and servo valve area gradient, $x_v$ is the spool valve position, and $u$ is the input current to the servo valve.

After summing forces along the line of action of the actuators on the control masses, the equations of motion of the left and right control masses, together with the actuator model, are given by

$$m_d \ddot{d}_i = F_i^a - M_i \cos\phi - N_i \sin\phi \tag{6–74}$$

$$\dot{F}^a{}_i = -\beta F_i^a - \alpha A \dot{d}_i + \alpha A x_{v_i} \sqrt{P_s - sgn(x_{v_i}) \frac{F_i^a}{A}} \tag{6–75}$$

$$\tau \dot{x}_{v_i} = -x_{v_i} + K u_i. \tag{6–76}$$

The subscript $i = \{L, F\}$ is used to indicate left and right quantities respectively.

### 6.4.2 Control Design

This section details the design of control design for the hydraulic actuators geared towards improvement of the body roll dynamics. First, the control laws are designed, and the resulting closed loop error system given. The desired actuator forces required to achieved a desired roll behavior are designed using a model reference adaptive control and sliding mode techniques[55, 73, 106–108], then the necessary servo current command to the spool valve is designed from the actuator dynamics using an adaptive singular perturbation approach[76]. Next, a Lyapunov-based stability analysis is carried out for the overall closed loop error dynamics to guarantee the convergence of the tracking error and boundedness of the system states. The control development is done hierarchically. First for the vehicle body roll, then for the control masses, and finally for the hydraulic actuators.

#### 6.4.2.1 Vehicle Body Roll

Again, the desired reference roll model is given by

$$I_s\ddot{\phi}_m + k_2\dot{\phi}_m + k_1\phi_m = 0, \tag{6–77}$$

(6–78)

where

$$k_1 = \omega_1, \tag{6–79}$$

$$k_2 = \sqrt{\frac{\omega_2^2}{I_s} + 2\omega_1} \tag{6–80}$$

were designed to minimize

$$J = \int_0^\infty \left(\omega_1^2\phi_m(t)^2 + \omega_2^2\dot{\phi}_m(t)^2 + \left(k_1\phi_m(t) + k_2\dot{\phi}_m(t)\right)^2\right)dt \tag{6–81}$$

subject to (6–77), where $\omega_1,$ and $\omega_2$ are performance weights used to penalize the performance index with respect to roll and roll rate respectively. The performance index

in (6–81) is chosen to ensure smooth and bounded roll dynamics of the vehicle body, with the performance weights specifying a trade-off between achieved boundedness (controlled by $k_1$) and smoothness (controlled by $k_2$) of the ride.

Let

$$e(t) = \phi(t) - \phi_m(t) \tag{6–82}$$

be the tracking error defining how well the roll dynamics in (6–32) tracks the reference model in (6–77). The objective is then to drive the tracking error to as small as possible using the actuator forces. Taking the first and second derivatives of (6–82) and subtracting (6–77) from (6–32) yields

$$I_s\ddot{e} + k_2\dot{e} + k_1 e = M_c - (k_2 - b_{sb})\,\dot{\phi} - (k_1 - k_{sb})\,\phi, \tag{6–83}$$

where $k_{sb}$, $b_{sb}$ are the stiffness and damping due to the sway bar and other compliance and damping elements that have indirect or direct influence on the roll dynamics. This part, which was neglected for the kinematic control, is included here for completion. To facilitate subsequent control design and analyses, the nonlinear lateral force given by the Pacejka formula is approximated as

$$F_{yj} = \sum_{i=1}^{n} Q_i L_i(s_j) \tag{6–84}$$

$$= \mathbf{L}(s_j)^T \mathbf{Q}, \tag{6–85}$$

where the regression matrix $R(s_j)$ and the constant coefficient vector $Q$ are given by

$$\mathbf{L}(s_j) = \begin{bmatrix} L_1(s_j) & L_2(s_j) & \dots & L_n(s_j) \end{bmatrix}^T, \tag{6–86}$$

$$\mathbf{Q} = \begin{bmatrix} Q_1 & Q_2 & \dots & Q_n \end{bmatrix}^T, \tag{6–87}$$

with

$$L_i(s_j) = \sin\left((2i-1)\tan^{-1}(s_j)\right), \quad i = 1, 2, \dots, n \tag{6–88}$$

being the set of bases functions. Other bases functions can be used (e.g polynomial [109], rational function [110]). The functions in (6–88) are used as basis for the lateral tire force approximation because they preserve the form given in the Magic formula. Fig. 6-14 shows the resulting approximation for $n = 10$, where the ideal weight vector Q was obtained using a least square approach.

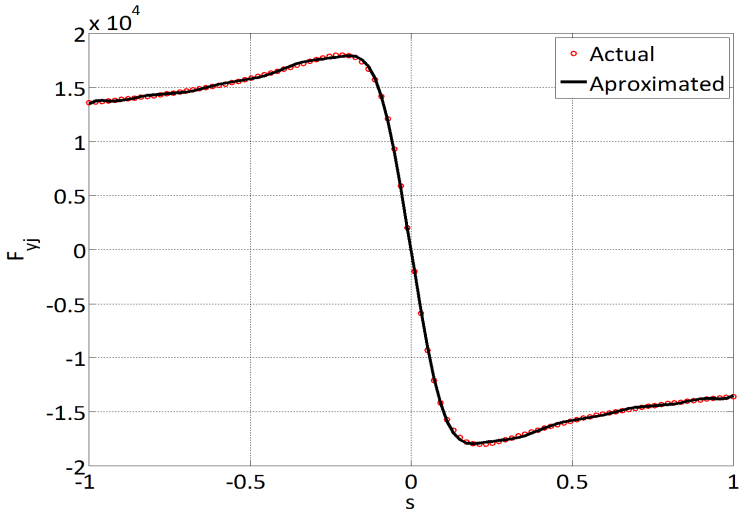


Figure 6-14. Lateral tire force approximation

Thus, the roll error dynamics in (6–83) becomes

$$I_s\ddot{e} + k_2\dot{e} + k_1 e - \mathbf{L}^T\widetilde{\mathbf{Q}}z + Y\widetilde{h}_2 = f_\phi, \tag{6–89}$$

where

$$f_\phi = g_L d_L + g_R d_R - Y\hat{h}_2 + \mathbf{L}^T\hat{\mathbf{Q}}z - (k_2 - b_{sb})\dot{\phi} - (k_1 - k_{sb})\phi, \tag{6–90}$$

and $\hat{h}_2, \hat{\mathbf{Q}}$ are the adaptive estimates of the unknown system constant parameters $h_2, \mathbf{Q}$, with the corresponding estimation errors given by

$$\widetilde{h}_2 = h_2 - \hat{h}_2, \tag{6–91}$$

$$\widetilde{\mathbf{Q}} = \mathbf{Q} - \hat{\mathbf{Q}}. \tag{6–92}$$

The parenthesized arguments have been dropped unless otherwise required for clarity. Let

$$d_L^* = d_0 + \Delta_L, \tag{6–93}$$

$$d_R^* = d_0 + \Delta_R, \tag{6–94}$$

where

$$\Delta_L, \Delta_R = \arg\min \left\{ |f_\phi| : -\Delta \leq \Delta_L, \Delta_R \leq \Delta \right\}, \tag{6–95}$$

be the desired displacement of the control masses. $\Delta$ defines the physical limits on the allowable positions of the control masses. The optimization in (6–95) defines a control allocation problem. Control allocation approach is generally used when different possible control choices can produce the same result. This usually happens when the number of effectors exceeds the state dimension, as the case in this paper. The general control allocation problem, as well as existing solution methods, are well expounded upon in [103, 104]. However, due to the special form of (6–90), the solution to (6–95) is obtained sequentially as follows

$$\Delta_L = \text{clip}\left( \frac{f_\phi^0}{g_L}, -\Delta, \Delta \right), \tag{6–96}$$

$$\Delta_R = \text{clip}\left( \frac{f_\phi^0 - g_L \Delta_L}{g_R}, -\Delta, \Delta \right), \tag{6–97}$$

where the saturation function, clip$(\ldots)$, is defined as

$$\text{clip}\,(x, a, b) \triangleq \begin{cases} a, & \text{if } x < a \\ x, & \text{if } a \leq x \leq b \\ b, & \text{if } x > b \end{cases} \tag{6–98}$$

$$= \min\{\max\{a, x\}, b\}, \tag{6–99}$$

and

$$f_\phi^0 = (g_L + g_R)\, d_0 - Y\hat{h}_2 + \mathbf{L}^T\hat{\mathbf{Q}}z - (k_2 - b_{sb})\,\dot{\phi} - (k_1 - k_{sb})\,\phi. \tag{6–100}$$

Consequently, let $\varepsilon_d$ be the residual value of $f_\phi^0$ after the optimization above. Also, let

$$r_1(t) = \dot{e}(t) + \alpha_1 e(t) \tag{6–101}$$

defines a sliding surface for the roll error dynamics. Then, the corresponding closed loop roll error dynamics is given by

$$I_s\dot{r}_1 = \varepsilon_d - (k_2 - \alpha_1 I_s)\, r_1 - (k_1 - \alpha_1\,(k_2 - \alpha_1))\, e + \mathbf{L}^T\widetilde{\mathbf{Q}}z - Y\widetilde{h}_2. \tag{6–102}$$

#### 6.4.2.2 Control Masses

In order to ensure smoothness of the ensuing motion of the control masses, the desired trajectory of the control masses is given by the following first-order low pass filter dynamics

$$\epsilon\dot{d}_i^d = -d_i^d + d_i^*, \quad i = \{L, R\}. \tag{6–103}$$

Let

$$r_i = \dot{e}_{d_i} + \alpha_2 e_{d_i}, \tag{6–104}$$

defines a sliding surface for the position tracking error

$$e_{d_i} = d_i - d_i^d \tag{6–105}$$

of the control masses, where $\alpha_2$ is a positive control gain. Differentiating (6–104) and substituting the control mass dynamics in (6–74) yield the closed loop tracking error dynamics

$$m_d \dot{r}_i = -\left(k_3 - \alpha_2 m_d\right) r_i - \alpha_2 m_d e_{d_i} - N_i + e_{F_i}, \tag{6–106}$$

where the desired actuator force is given by

$$F_i^d = k_3 r_i + M_i \cos\phi + N_i \sin\phi, \tag{6–107}$$

and the actuator force tracking error is given by

$$e_{F_i} = F_i^a - F_i^d. \tag{6–108}$$

$k_3 > 0$ is a control gain, and the desired position dynamics $N_i = m_d \ddot{d}_i^d$ is assumed to be upper bounded as follows

$$|N_i| \leq c_i \tag{6–109}$$

#### 6.4.2.3 Hydraulic Actuators

In order to simplify the controller design for the actuators, the spool valve dynamics is canceled by using a singular perturbation technique [75]. The control input is designed as

$$u_i = -K_f x_{v_i} + \frac{1 + KK_f}{K} u_{s_i}, \quad i = \{L, F\} \tag{6–110}$$

where $u_{s_i}$ is a slow control in time and $K_f$ is a positive design control gain. Consequently, the valve psuedo-closed loop dynamics is given by

$$\varepsilon \dot{x}_{v_i} + x_{v_i} = u_{s_i}, \tag{6–111}$$

where

$$\varepsilon = \frac{\tau}{1 + KK_f} \tag{6–112}$$

is the perturbation constant. The pseudo-closed loop in (6–111) has a quasi-steady state solution, $x_{v_i}(\varepsilon = 0) \triangleq \bar{x}_{v_i}$, given by

$$\bar{x}_{v_i} = u_{s_i}. \tag{6–113}$$

Using the fast time scale $\nu = \frac{t}{\varepsilon}$ and Tichonov's Theorem [75] yields

$$x_{v_i} = \bar{x}_{v_i} + \eta + O(\varepsilon), \tag{6–114}$$

$$\frac{d\eta}{d\nu} = -\eta, \tag{6–115}$$

where $\eta(\nu)$ is a boundary layer correction term. It is seen that $\eta(\nu)$ decays exponentially in the fast time scale. Typically, the time constant $\tau$ in the actual system is designed to satisfy $0 < \varepsilon \ll 1$ [76]. Therefore, by choosing the control gain $K_f$ large enough, the perturbation constant can be made as small as possible. As a result, $\eta + O(\varepsilon)$ becomes negligibly small. Thus, the actuator dynamics in (6–75) becomes

$$\dot{F}_i^a = f(F_i^a, \dot{d}_i) + g(F_i^a, x_{v_i}) u_{s_i}, \tag{6–116}$$

where

$$f(F_i^a, \dot{d}_i) = -\beta F_i^a - \alpha A \dot{d}_i \tag{6–117}$$
$$\triangleq f_i,$$
$$g(F_i^a, x_{v_i}) = \gamma A \sqrt{P_s - \text{sgn}(x_{v_i}) \frac{F_i^a}{A}} \tag{6–118}$$
$$\triangleq g_i.$$

Functions $f(F_i^a, \dot{d}_i)$ and $g(F_i^a, x_{v_i})$ , hence the dynamics in (6–116), contain unknown system parameters $\beta, \alpha$ and $\gamma$. Therefore, an adaptive control approach is used to design the control $u_{s_i}$.

Thus, the actuator force closed loop tracking error dynamics is given by

$$\dot{e}_{F_i} = \dot{F}_i^a - \dot{F}_i^d, \tag{6–119}$$
$$= f_i + g_i u_{s_i} - \dot{F}_i^d \tag{6–120}$$
$$= f_i - \frac{g_i}{\hat{g}_i}\hat{f}_i - g_i k_u e_{F_i} - \dot{F}_i^d + \frac{g_i}{\hat{g}_i}\hat{\dot{F}}_i^d + g_i \left( u_{s_i} + \frac{\hat{f}_i}{\hat{g}_i} + k_u e_{F_i} - \frac{\hat{\dot{F}}_i^d}{\hat{g}_i} \right). \tag{6–121}$$

The slow control $u_{s_i}$ is designed as follows

$$u_{s_i} = -\frac{\hat{f}_i}{\hat{g}_i} - k_u e_{F_i} + \frac{\hat{\dot{F}}_i^d}{\hat{g}_i} \tag{6–122}$$

where $\hat{f}_i$ and $\hat{g}_i$ are the estimates of $f_i$ and $g_i$ respectively, and the derivative $\dot{F}_i^d$ of the desired force is approximated using the high gain observer [55]

$$\varepsilon_2 \dot{\mathbf{p}} = A\mathbf{p} + \mathbf{b}F_i^d \tag{6–123}$$
$$\hat{\dot{F}}_i^d = \frac{1}{\varepsilon_2}\mathbf{c}^T\mathbf{p}, \tag{6–124}$$

where

$$A = \begin{bmatrix} -1 & 1 \\ -1 & 0 \end{bmatrix}, \mathbf{b} = \begin{bmatrix} 1 \\ 1 \end{bmatrix}, \mathbf{c} = \begin{bmatrix} 0 \\ 1 \end{bmatrix}, \varepsilon_2 \ll 1.$$

It can be shown (see [55]) that the estimation error, $\widetilde{\dot{F}}_i^d = \dot{F}_i^d - \hat{\dot{F}}_i^d$ decays very fast to the ball $|\widetilde{\dot{F}}_i^d| < O(\varepsilon_2)$. Thus, the actuator force closed loop tracking error system becomes

$$\dot{e}_{F_i} = \widetilde{f}_i - \frac{\hat{f}_i}{\hat{g}_i}\widetilde{g}_i - gk_u e_{F_i} - \widetilde{\dot{F}}_i^d + \frac{\hat{\dot{F}}_i^d}{\hat{g}_i}\widetilde{g}_i \tag{6–125}$$

$$= \widetilde{f}_i + \left(\frac{\hat{\dot{F}}_i^d - \hat{f}_i}{\hat{g}_i}\right)\widetilde{g}_i - gk_u e_{F_i} - \widetilde{\dot{F}}_i^d, \tag{6–126}$$

where

$$\widetilde{f}_i = f_i - \hat{f}_i = -\widetilde{\beta}_i F_i^a - \widetilde{\alpha}_i A\dot{d}_i, \tag{6–127}$$

$$\widetilde{g}_i = g_i - \hat{g}_i = \widetilde{\gamma}_i A\sqrt{P_s - \mathrm{sgn}(x_{v_i})\frac{F_i^a}{A}}, \tag{6–128}$$

where

$$\widetilde{\beta}_i = \beta - \hat{\beta}_i, \tag{6–129}$$

$$\widetilde{\alpha}_i = \alpha - \hat{\alpha}_i, \tag{6–130}$$

$$\widetilde{\gamma}_i = \gamma - \hat{\gamma}_i, \tag{6–131}$$

are the parameter estimation errors.

### 6.4.3 Stability Analysis

The overall closed loop error system is

$$I_s\dot{r}_1 = \varepsilon_d - (k_2 - \alpha_1 I_s)\, r_1 - (k_1 - \alpha_1 (k_2 - \alpha_1))\, e + \mathbf{L}^T\widetilde{\mathbf{Q}}z - Y\widetilde{h}_2, \tag{6–132}$$

$$m_d\dot{r}_i = -(k_3 - \alpha_2 m_d)\, r_i - \alpha_2 m_d e_{d_i} - N_i + e_{F_i}, \tag{6–133}$$

$$\dot{e}_{F_i} = \widetilde{f}_i + \left(\frac{\hat{\dot{F}}_i^d - \hat{f}_i}{\hat{g}_i}\right)\widetilde{g}_i - gk_u e_{F_i} - \widetilde{\dot{F}}_i^d. \tag{6–134}$$

**Theorem 6.2.** *Given the adaptive update laws*

$$\dot{\hat{h}}_2 = Proj\left(\hat{h}_2,\ -L_h Y r_1\right), \tag{6–135}$$

$$\dot{\hat{\boldsymbol{Q}}} = Proj\left(\hat{\boldsymbol{Q}},\ L_Q \boldsymbol{L} z r_1\right), \tag{6–136}$$

$$\dot{\hat{\alpha}}_i = Proj\left(\hat{\alpha}_i,\ -L_\alpha A e_{F_i} \dot{d}_i\right), \tag{6–137}$$

$$\dot{\hat{\beta}}_i = Proj\left(\hat{\beta}_i,\ -L_\beta F_i^a e_{F_i}\right), \tag{6–138}$$

$$\dot{\hat{\gamma}}_i = Proj\left(\hat{\gamma}_i,\ \frac{L_\gamma}{\hat{\gamma}_i}\left(\hat{F}_i^d - \hat{f}_i\right) e_{F_i}\right), \tag{6–139}$$

*where $L_h, L_\alpha, L_\beta, L_\gamma$ are positive adaptation gain constants, and $L_Q$ is a positive definite adaptation gain matrix. If the control gains $k_1$, and $k_2$ are chosen to satisfy the following sufficient conditions*

$$k_2 - \alpha_1 l_s > \rho_1 + \rho_2 \tag{6–140}$$

$$k_1 - \alpha_1 \left(k_2 - \alpha_1 l_s\right) > \rho_3, \tag{6–141}$$

$$k_3 > \rho_4 + \frac{1}{2}, \tag{6–142}$$

$$g_i k_u > \rho_5 + \rho_6 + \frac{1}{2}, \tag{6–143}$$

$$\rho_1, \rho_2, \rho_3, \rho_4, \rho_5, \rho_6 > 0,$$

*then the closed loop system in (6–132)-(6–134) is uniformly ultimately bounded*[2] *with respect to the closed ball*

$$B_r = \left\{\boldsymbol{\chi} : \|\boldsymbol{\chi}\|^2 \leq \frac{\lambda_1}{\lambda_2}\sigma\right\}, \tag{6–144}$$

[2] A signal $\mathbf{x}(t)$ is uniformly ultimately bounded (UUB) with respect to a closed ball $B_r$ if for all $r > 0$, there exists $T(r)$ such that $\|\mathbf{x}(t_0)\| \leq r$ implies that $\mathbf{x}(t) \in B(r)$, $\forall t > t_0 + T$

*where*

$$\lambda_1 = \frac{1}{2}\max\left\{I_s, \rho_3, \frac{1}{L_h}, \lambda_{max}\left\{L_Q^{-1}\right\}, m_d, \alpha_2 m_d, \frac{1}{L_\alpha}, \frac{1}{L_\beta}, \frac{1}{L_\gamma}\right\}, \tag{6–145}$$

$$\lambda_2 = \min\left\{\rho_1, \alpha_1, \alpha_2, \alpha_2 m_d, \alpha_2^2 m_d, \rho_5, 1\right\}, \tag{6–146}$$

$$\sigma = \frac{\varepsilon_d^2}{4\rho_2} + \frac{1}{4\rho_4}\left(c_L^2 + c_R^2\right) + \frac{O(\varepsilon_2)^2}{2\rho_6} + c_\theta^2 \tag{6–147}$$

*with*

$$\widetilde{\mathbf{\Theta}} = \begin{bmatrix} \widetilde{h}_2 & \widetilde{\mathbf{Q}}^T & \widetilde{\alpha}_L & \widetilde{\alpha}_R & \widetilde{\beta}_L & \widetilde{\beta}_R & \widetilde{\gamma}_L & \widetilde{\gamma}_R \end{bmatrix}^T \tag{6–148}$$

*satisfying*

$$\|\widetilde{\mathbf{\Theta}}\| \leq c_\theta, \quad c_\theta > 0. \tag{6–149}$$

*Proof.* Consider the candidate Lyapunov function

$$V = \frac{I_s}{2} r_1^2 + \frac{\rho_3}{2}\phi^2 + \frac{1}{2L_h}\widetilde{h}_2^2 + \frac{1}{2}\widetilde{\mathbf{Q}}^T L_Q^{-1}\widetilde{\mathbf{Q}} + \frac{1}{2}\sum_{i=\{L,R\}}\left(m_d r_i^2 + \alpha_2 m_d e_{d_i}^2 + e_{F_i}^2 + \frac{1}{L_\alpha}\widetilde{\alpha}_i^2 + \frac{1}{L_\beta}\widetilde{\beta}_i^2 + \frac{1}{L_\gamma}\widetilde{\gamma}_i^2\right). \tag{6–150}$$

It's time derivative is

$$\dot{V} = I_s r_1 \dot{r}_1 + \rho_3\phi\left(r_1 - \alpha_1\phi\right) - \frac{\widetilde{h}_2\dot{\hat{h}}_2}{L_h} - \widetilde{\mathbf{Q}}^T L_Q^{-1}\dot{\hat{\mathbf{Q}}} + \sum_{i=\{L,R\}}\left(m_d r_i \dot{r}_i + \alpha_2 m_d e_{d_i}\left(r_i - \alpha_2 e_{d_i}\right) + e_{F_i}\dot{e}_{F_i} - \frac{\widetilde{\alpha}_i\dot{\hat{\alpha}}_i}{L_\alpha} - \frac{\widetilde{\beta}_i\dot{\hat{\beta}}_i}{L_\beta} - \frac{\widetilde{\gamma}_i\dot{\hat{\gamma}}_i}{L_\gamma}\right), \tag{6–151}$$

which, after substituting the closed loop error dynamics (6–132)-(6–134) and applying the update laws (6–135)-(6–139), becomes

$$\begin{aligned}\dot{V} &\leq r_1\left(-\rho_1 r_1 - \rho_2 r_1 + \varepsilon_d\right) - \alpha_1\phi^2 \\ &+ \sum_{i=\{L,R\}}\left(r_i\left(-\alpha_2 m_d r_i - \rho_4 r_i - N_i\right) + e_{F_i}\left(-\rho_5 e_{F_i} - \rho_6 e_{F_i} + \widetilde{\dot{F}}_i^d\right)\right) \qquad (6\text{–}152)\\ &\leq -\rho_1 r_1^2 - \alpha_1\phi^2 - |r_1|\left(\rho_2|r_1| - |\varepsilon_d|\right) \\ &+ \sum_{i=\{L,R\}}\left(-\alpha_2 m_d r_i^2 - \alpha_2^2 m_d e_{d_i}^2 - |r_i|\left(\rho_4|r_i| - c_i\right) - \rho_5 e_{F_i}^2 - |e_{F_i}|\left(\rho_6|e_{F_i}| - O(\varepsilon_2)\right)\right), \qquad (6\text{–}153)\end{aligned}$$

Using the boundedness property of the parameter estimation error in (6–149), due to the projection operator [111], the inequality in (6–153) yields

$$\begin{aligned}\dot{V} &\leq -\rho_1 r_1^2 - \alpha_1\phi^2 + \sum_{i=\{L,R\}}\left(-\alpha_2 m_d r_i^2 - \alpha_2^2 m_d e_{d_i}^2 - \rho_5 e_{F_i}^2\right) - \|\widetilde{\Theta}\|^2 + \sigma \qquad (6\text{–}154)\\ &\leq -\lambda_2\|\boldsymbol{\chi}\|^2 + \sigma, \qquad (6\text{–}155)\\ &\leq -\frac{\lambda_2}{\lambda_1}V + \sigma, \qquad (6\text{–}156)\end{aligned}$$

where

$$\boldsymbol{\chi} = \begin{bmatrix} r_1 & \phi & r_L & e_{d_L} & r_R & e_{d_R} & \widetilde{\boldsymbol{\Theta}}^T \end{bmatrix}^T. \qquad (6\text{–}157)$$

Using the Comparison Lemma [55], it follows that

$$V(t) \leq \frac{\lambda_1}{\lambda_2}\sigma + \left(V(t_0) - \frac{\lambda_1}{\lambda_2}\sigma\right)\exp\left(-\frac{\lambda_2}{\lambda_1}(t - t_0)\right). \qquad (6\text{–}158)$$

Thus, any trajectory starting outside of $B_r$ will approach $B_r$ monotonically, and any trajectory starting inside $B_r$ will remain in $B_r$ . This shows that the system is uniformly ultimately bounded[112]. □

### 6.4.4 Simulation

Similar to the Kinematic Control, simulations are carried out using the same steering commands as in the previous section. However, unlike the kinematic control case, only the response for the font axle is reported. This is because, as can be seen in kinematic control case, the performance of the system is similar for both axles. The results, shown in the figures below, also show that by using the actuated variable stiffness mechanism together with the control developed in the previous sections, the roll angle and roll rates are reduced by more than 50%.

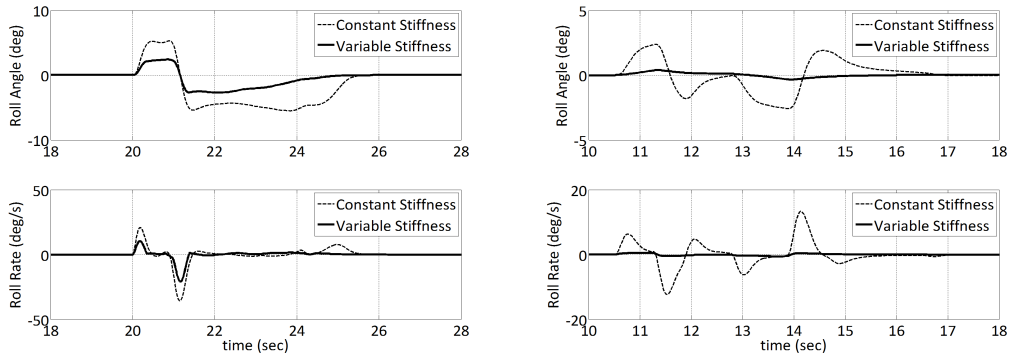


A Fishhook B Double lane change

Figure 6-15. Roll response

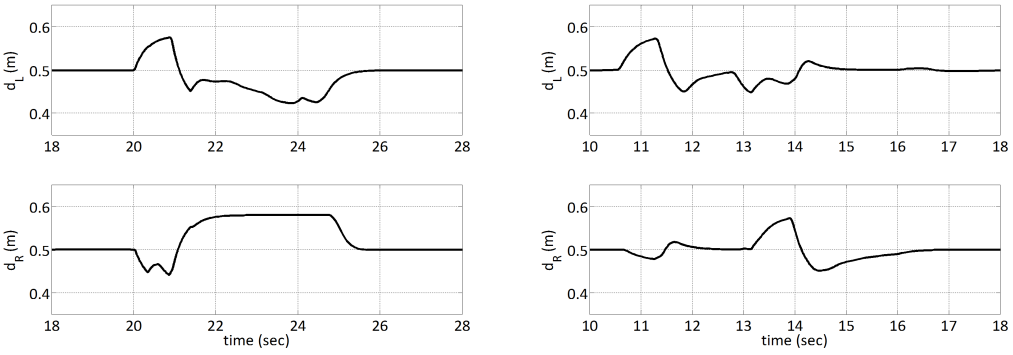


A Fishhook B Double lane change

Figure 6-16. Control mass displacement

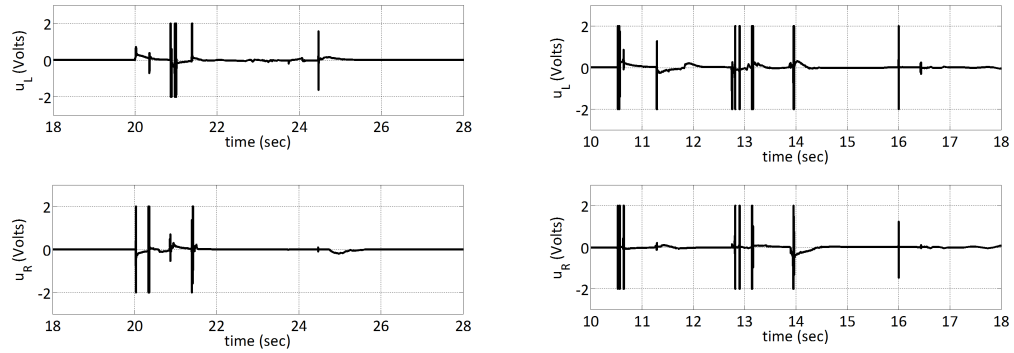


A Fishhook B Double lane change

Figure 6-17. Voltage command

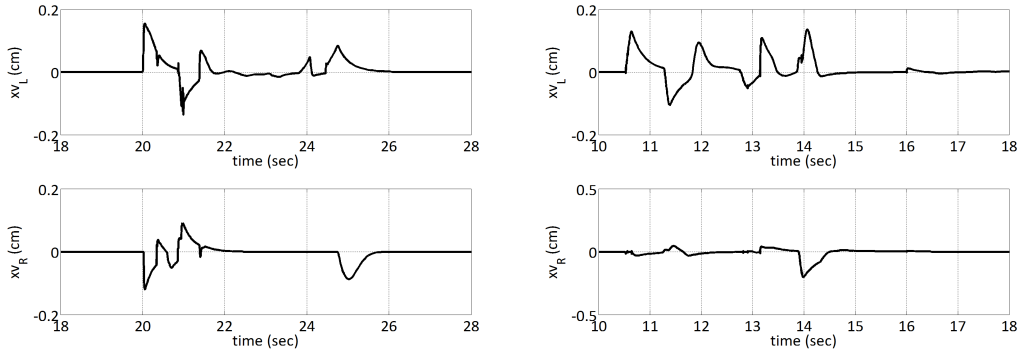


A Fishhook B Double lane change

Figure 6-18. Spool valve response

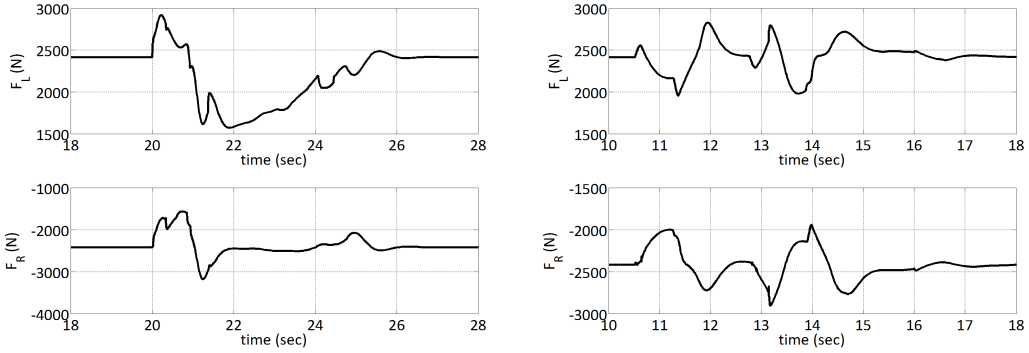


A Fishhook B Double lane change

Figure 6-19. Hydraulic force output

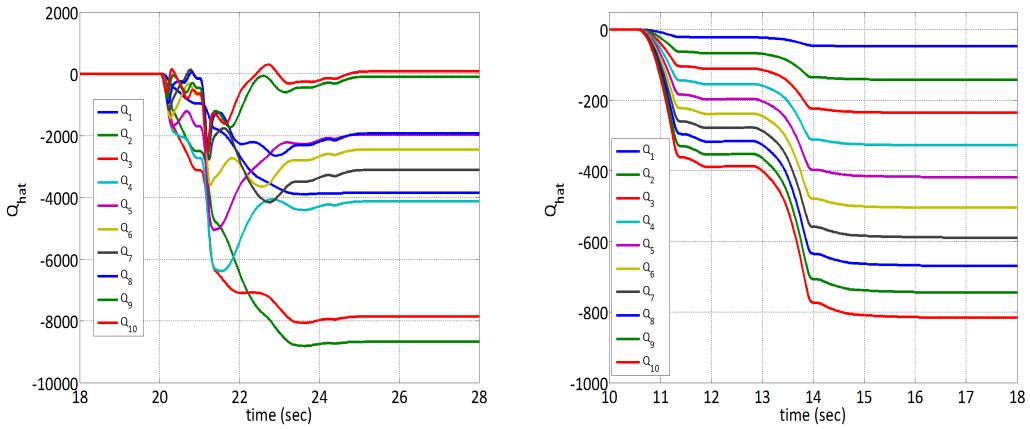


A Fishhook B Double lane change

Figure 6-20. Adaptive parameter estimation history, $\hat{\mathbf{Q}}$

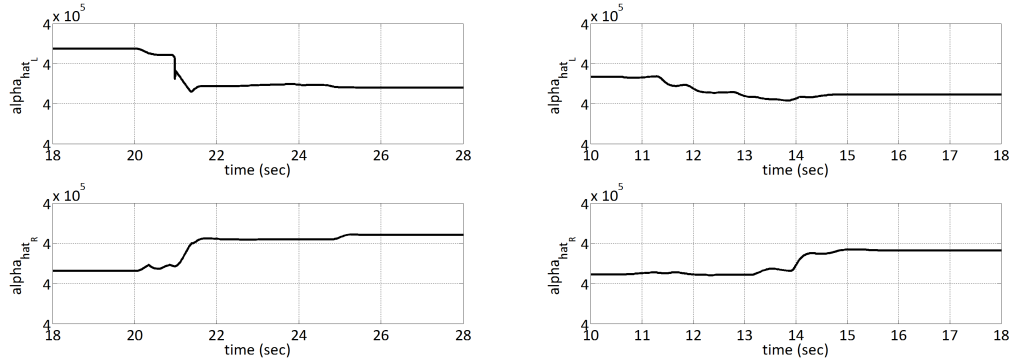


A Fishhook B Double lane change

Figure 6-21. Adaptive parameter estimation history, $\hat{\alpha}$

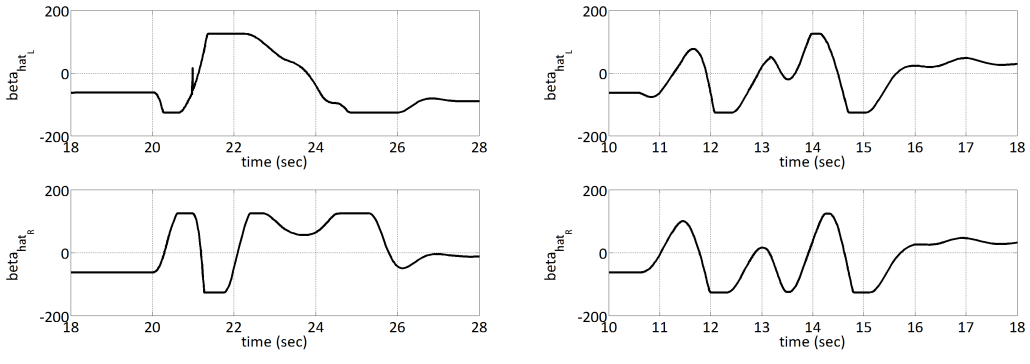


A Fishhook B Double lane change

Figure 6-22. Adaptive parameter estimation history, $\hat{\beta}$

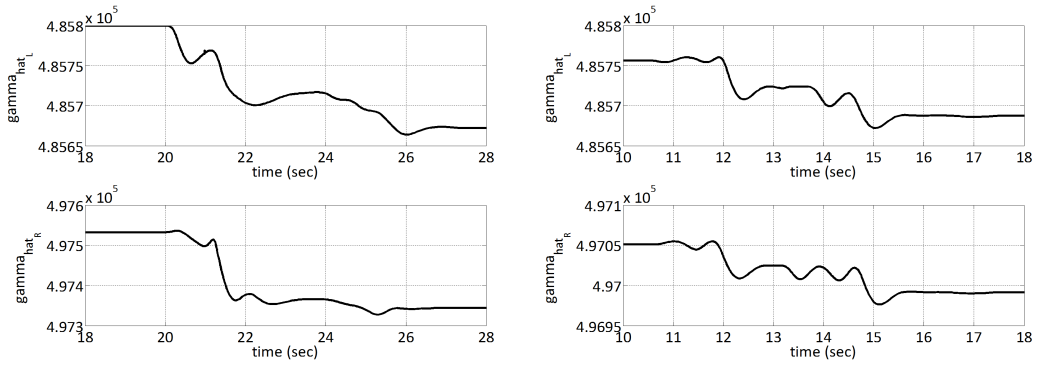


A Fishhook B Double lane change

Figure 6-23. Adaptive parameter estimation history, $\hat{\gamma}$

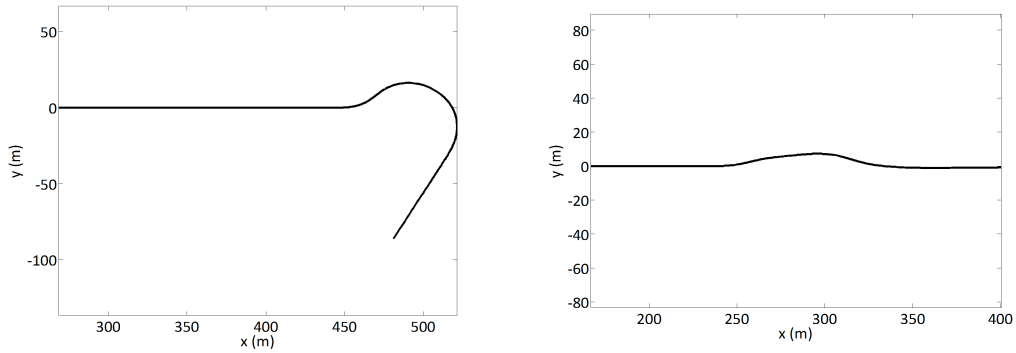


A Fishhook B Double lane change

Figure 6-24. Vehicle trajectory

# CHAPTER 7
# CONCLUSIONS AND FUTURE WORK

## 7.1 Conclusion

The idea of improving the performance of vehicle suspension systems is an active area of research. Past approaches utilize one of three techniques; adaptive, semi-active, or fully active suspension. This research considered the design, analyses, simulation, and experimentation of a new variable stiffness suspension system. The design was based on the concept of a variable stiffness mechanism. The mechanism, which is a simple arrangement of two springs, a lever arm, and a pivot bar, has an effective stiffness that is a rational function of the horizontal position of the pivot. The effective stiffness was varied by changing the position of the pivot while keeping the point of application of the external force constant. The overall suspension system consists of a horizontal control strut and a vertical strut. The main idea was to vary the load transfer ratio by moving the location of the point of attachment of the vertical strut to the car body. This movement was controlled passively, semi-actively, and actively using the horizontal strut.

A theoretical justification for modulating the stiffness of a suspension system, alongside the damping, was presented. It was shown that a better performance, in terms of ride comfort and handling, is achievable by varying the stiffness alongside the damping coefficient over varying either damping or stiffness alone. Two additional control laws were presented for varying the damping and stiffness of a semi-active suspension based on a quarter car model. The first varied the damping and stiffness sequentially while the second varied them simultaneously.

The new variable stiffness mechanism was introduced. The expression for the effective stiffness was derived. A reverse analysis was also carried out on the mechanism. Special design cases were considered. The dynamic equation of the

system was derived and used to deduce the natural frequency of the mechanism from which some insights were gained on the dynamic behavior of the mechanism.

The incorporation of the new variable stiffness mechanism into vehicle suspension design was considered. The concept used “reciprocal actuation” to effectively transfer energy between a vertical traditional strut and a horizontal oscillating control mass, thereby improving the energy dissipation of the overall suspension. Due to the relatively fewer number of moving parts, the concept can easily be incorporated into existing traditional front and rear suspension designs. An implementation with a double wishbone was shown. A detailed $\mathcal{L}_2$-gain analysis was used to show that the resulting variable stiffness suspension system has much better performance than the traditional constant stiffness counterpart. The design was extended to incorporate semi-active and active actuators.

The variable stiffness architecture was also used in the suspension system to counteract the body roll moment, thereby enhancing the roll stability of the vehicle. The lateral dynamics of the system was developed using a bicycle model. The accompanying roll dynamics were also developed and validated using experimental data. The positions of the left and right control masses were optimally allocated to reduce the effective body roll and roll rate. Simulation results show that the resulting variable stiffness suspension system has more than 50% improvement in roll response over the traditional constant stiffness counterparts. The simulation scenarios examined were; the fishhook maneuver and the ISO 3888-2 double lane change maneuvers. A combined vibration isolation and roll stabilization performance improvement was also examined.

## 7.2 Future Work

In this research, only the roll and vibration isolation performance of the newly designed variable stiffness suspension system were considered. The examination of the pitch performance, and possible influence on the yaw dynamics of the vehicle is

still an open area of research. Also, a combination of vibration, roll, pitch, and yaw performances using a full car model would be an interesting research.

With respect to vibration isolation performance enhancement, the behavior of the front suspensions can be used to build a disturbance observer for the road input. The observed road disturbance can then be fed forward to improve the behavior of the rear suspension. This would provide some sort of preview information for the rear suspension without using expensive preview equipments.

One more interesting aspect of this research is the final implementation of the variable stiffness design in a real vehicle. When this is done, more realistic experiments can be conducted.

# APPENDIX
# PROOF OF THEOREMS 2.1 AND 2.2

## A.1 Proof of Theorem 2.1

*Proof.* Define the Hamiltonian

$$H \triangleq g(\mathbf{x}, v) + \mathbf{p}^T(A\mathbf{x} + \phi(\mathbf{x})v) \tag{A–1}$$

where $\mathbf{p}$ is the Lagrange multiplier vector for the dynamic constraint (2–9). Using calculus of variations, the necessary conditions for optimality are given by

$$-\dot{\mathbf{p}} = \frac{dg}{d\mathbf{x}} + \left(A^T + v\frac{\partial\phi(\mathbf{x})}{\partial\mathbf{x}}\right)\mathbf{p} \tag{A–2}$$

$$0 = \frac{\partial g}{\partial v} + \mathbf{p}^T\phi(\mathbf{x}). \tag{A–3}$$

From (A–3)

$$w(\mathbf{x})\left(-\frac{2\mathbf{a}^T\mathbf{x}}{m_s} + \frac{2w(\mathbf{x})}{m_s^2}v - \mathbf{b}^T\mathbf{p}\right) = 0. \tag{A–4}$$

If $w(\mathbf{x}) \neq 0$ then

$$v^* = \frac{m_s}{2w(\mathbf{x})}\left(2\mathbf{a}^T\mathbf{x} + m_s\mathbf{b}^T\mathbf{p}\right). \tag{A–5}$$

Substituting (A–5) in (A–2) yields

$$\begin{aligned} -\dot{\mathbf{p}} &= 2Q\mathbf{x} - \frac{2v^*}{m_s}\left(w(\mathbf{x})\mathbf{a} + \mathbf{T}\mathbf{a}^T\mathbf{x}\right) \\ &\quad + \frac{2w(\mathbf{x})}{m_s^2}v^{*2}\mathbf{T} + A^T\mathbf{p} - v^*\mathbf{T}\mathbf{b}^T\mathbf{p} \\ &= \left(A^T - m_s^2\mathbf{a}\mathbf{b}^T\right)\mathbf{p} + 2\left(Q - \mathbf{a}\mathbf{a}^T\right)\mathbf{x} \\ &= \bar{A}\mathbf{p} + 2\bar{Q}\mathbf{x}. \end{aligned} \tag{A–6}$$

Similarly, susbstituting (A–5) in the deterministic dynamic constraint (2–9) yields

$$\begin{aligned}\dot{\mathbf{x}} &= A\mathbf{x} - \frac{m_s}{2}\left(m_s\mathbf{b}^T\mathbf{p} + 2\mathbf{a}^T\mathbf{x}\right)\mathbf{b} \\ &= \left(A - m_s^2\mathbf{b}\mathbf{a}^T\right)\mathbf{x} - \frac{m_s^2}{2}\mathbf{b}\mathbf{b}^T\mathbf{p} \\ &= \bar{A}^T\mathbf{x} - \bar{B}\mathbf{p}. \end{aligned} \tag{A–7}$$

Putting (A–6) and (A–7) together yields the homogeneous linear ordinary differential equation (A–8) in terms of the state $\mathbf{x}$ and costate $\mathbf{p}$.

$$\begin{bmatrix} \dot{\mathbf{x}} \\ \dot{\mathbf{p}} \end{bmatrix} = \begin{bmatrix} \bar{A}^T & -\bar{B} \\ -2\bar{Q} & -\bar{A} \end{bmatrix} \begin{bmatrix} \mathbf{x} \\ \mathbf{p} \end{bmatrix}. \tag{A–8}$$

Now, let

$$\mathbf{p} = P\mathbf{x} \tag{A–9}$$

where $P \in \Re^{4\times 4}$ is a positive-definite matrix. Substituting (A–9) into (A–6) yields

$$\begin{aligned} &-\left(\dot{P}\mathbf{x} + P\dot{\mathbf{x}}\right) = \bar{Q}\mathbf{x} + \bar{A}P\mathbf{x} \\ \Longrightarrow \\ &\left(\dot{P} + P(\bar{A}^T - \bar{B}^T P) + \bar{Q} + \bar{A}P\right)\mathbf{x} = \mathbf{0} \end{aligned}$$

which, provided $\mathbf{x} \neq \mathbf{0}$ reduces to the the Riccati equation

$$\dot{P} + P\bar{A}^T + \bar{A}P - P\bar{B}^T P + \bar{Q} = 0. \tag{A–10}$$

Now, after some algebraic manipulations, $g(\mathbf{x}^*, v^*)$ becomes

$$g(\mathbf{x}^*, v^*) = \frac{1}{2}\mathbf{x}^T\left(\bar{Q} + P\bar{B}P\right)\mathbf{x} \tag{A–11}$$

$$= -\frac{1}{2}\frac{d}{dt}(\mathbf{x}^T P\mathbf{x}). \tag{A–12}$$

Thus the value function $J^* \triangleq J(\mathbf{x}^*, v^*)$ is given by

$$J^* = \int_{t_0}^{t_f} g(\mathbf{x}^*, v^*)dt = -\frac{1}{2}\mathbf{x}^T P\mathbf{x}\Big|_{t_0}^{t_f}.$$

Imposing the boundary condition $P(t_f) = 0$ on the Riccati equation (A–10) yields

$$J^* = \frac{1}{2}\mathbf{x}^T(t_0)P\mathbf{x}(t_0). \tag{A–13}$$

□

## A.2 Proof of Theorem 2.2

*Proof.* The Hamiltonian (A–1) is modified as

$$H = g(\mathbf{x}, v) + \mathbf{p}^T(A\mathbf{x} + \phi(\mathbf{x})v) - \lambda_1 v + \lambda_2(v - \bar{v}), \tag{A–14}$$

where $\lambda_1, \lambda_2 \geq 0$ are the Lagrange multipliers for the inequality constraint (2–10).

Similarly, the necessary conditions for optimality are

$$-\dot{\mathbf{p}} = \frac{dg}{d\mathbf{x}} + \left(A^T + v\frac{\partial\phi(\mathbf{x})}{\partial\mathbf{x}}\right)\mathbf{p} \tag{A–15}$$

$$0 = \frac{\partial g}{\partial v} + \mathbf{p}^T\phi(\mathbf{x}) - \lambda_1 + \lambda_2. \tag{A–16}$$

(A–16) yields

$$\begin{aligned} v &= \frac{m_s^2}{2w(\mathbf{x})}\left(\frac{2\mathbf{a}^T\mathbf{x}}{m_s} + \mathbf{b}^T\mathbf{p}\right) + \frac{m_s^2}{2w(\mathbf{x})^2}(\lambda_1 - \lambda_2) \\ &= \frac{m_s^2}{2w(\mathbf{x})^2}\left(v' + \lambda_1 - \lambda_2\right), \end{aligned} \tag{A–17}$$

where

$$v' = \frac{w(\mathbf{x})}{m_s}\left(2\mathbf{a}^T\mathbf{x} + m_s\mathbf{b}^T\mathbf{p}\right). \tag{A–18}$$

There are three possibilities for the values of $\lambda_1$ and $\lambda_2$.

Case 1: ($\lambda_1 > 0, \lambda_2 = 0$)

$$\frac{\partial H}{\partial \lambda_1} = \frac{m_s^2}{2w(\mathbf{x})^2}(v' + \lambda_1) = 0$$

$$\Longrightarrow$$

$$\lambda_1 = \begin{cases} 0 & \text{if } v' > 0 \\ -v' & \text{if } v' \leq 0. \end{cases} \tag{A–19}$$

Case 2: ($\lambda_1 = 0, \lambda_2 = 0$)

$$v = \frac{m_s^2}{2w(\mathbf{x})^2} v' \tag{A–20}$$

Case 3: ($\lambda_1 = 0, \lambda_2 > 0$)

$$\frac{\partial H}{\partial \lambda_2} = \frac{m_s^2}{2w(\mathbf{x})^2}(v' - \lambda_2) - \bar{v} = 0$$

$$\Longrightarrow$$

$$\lambda_2 = \begin{cases} 0 & \text{if } v' < \frac{2w(\mathbf{x})^2}{m_s^2}\bar{v} \\ v' - \frac{2w(\mathbf{x})^2}{m_s^2}\bar{v} & \text{if } \frac{2w(\mathbf{x})^2}{m_s^2}\bar{v} \leq v'. \end{cases} \tag{A–21}$$

Putting the results for the cases together yields

$$\begin{aligned} &\lambda_1 = -v', \lambda_2 = 0 && \text{if } v' \leq 0 \\ &\lambda_1 = \lambda_2 = 0 && \text{if } 0 < v' < \tfrac{2w(\mathbf{x})^2}{m_s^2}\bar{v} \\ &\lambda_1 = 0, \lambda_2 = v' - \tfrac{2w(\mathbf{x})^2}{m_s^2}\bar{v} && \text{if } v' \geq \tfrac{2w(\mathbf{x})^2}{m_s^2}\bar{v}. \end{aligned} \tag{A–22}$$

Thus (A–17) becomes

$$v = \begin{cases} 0 & \text{if } v' \leq 0 \\ \frac{m_s^2}{2w(\mathbf{x})^2} v' & \text{if } 0 < v' < \frac{2w(\mathbf{x})^2}{m_s^2}\bar{v} \\ \bar{v} & \text{if } v' \geq \frac{2w(\mathbf{x})^2}{m_s^2}\bar{v} \end{cases}. \tag{A–23}$$

The deterministic dynamic constraint (2–9) and (A–15) then become

$$\begin{bmatrix} \dot{\mathbf{x}} \\ \dot{\mathbf{p}} \end{bmatrix} = \begin{cases} \begin{bmatrix} A & 0 \\ -2Q & -A^T \end{bmatrix} \begin{bmatrix} \mathbf{x} \\ \mathbf{p} \end{bmatrix} & \text{if } \mathbf{x} \in \mathcal{R}_1 \\ \begin{bmatrix} \bar{A}^T & -\bar{B} \\ -2\bar{Q} & -\bar{A} \end{bmatrix} \begin{bmatrix} \mathbf{x} \\ \mathbf{p} \end{bmatrix} & \text{if } \mathbf{x} \in \mathcal{R}_2 \\ \begin{bmatrix} \hat{A}_1 & 0 \\ -Q^* & -\hat{A}_1^T \end{bmatrix} \begin{bmatrix} \mathbf{x} \\ \mathbf{p} \end{bmatrix} & \text{if } \mathbf{x} \in \mathcal{R}_3 \end{cases} \tag{A–24}$$

where $\hat{A}_1 = A - \bar{v}\mathbf{b}\mathbf{T}^T$, $Q^* = \bar{Q} + \frac{2}{m_s^2}(\bar{v}\mathbf{T} - m_s\mathbf{a})(\bar{v}\mathbf{T} - m_s\mathbf{a})^T$ and $\mathcal{R}_1, \mathcal{R}_2$and $\mathcal{R}_3$ are as defined in section 2.2. Thus, using the relationship (A–9) yields the Riccati equation (2–17).

Now, let

$$V_a = \mathbf{x}^T P_a \mathbf{x} \tag{A–25}$$

where, $P_a$ is defined in Theorem 2.2. The associated value function of the fully active optimal control[9] is

$$J_a = \mathbf{x}^T(t_0) P_a \mathbf{x}(t_0). \tag{A–26}$$

Then, for the deterministic semi-active suspension

$$\begin{aligned} \dot{V}_a &= \dot{\mathbf{x}}^T P_a \mathbf{x} + \mathbf{x}^T P_a \dot{\mathbf{x}} \\ &= \mathbf{x}^T \left( A^T P_a + P_a A \right) \mathbf{x} + v \left( \phi^T(\mathbf{x}) P_a \mathbf{x} + \mathbf{x}^T P_a \phi(\mathbf{x}) \right) \end{aligned}$$

which, using (2–22) and $g(\mathbf{x}, v)$ defined in (2–5), becomes

$$\dot{V}_a = -g(\mathbf{x}, v) + \left( \frac{w(\mathbf{x})v}{m_s} - \left( m_s \mathbf{b}^T P_a + \mathbf{a}^T \right) \mathbf{x} \right)^2. \tag{A–27}$$

Integrating both sides and using the boundary condition $\mathbf{x}(t_f) = \mathbf{0}$ yields

$$-V_a(t_0) = -J(\mathbf{x}^*, v^*) + \int_{t_0}^{t_f} \left( \frac{w(\mathbf{x}^*)v^*}{m_s} - \left( m_s \mathbf{b}^T P_a + \mathbf{a}^T \right) \mathbf{x}^* \right)^2 dt \tag{A–28}$$

from which (2–21) follows. □

REFERENCES


[1] W.B. Adams *English Pleausre Carriages*, C. Knight & Co., 1837.

[2] chroniclingamerica.loc.gov, The Washington Times, Sunday 30 June,; .

[3] K.K. Jain and R.B. Asthana *Automobile Engineering*, Tata McGraw-Hill, 2002.

[4] J.C. Dixon *Suspension Geometry and Computation*, John Wiley & Sons Ltd, 2009.

[5] G. Genta and L. Morello *The Automotive Chassis, Vol. 1: Components Design*, Vol. 1, Springer, 2009.

[6] Ingolstadt, *Audi TT coupé '07 - Suspension System*, , Service Training, Self Study Programme 381, 2006.

[7] R. Alkhatib, G.N. Jazar, and M.F. Golnaraghi, *Optimal design of Passive Linear Suspension Using Genetic Algorithm*, Journal of Sound and vibration 275 (2004), pp. 665–691.

[8] R.A. Williams, *Automotive active suspensions. Part 1: basic principles*, in *Proceedings of IMechE*, Vol. 211, 1997, pp. 415–426.

[9] T. Butsuen, *The Design of Semi-active Suspensions for Automotive Vehicles*, Massachussets Institute of Technology, 1989.

[10] H.E. Tseng and J.K. Hedrick, *Semi-Active Control Laws - Optimal and Sub-Optimal*, Vehicle System Dynamics 23 (1994), pp. 545–569.

[11] M. Valasek and W. Kortum, *Nonlinear control of semi-active road-friendly truck suspension*, in *Proceedings AVEC 98*, Nagoya, 1998, pp. 275–280.

[12] M. Valasek and W. Kortum, 2001, Semi-Active Suspension Systems II. in *The Mechanical Systems Design Handbook; Modeling, Measurement and Control* CRC Press LLC.

[13] D. Karnopp, M. Crosby, and R. Harwood, *Vibration control using semi-active force generators*, Journal of Engineering for Industry 96 (1974), pp. 619–626.

[14] D. Karnopp, *Active damping in road vehicle suspension systems*, Vehicle System Dynamics 12 (1983), pp. 291–316.

[15] D. Karnopp and G. Heess, *Electronically controllable vehicle suspensions*, Vehicle System Dynamics 20 (1991), pp. 207–217.

[16] W.J. Evers, A. Teehuis, A. Knaapvan der , I. Besselink, and H. Nijmeijer, *The Electromechanical Low-Power Active Suspension: Modeling, Control, and Prototype Testing*, Journal of Dynamic Systems, Measurement, and Control 133 (2011).

[17] A.C.M. Knaapvan der , A.P. Teerhuis, R.B.G. Tinsel, and R.M.A.F. Vershuren, *Active Suspension Assembly for a Vehicle*, International Patent No. 2008/049845. (2008).

[18] A. Ashfak, A. Saheed, K.K. Abdul-Rasheed, and J.A. Jaleel, *Design, Fabrication and Evaluation of MR Damper*, World Academy of Science, Engineering and Technology 53 (2009).

[19] I. Fialho and G.J. Balas, *Road Adaptive Active Suspension Design Using Linear Parameter-Varying Gain-Scheduling*, IEE Transactions on control systems technology 10 (2002), pp. 43–54.

[20] A.L. Do, O. Sename, and L. Dugard, *An LPV Control Approach for Semi-active Suspension Control with Actuator Constraints*, in *2010 American Control Conference*, 2010.

[21] R.A. Williams, A. Best, and I.L. Crawford, *Refined low frequency active suspension*, in *Proceedings of IMechE International Conference*, November, , 1993, pp. 285–300.

[22] S. Ikenaga, F. Lewis, J. Campos, and L. Davis, *Active suspension control of ground vehicle based on a full-vehicle model*, in *American Control Conference, 2000. Proceedings of the 2000*, Vol. 6, 2000, pp. 4019–4024.

[23] W. Jones, *Easy ride: Bose Corp. uses speaker technology to give cars adaptive suspension*, Spectrum, IEEE 42 (2005), pp. 12–14.

[24] D. Karnopp and D. Margolis, *Adaptive suspension concepts for road vehicles*, Vehicle System Dynamics 13 (1984), pp. 145–160.

[25] L. Woods, Computer Optimized Adaptive Suspension System Having Combined Shock Absorber/Air Spring Unit; EP Patent 0,080,291.

[26] B.F. Spencer, S.J. Dyke, M.K. Sain, and J.D. Carlson, *Phenomenological model of a magnetorheological damper*, ASCE Journal of Engineering Mechanics (1996).

[27] J.W. Kim, Y.H. Cho, H. Lee, and S.B. Choi, *Electrorheological Semi-Aactive damper: Polyaniline based ER system*, Journal of Intelligent Matrial Systems and Structures 13 (2002), pp. 509–513.

[28] O.M. Anubi and C. Crane, *Semi-global Output Feedback Asymptotic Tracking for an Under-actuated Variable Stiffness Mechanism*, in *Proceedings of the 13th IFTOMM World Congress in Mechanism and Machine Science*, June, , 2011.

[29] A. Knaapvan der , *Design of a Low Power Anti-Roll/Pitch System for a Passenger Car*, Delft University of Technology, 1989.

[30] P.J.T. Venhovens and A.C.M. Knaapvan der , *Delft Active Suspension (DAS). Background Theory and Physical Realization*, Smart Vehicles (1995), pp. 139–165.

[31] D. Karnopp, M. Crossby, and R. Harwood, *Vibration Control Using Semi-Active Force Generators*, Journal of Engineering for Industry 96 (1974), pp. 619–626.

[32] S.M. Savaresi, E. Silani, and S. Bittanti, *Acceleration-Driven Damper (ADD): An Optimal Control Algorithm for Comfort-Oriented Semi-Active Suspensions*, ASME Journal of Dynamic Systems, Measurement and Control 127 (2005), pp. 218–229.

[33] S.M. Savaresi and C. Spelta, *Mixed Sky-Hook and ADD: Approaching the Filtering Limits of Semi-Active Suspension*, ASME Journal of Dynamic Systems, Measurement and Control 129 (2007), pp. 382–392.

[34] K.S. Hong, D.S. Joen, and H.C. Sohn, *A New Modeling of the Macpherson Suspension System and its Optimal Pole-Placement Control*, in *Proceedings of the 7th Mediterranean Conference on Control and Automation (MED99) Haifa, Israel*, 1999.

[35] M.S. Fallah, *New Dynamic Modeling and Practical Control Design for MacPherson Suspension System*, Concordia University, Montreal, Quebec, Canada, 2010.

[36] O.M. Anubi and C.D. Crane, *Nonlinear Control of Semi-active MacPherson Suspension System*, in *ASME 2012 International Design Engineering Technical Conferences & Computers and Information in Engineering Conference*, 2012.

[37] C.D.C. Olugbenga Moses Anubi and W. Dixon, *Nonlinear Disturbance Rejection for Semi-active MacPherson Suspension System*, in *ASME Dynamic Systems and Control Conference, Ft. Lauderdale, FL*, 2012.

[38] S. Guo, S. Yang, and C. Pan, *Dynamic Modeling of Magnetorheological Damper Behaviors*, Journal of Intelligent Matrial Systems and Structures 17 (2006), pp. 3–14.

[39] H. Tanghirad and E. Esmailzadeh, *Automobile Passenger Comfort Assured through LQG/LQR Active Suspension*, Journal of Vibration Control 4 (1998), pp. 603–618.

[40] E. Elbeheiry, D. Karnopp, and A. Abdelraaouf, *Suboptimal Control Design of Active and Passive Suspensions Based on a Full car Model*, Vehicle System Dynamics 26 (1996), pp. 197–222.

[41] F. Lin *Robust Control Design: An Optimal Control Approach*, John Wiley & Sons Ltd, West Sussex, England, 2007.

[42] H.D.T. E. Ono S. Hosoe and Y. Hayashi, *Nonlinear $H_\infty$ Control of Active Suspension*, Vehicle System Dynamics Supplement 25 (1996), pp. 489–501.

[43] A. Zin, O. Sename, M. Basset, L. Dugard, and G. Gissinger, *A nonlinear vehicle bicycle model for suspension and handling control studies*, in *Proceedings of the IFAC Conference on Advances in Vehicle Control and Safety (AVCS), Genova, Italy*, October, , 2004, pp. 638–643.

[44] J.H. Taylor, 1999, Describing Functions. in *Electrical Engineering Encyclopedia* John Wiley and Sons, Inc, New York.

[45] J. Jerz, Variable Stiffness Suspension System; US Patent 3,559,976.

[46] T. Kobori, M. Takahashi, T. Nasu, N. Niwa, and K. Ogasawara, *Seismic response controlled structure with active variable stiffness system*, Earthquake Engineering and Structural Dynamics 22 (1993), pp. 925–941.

[47] I. Youn and A. Hac, *Semi-active suspension with adaptive capability*, Journal of Sound and Vibration 180 (1995), pp. 475–492.

[48] Y. Liu, H. Matsuhisa, and H. Utsuno, *Semi-active vibration isolation system with variable stiffness and damping control*, Journal of Sound and Vibration 313 (2008), pp. 16 – 28.

[49] O.M. Anubi, C. Crane, and S. Ridgeway, *Design and Analysis of a Variable Stiffness Mechanism*, in *Proceedings IDETC/CIE2010. ASME 2010 International Design Engineering Technical Conferences & Computers and Information in Engineering Conference*, 2010.

[50] F.L. Lewis, D.M. Dawson, and C.T. Abdallah *Robot Manipulator Control, Theory and Practice*, 2nd Marcel Dekker, Inc., 2004.

[51] J. Ball and J. Helton, $H_\infty$ *control for nonlinear plants: Connections with differential games*, in *Proceedings of the 28th Conference on Decision and Control*, Tampa, Florida, 1989, pp. 956–962.

[52] J. Helton and M. James *Extending* $H_\infty$ *Control to Nonlinear Systems*, SIAM, 1999.

[53] P. Soravia, $H_\infty$ *Control for Nonlinear Systems: Differential and Viscosity Solutions*, SIAM Journal of Control and Optimization 34 (1996), pp. 1071–1097.

[54] A.J. Schaftvan der $\mathcal{L}_2$*-Gain and Passivity Techniques in Nonlinear Control*, Springer: Berlin, 1996.

[55] H. Khalil and J. Grizzle *Nonlinear systems*, Vol. 3, Prentice Hal,l New Jersey, 1996.

[56] NHTSA, New Passenger Car Fleet Average Characterisitcs; .

[57] J. Schoukens, R. Pintelon, Y. Rolain, and T. Dobrowiecki, *Frequency Response Function Measurements in the Presence of Nonlinear Distortions*, Automatica 37 (2001), pp. 939–946.

[58] A.J. Stack and F.J. Doyle, *A Measure for Control Relevant Nonlinearity*, in *American Control Conferencel, Seattle*, 1995, pp. 2200–2204.

[59] I. 2631-1 *International Organization of Standardization. Mechanical Vibration and Shock - Evaluation of Human Exposure to Whole Body Vibration. Part 1: General Requirement.*, Geneva, 1997.

[60] Y. Starosvetsky and O. Gendelman, *Vibration absorption in systems with a nonlinear energy sink: Nonlinear damping*, Journal of Sound and Vibration 324 (2009), pp. 916–939.

[61] A. Vakakis, *Inducing passive nonlinear energy sinks in vibrating systems*, Trans ASME, J. Vib. Acoust. 123 (2001), pp. 324–332.

[62] E. Gourdon and C. Lamarque, *Nonlinear energy sink with uncertain parameters*, Journal of computational and nonlinear dynamics 1 (2006), pp. 187–195.

[63] X. Jiang, D.M. McFarland, L.A. Bergman, and A.F. Vakakis, *Steady state passive nonlinear energy pumping in coupled oscillators: theoretical and experimental results*, Nonlinear Dynamics 33 (2003), pp. 87–102.

[64] A.F. Vakakis, L. Manevitch, O. Gendelman, and L. Bergman, *Dynamics of linear discrete systems connected to local, essentially non-linear attachments*, Journal of Sound and Vibration 264 (2003), pp. 559–577.

[65] O. Gendelman and Y. Starosvetsky, *Quasi-periodic response regimes of linear oscillator coupled to nonlinear energy sink under periodic forcing*, Journal of applied mechanics 74 (2007), pp. 325–331.

[66] O. Gendelman, Y. Starosvetsky, and M. Feldman, *Attractors of harmonically forced linear oscillator with attached nonlinear energy sink I: Description of response regimes*, Nonlinear Dynamics 51 (2008), pp. 31–46.

[67] Y. Starosvetsky and O. Gendelman, *Attractors of harmonically forced linear oscillator with attached nonlinear energy sink. II: Optimization of a nonlinear vibration absorber*, Nonlinear Dynamics 51 (2008), pp. 47–57.

[68] O. Gendelman, L. Manevitch, A.F. Vakakis, and R. M'CLOSKEY, *Energy pumping in nonlinear mechanical oscillators: Part I: Dynamics of the underlying Hamiltonian systems*, Journal of Applied Mechanics 68 (2001), pp. 34–41.

[69] O.V. Gendelman, *Transition of energy to a nonlinear localized mode in a highly asymmetric system of two oscillators*, Nonlinear dynamics 25 (2001), pp. 237–253.

[70] O. Gendelman and A.F. Vakakis, *Energy pumping in nonlinear mechanical oscillators: Part II: Resonance Capture*, Journal of Applied Mechanics 68 (2000), pp. 42–48.

[71] O.M. Anubi, D.R. Patel, and C.D. Crane III, *A new variable stiffness suspension system: passive case*, Mechanical Sciences 4 (2013), pp. 139–151.

[72] J. Smoker, A. Baz, and L. Zheng, *Virtual Reality Simulation of Active Car Suspension System*, International Journal of Virtual Reality 8 (2009), pp. 75–82.

[73] A. Alleyne and J. Hedrick, *Nonlinear adaptive control of active suspensions*, Control Systems Technology, IEEE Transactions on 3 (1995), pp. 94–101.

[74] H. Merritt *Hydraulic control systems*, Wiley New York, 1967.

[75] P. Kokotovic, H. Khali, and J. O'reilly *Singular perturbation methods in control: analysis and design*, Vol. 25, Society for Industrial Mathematics, 1987.

[76] E. Kim, *Nonlinear indirect adaptive control of a quarter car active suspension*, in *Control Applications, 1996., Proceedings of the 1996 IEEE International Conference on*, 1996, pp. 61–66.

[77] L.B.S. H. Laalej Z. Q and P. Martynowicz, *MR damper based implementation of nonlinear damping for a pitch plane suspension system*, Smart Materials and Structures 21 (2012).

[78] M.A. Xubin Song and S.C. Sotuhward, *Modeling Magnetorheological Dampers with Application of Nonparametric Approach*, Journal of Intelligent Material Systems and Structures 16 (2005), pp. 421–432.

[79] E. Guglielmino, T. Sireteanu, C.W. Stammers, G. Ghita, and M. Giuclea *Semi-active Suspension Control: Improved Vehicle Ride and Road Friendliness*, Springer, 2008.

[80] Y.K. Wen and M. Asce, *Method for Random Vibration of Hysteric Systems*, Journal of the Engineering Mechanics Division 102 (1976), pp. 249–263.

[81] I.H. Shames and F.A. Cozzarelli *Elastic and Inelastic Stress Analysis*, Taylor & Francis, NJ, 1997.

[82] J. Koo, F. Goncalves, and M. Ahmadian, *A comprehensive analysis of the response time of MR dampers*, Smart materials and structures 15 (2006), p. 351.

[83] G.J. Forkenbrok, W. Garrot, M. Heitz, and B.C. O'Harra., *A comprehensive experimental examination of test maneuvers that may induce on-road, untripped, light vehicle rollover -phase iv of NHTSA's light vehicle rollover research program*, , National Highway Traffic Saftety Administration, 2002.

[84] M. Walz, *Trends in the static stability factor of passenger cars, light trucks, and vans*, , 2005.

[85] D. Sampson, *Active roll control of articulated heavy vehicles*, University of Cambridge UK, 2000.

[86] C. Carlson and J. Gerdes, *Optimal rollover prevention with steer by wire and differential braking*, in *Proceedings of IMECE*, 2003, pp. 16–21.

[87] B. Chen and H. Peng, *Differential-braking-based rollover prevention for sport utility vehicles with human-in-the-loop evaluations*, Vehicle System Dynamics 36 (2001), pp. 359–389.

[88] L. Palkovics, A. Semsey, and E. Gerum, *Roll-over prevention system for commercial vehicles–additional sensorless function of the electronic brake system*, Vehicle System Dynamics 32 (1999), pp. 285–297.

[89] V. Tsourapas, D. Piyabongkarn, A. Williams, and R. Rajamani, *New method of identifying real-time Predictive Lateral load Transfer Ratio for rollover prevention systems*, in *American Control Conference, 2009. ACC'09.*, 2009, pp. 439–444.

[90] M. Theriault *Great Maritime Inventions 1833-1950*, Goose Lane Editions, 2001.

[91] S. De Molina and S. Deferme, Passive anti-roll system; US Patent 6,220,406.

[92] P. Bock and G. O'rourke, Anti-roll system for wheeled vehicles; US Patent 5,383,680.

[93] J. Kincad, B. Mattila, and T. Ignatius, Semi-active anti-roll system; US Patent 6,428,019.

[94] I. AGNER, Anti-roll System; WO Patent 2,004,085,178.

[95] M. Nishikawa, Anti-roll system for vehicles; US Patent 4,345,661.

[96] M. Lund, Anti-roll system for a vehicle; US Patent 4,589,678.

[97] ———, Anti-roll system with tilt limitation; US Patent 5,040,823.

[98] M. Lund and G. Garrabrant, Anti-roll system with tilt limitation; US Patent 4,966,390.

[99] R. Jazar *Vehicle Dynamics: Theory and Application*, Springer, 2008.

[100] R. Rajamani *Vehicle dynamics and control*, Springer, 2011.

[101] L. Ray, *Nonlinear state and tire force estimation for advanced vehicle control*, Control Systems Technology, IEEE Transactions on 3 (1995), pp. 117–124.

[102] H. Pacejka and E. Bakker, *The magic formula tyre model*, Vehicle system dynamics 21 (1992), pp. 1–18.

[103] M. Oppenheimer, D. Doman, and M. Bolender, *Control allocation for over-actuated systems*, in *Control and Automation, 2006. MED'06. 14th Mediterranean Conference on*, 2006, pp. 1–6.

[104] M. Bodson, *Evaluation of optimization methods for control allocation*, in *AIAA Guidance, Navigation, and Control Conference and Exhibit*, 2001.

[105] International Standard ISO 3888-2: Passenger Cars - test track for a severe lane-change maneuver - part2: Obstacle avoidance; .

[106] K. Nam and A. Araposthathis, *A model reference adaptive control scheme for pure-feedback nonlinear systems*, Automatic Control, IEEE Transactions on 33 (1988), pp. 803–811.

[107] P. Ioannou and J. Sun, *Robust adaptive control*, (1996).

[108] G. Kreisselmeier and B. Anderson, *Robust model reference adaptive control*, Automatic Control, IEEE Transactions on 31 (1986), pp. 127–133.

[109] B. Badji, E. Fenaux, M. El Bagdouri, and A. Miraoui, *Nonlinear single track model analysis using Volterra series approach*, Vehicle System Dynamics 47 (2009), pp. 81–98.

[110] S.Ç. Baslamisli, İ.E. Köse, and G. Anlaş, *Gain-scheduled integrated active steering and differential control for vehicle handling improvement*, Vehicle System Dynamics 47 (2009), pp. 99–119.

[111] G.C. Goodwin and K.S. Sin *Adaptive filtering prediction and control*, Dover Publications, 2009.

[112] M. Corless and G. Leitmann, *Continuous state feedback guaranteeing uniform ultimate boundedness for uncertain dynamic systems*, Automatic Control, IEEE Transactions on 26 (1981), pp. 1139–1144.

[113] O.M. Anubi, D. Patel, and C.D. Crane, *Passive Variable Stiffness Suspension System*, ASME Early Career Technical Journal 11 (2012).

[114] T. Butz and Stryk Ovon *Modeling and Simulation of Rheological Fluid Devices*, Technische Universität München, Germany, 1999 Preprint SFB-438-9911.

[115] C.Collete and A. Preumont, *High frequency energy transfer in semi-active suspension*, Journal of Sound and Vibration 329 (2010), pp. 4604–4616.

[116] N. Ciblak and H. Lipkin, *Synthesis of Stiffness by Springs*, in *Proceedings of DETC'98*, September, , 1998.

[117] H. Dugoff, P. Fancher, and L. Segel, *Tire performance characteristics affecting vehicle response to steering and braking control inputs*, , 1969.

[118] E. Elbeheiry, D. Karnopp, and A. Abdelraaouf, *Advanced Ground Vehicle Suspension System - a Classified Biography*, Vehicle System Dynamics 24 (1995), pp. 231–258.

[119] H. FRAHM, Vibrations of Bodies; US Patent 989,958.

[120] G. Genta and L. Morello *The Automotive Chassis, Vol. 2: System Design*, Vol. 1, Springer, 2009.

[121] G. Holler, Antilock braking system based roll over prevention; US Patent 6,741,922.

[122] J.B. Hunt *Dynamic vibration absorbers*, Mechanical Engineering Publications, 1979.

[123] A. Isidori and A. Astolfi, *Disturbance Attenuation and $H_\infty$ Control via Measurement Feedback in Nonlinear Systems*, IEEE Trans. Automat. Contr 37 (1992), pp. 1283–1293.

[124] L. Jansen and S. Dyke, *Semiactive control strategies for MR dampers: comparative study*, Journal of Engineering Mechanics 126 (2000), pp. 795–803.

[125] J. Ji and N. Zhang, *Suppression of the primary resonance vibrations of a forced nonlinear system using a dynamic vibration absorber*, Journal of Sound and Vibration 329 (2010), pp. 2044–2056.

[126] A. Kalyani, M. Ahuja, A. Kumar, R. Kumar, K. Dhuri, and N. Tambe, Systems and Methods Providing Variable Spring Stiffness for Weight Management in a Vehicle; US Patent 20,120,049,479.

[127] L. Kitis, B. Wang, and W. Pilkey, *Vibration reduction over a frequency range*, Journal of Sound and Vibration 89 (1983), pp. 559–569.

[128] C.S. Kyle and P.N. Roschke, *Fuzzy Modeling of a Magnetorheological Damper using ANFIS*, in *IEEE Fuzzy Conference*, San Antonio, Texas, USA, 2000.

[129] G. Leitmann, *Semiactive control for vibration attenuation*, Journal of Intelligent Material Systems and Structures 5 (1994), pp. 841–846.

[130] F. Lin *Robust Control Design: An Optimal Control Approach*, John Wiley & Sons Ltd, West Sussex, England, 2007.

[131] J. Lin and J. Kanellakopoulos, *Road-adaptive nonlinear design of active suspensions*, in *American Control Conference, 1997. Proceedings of the 1997*, Vol. 1, 1997, pp. 714–718.

[132] Y. Liu, H. Matsuhisa, and H. Utsuno, *Semi-active vibration isolation system with variable stiffness and damping control*, Journal of sound and vibration 313 (2008), pp. 16–28.

[133] J. Lu, *A frequency-adaptive mutli-objective suspension control strategy.*, ASME Journal of Dynamic Systems, Measurement, and Control 126 (2004), pp. 700–707.

[134] S. Masri, *On the stability of the impact damper*, Trans ASME, J. Appl. Mech. 33 (1966), pp. 586–592.

[135] D.J. Mead and D. Meador *Passive vibration control*, Wiley, 1998.

[136] P. Muller, K. Popp, and W. Schiehlen, *Covariance analysis of nonlinear stochastic guideway-vehicle-systems*, in *Proceedings of the Sixth IAVSD Symposium*, 1979, pp. 337–351.

[137] S. Natsiavas, *Steady state oscillations and stability of non-linear dynamic vibration absorbers*, Journal of Sound and Vibration 156 (1992), pp. 227–245.

[138] A.H. Nayfeh and D.T. Mook *Nonlinear oscillations*, Wiley-VCH, 2008.

[139] J. Ormondroyd, *Theory of the dynamic vibration absorber*, Transaction of the ASME 50 (1928), pp. 9–22.

[140] A. Pavlov, N. Wouwvan de , and H. Nijmeijer, *Frequency response functions and Bode plots for nonlinear convergent systems*, in *Proceedings of the 45th IEEE Conference on Decision & Control*, December, , 2006.

[141] R. Rajamani and S. Larparisudthi, *On invariant points and thier influence on active vibration isolation*, Mechatronics 14 (2004), pp. 175–198.

[142] R.E. Roberson, *Synthesis of a nonlinear dynamic vibration absorber*, Journal of the Franklin Institute 254 (1952), pp. 205–220.

[143] A.J. Schaftvan der , $\mathcal{L}_2$*-Gain Analysis of Nonlinear Systems and Nonlinear State Feedback* $H_\infty$, IEEE Trans. Automat. Contr 37 (1992), pp. 770–784.

[144] J. Shaw, S.W. Shaw, and A.G. Haddow, *On the response of the non-linear vibration absorber*, International Journal of Non-Linear Mechanics 24 (1989), pp. 281–293.

[145] C. Spelta, F. Previdi, S. Savaresi, P. Bolzern, M. Cutini, and C. Bisaglia, *A novel control strategy for semi-active suspensions with variable damping and stiffness*, in *American Control Conference (ACC), 2010*, 2010, pp. 4582–4587.

[146] C. Spelta, F. Previdi, S. Savaresi, P. Bolzern, M. Cutini, C. Bisaglia, and S. Bertinotti, *Performance analysis of semi-active suspensions with control of variable damping and stiffness*, Vehicle System Dynamics 49 (2011).

[147] B.F. Spencer, G. Yang, J.D. Carlson, and M.K. Sain, *Smart Dampers for Seismic Protection of Structures: A Full Scale Study*, in *Second World Conference on Structural Control*, Kyoto, Japan, 1998.

[148] Y. Starosvetsky and O. Gendelman, *Attractors of harmonically forced linear oscillator with attached nonlinear energy sink. II: Optimization of a nonlinear vibration absorber*, Nonlinear Dynamics 51 (2008), pp. 47–57.

[149] K. Sung, Y. Han, K. Lim, and S. Choi, *Discrete-time fuzzy sliding mode control for a vehicle suspension system featuring an electrorheological fluid damper*, Smart materials and structures 16 (2007), p. 798.

[150] N. Tischler and A.A. Goldenberg, *Stiffness control for geared manipulators*, in *Proceedings 2001 ICRA. IEEE International Conference on Robotics and Automation*, Vol. 3, 2001, pp. 3042–3046.

[151] E. Wang, X. Ma, S. Rakheja, and C. Su, *Semi-active control of vehicle vibration with MR-dampers*, in *Decision and Control, 2003. Proceedings. 42nd IEEE Conference on*, Vol. 3, 2003, pp. 2270–2275.

[152] G. Yao, F. Yap, G. Chen, W. Li, and S. Yeo, *MR damper and its application for semi-active control of vehicle suspension system*, Mechatronics 12 (2002), pp. 963–973.

[153] J. Yao and C. Song, *Simulation and Analysis of Variable Stiffness Double- layer Vibration Isolation System*, Journal of Wuhan University of Technology(Information & Management Engineering) 32 (2010).

[154] J. Yim and J.H. Park, *Nonlinear $H_\infty$ Control of Robotic Manipulator*, in *IEEE Conference on System, Man and Cybernetics,SMC, Tokyo, Japan*, October, , 1999, pp. 960–965.

[155] M. Yokoyama, J. Hedrick, and S. Toyama, *A model following sliding mode controller for semi-active suspension systems with MR dampers*, in *American Control Conference, 2001. Proceedings of the 2001*, Vol. 4, 2001, pp. 2652–2657.

[156] M. Zapateiro, F. Pozo, H. Karimi, and N. Luo, *Semiactive Control Methodologies for Suspension Control With Magnetorheological Dampers*, Mechatronics, IEEE/ASME Transactions on (2012), pp. 1–11.

[157] L. Zuo and S. Nayfeh, *Low order continuous-time filters for approximation of the ISO 2631-1 human vibration sensitivity weightings*, Journal of Sound and Vibration 265 (2003), pp. 459–465.

[158] L. Zuo and S.A. Nayfeh, *Structured $H_2$ Optimization of Vehicle Suspensions Based on Multi-Wheel Models*, Vehicle System Dynamics 40 (2003), pp. 351–371.

## BIOGRAPHICAL SKETCH

Olugbenga Moses Anubi received his B.S (Hons) in systems engineering from the University of Lagos, Nigeria in 2006. He then served in the Nigerian National Youth Service Corp (NYSC) in 2007. He is currently completing his doctoral degree in Mechanical Engineering at the Center for Intelligent Machines and Robotics (CIMAR), at the University of Florida, Gainesville. His research interests are; Vehicle System Dynamics and Control, Suspension Design and Analysis, Nonlinear Control, Robust Control, Optimal Control, Robotics. He is a member of the American Society of Mechanical Engineers (ASME), and the Society of Automotive Engineers (SAE)